Probabilistic Reliability Assessment for Non-Linear Finite Element Analysis of Reinforced Concrete Beams

MSc Thesis

by

M.A.A. Strookman

to obtain the degree of Master of Science
at the Delft University of Technology,
to be defended publicly on Wednesday May 12, 2021 at 09:00 AM.

Student number:	4282981	
Project duration:	June 29, 2020 – May 12, 2021	
Thesis committee:	Dr. ir. O. Morales Napoles,	TU Delft, supervisor
	Dr. ir. M.A.N. Hendriks,	TU Delft
	Dr. ir. C.B.M. Blom,	TU Delft
	Ir. A.S. Greeuw	Dura Vermeer
	Ir. J. Meijdam	Dura Vermeer

This thesis is confidential and cannot be made public until April 30, 2021.

Abstract

Non-linear finite element analysis (NLFEA) is a powerful numerical solution method that can enhance accurate determination of the structural resistance for a more efficient design. However, the implementation of NLFEA for the design of reinforced concrete structures is lagging behind as related uncertainties have not been quantified adequately yet.

Multiple studies have been conducted to evaluate the effect of modelling choices, which has led to the RTD1016 Dutch Guideline. This guideline enables a better quantification of the uncertainties related to NLFEA for the proposed solution strategy. In this research, a full probabilistic approach is applied to improve the quantification of uncertainties related to NLFEA, and thereby enhance its application for the design of reinforced concrete structures. In particular, to the ultimate limit state (ULS) of simply supported beams subjected to both ductile and brittle failure modes.

To achieve this goal, 48 benchmark beams were selected from literature for calibration purposes. Material induced uncertainties of concrete and reinforcement were incorporated through an optimized Latin hypercube sampling strategy. The beams were modelled in a 2D plane in software program *Diana* based on a total strain crack model and Von Mises plasticity. A displacement-controlled analysis was performed to determine the numerical ultimate resistance. In total, 1104 analysis were performed of which the model uncertainty was quantified and the failure mode was determined by the ductility index. Based on this, a global reliability method was defined as a function of the failure mode. A comparison with existing reliability methods was made in terms of accuracy and robustness. Furthermore, a standalone multivariate non-parametric Bayesian network (NPBN) was developed that allows for extensive reliability assessment possibilities.

The research has shown how a full probabilistic approach with benchmarking can be applied. A reliability method as a function of the failure mode was proposed that showed improved efficiency compared to existing reliability methods (GRF,PRF,ECOV). For a 50 year design lifetime, a mean unity check of 77% was attained for the ductile failure mode and 66% for the brittle failure mode. For specific types of concrete and reinforcement, even higher efficiency can be obtained by reduced coefficients of variation of the material parameters. Furthermore, a NPBN was constructed which describes the NLFEA behavior of reinforced concrete beams. Additional research is necessary to improve the model application, but it has been demonstrated how such a model can be established and used for reliability assessment of reinforced concrete beams.

The findings of this study suggest that the design of reinforced concrete beams by NLFEA can be applied for efficient design, while respecting safety standards. The full probabilistic approach enabled an improved quantification of the design resistance. Thereby, this research contributes to the implementation of NLFEA for the design of reinforced concrete structures.

Keywords: Non-linear finite element analysis (NLFEA), Latin hypercube sampling (LHS), reinforced concrete beams, reliability method, ductility index, non-parametric Bayesian network (NPBN).

Preface

This research was conducted to complete the Master's program of the track Structural Engineering at the Faculty of Civil Engineering and Geosciences at Delft University of Technology. During the Bachelor's and Master's programs, I have acquired a lot of knowledge about the mechanics and design of civil engineering structures. This thesis gave me the opportunity to combine the knowledge from multiple disciplines, and perform a research that governs aspects of probabilistic, programming, mechanics and finite element analysis. This in-depth research has definitely improved my understanding and hopefully will help me to adequately solve civil engineering problems in the future. The research is intended to enhance the application of NLFEA in the design of reinforced concrete structures. It is presumed that this research contributes to safe and efficient design by NLFEA, and may it therefore be useful to other civil engineering practitioners.

My sincere appreciation goes to my graduation committee for their support during the research. I would like to thank Alex Greeuw and Jeroen Meijdam for the opportunity of the graduation internship at Dura Vermeer. They have inspired me to dive into the topic, and to link the research to practical use. I also want to thank the committee members of Delft University of Technology for their acknowledged expertise. Dr. ir. Oswaldo Morales-Nápoles on his expert knowledge and guidance on probabilistic, dr. ir. Max Hendriks for his extensive help in understanding and applying NLFEA, and dr. ir. Kees Blom for his constructive feedback related to the mechanics of reinforced concrete structures. The combined support has formed the foundation for the thesis lying in front of you.

M.A.A. Strookman
The Hague, April 2021

Contents

Nomenclature

Abbreviations

CC	Concrete Class
COV	Covariance
CoV	Coefficient of Variation
DT	Diagonal Tension
ECOV	Estimate of Coefficient of Variation
FC	Flexural Compression
FEM	Finite Element Model
FT	Flexural Tension
GRF	Global Resistance Factor
LFEA	Linear Finite Element Analysis
LHS	Latin Hypercube Sampling
MCS	Monte Carlo Simulation
NLFEA	Non-Linear Finite Element Analysis
NPBN	Non-Parametric Bayesian Network
PRF	Partial Resistance Factor
SLS	Service Limit State
ULS	Ultimate Limit State
VC	Shear Compression

Symbols

α	Sensitivity factor	[-]
β	Reliability index	[-]
β_{cr}	Minimum reducation factor of compressive strength due to lateral cracking	[-]
χ	Ductility index	[-]
γ	Safety factor	[-]
μ	Sample mean	[-]
ν	Poisson's ratio	[-]
ρ	Correlation coefficient	[-]
ρ_l	Longitudinal reinforcement ratio	[%]
σ	Sample standard deviation	[-]
σ_{xy}	Shear stress	[MPa]

θ	Model uncertainty	[-]
ε_{cu}	Ultimate strain concrete	[‰]
ε_{su}	Ultimate strain steel	[‰]
E_c	Young’s modules concrete	[MPa]
E_s	Young’s modules reinforcement steel	[MPa]
F	Point load	[kN]
f_u	Reinforcement ultimate strength	[MPa]
f_y	Reinforcement yield strength	[MPa]
f_{cd}	Concrete design compressive strength	[MPa]
f_{cm}	Concrete mean compressive strength	[MPa]
f_{ctm}	Concrete mean tensile strength	[MPa]
G_c	Concrete compressive fracture energy	[N/mm]
G_f	Concrete fracture energy	[N/mm]
K_n	Normal interface stiffness	[N/mm^3]
K_t	Tangential interface stiffness	[N/mm^3]
L	Span length	[m]
M_{Ed}	Bending moment	[kNm]
M_{Rd}	Bending moment resistance	[kNm]
P_f	Probability of failure	[-]
P_u	Ultimate load	[kN]
q	Distributed line load	[kN/m]
V	Coefficient of variation	[-]
V_{Ed}	Shear force	[kN]
V_{Rd}	Shear force resistance	[kN]
W	Plastic energy	[Nmm]
w_{crack}	Crack width	[mm]
w_{max}	Maximum deflection	[mm]

List of Figures

List of Tables

1 | Introduction

A large amount of civil engineering works in the Netherlands has been built in the period of 1955-1970, during economic resurgence after World War II. Many of this infrastructure has typically been designed for a lifetime of 50 to 70 years and are entering their end of lifetime in the coming decade. Existing structures either need replacement or should be reassessed for their remaining capacity based on their current status and present traffic loads. With economical and sustainable requirements in mind, both cases have led to an increased demand for accurate determination of the resistance of reinforced concrete structures. A large share of the reinforced concrete structures comprises bridges. Therefore, this research focuses on reinforced concrete beams as part of a bridge superstructure.

To date, the design of reinforced concrete structures has been carried out according to design rules as prescribed in the Eurocode (EN 1992-1-1)[1] and linear finite element analysis (LFEA). These methods have proven to result in safe structures for their designed lifetime, but are also known to be conservative as only the linear behaviour of materials is considered. The non-linear material behaviour beyond the linear response is not taken into account, while this has a significant impact on the ultimate limit state. In this context, non-linear finite element analysis (NLFEA) could offer a solution that considers the full mechanical behaviour and thereby enables a more accurate determination of the resistance of reinforced concrete structures.

Meanwhile, the application of NLFEA is already common practise in other fields of engineering. Amongst these fields of engineering are for example the design of shore protections and geotechnical design. The use of NLFEA in these engineering fields is widely used and accepted, which can be explained by the high complexity of problems dealing with either non-linear effects concerning geometry, contact or typical non-linear behaviour of materials. This raises the question of why the use of NLFEA is accepted in these fields of engineering, but not yet for the design of reinforced concrete structures.

The aversion to design reinforced concrete structures by NLFEA can be explained by the fact that the associated uncertainties have not been properly identified and quantified. General modelling choices and reliability methods were prescribed in *fib* Model Code 2010 [2]. In correspondence, Rijkswaterstaat[1] published guidelines on modelling choices for girder members. (Hendriks et al., Belletti et al.)[3,4] Multiple research have been conducted to further investigate the model uncertainty of NLFEA for different types of modelling choices and civil engineering structures. (Engen et al., Pacoste et al., de Putter)[5–7]. The combined efforts have resulted in a better understanding of modelling choices in NLFEA. However, existing reliability methods do not consider the failure mode while this has a significant impact on the model uncertainty. (Castaldo et al.)[8] Moreover, the model uncertainty is quantified through deterministic input parameters in these research. This semi-probabilistic approach does not adequately guarantee reliability levels and does not show the effect of related input parameters on the output.

To fill this gap in literature, a full probabilistic approach is considered that takes into account uncertainties due to material heterogeneity and modelling choices separately. It is presumed that an improved reliability method is feasible that complies with safety standards. Simultaneously, a more efficient reliability model can be obtained by distinction of the failure mode. An objective distinction between a ductile and brittle failure mode can be obtained by the ductility index, defined as a measure of the plastic energy absorbed by the reinforcement with respect to the total plastic energy dissipated in the system. (Engen et al.)[5] Therefore, this research aims to formulate an improved reliability method in terms of accuracy and robustness, and thereby enhance the implementation of NLFEA for design of reinforced concrete structures.

[1] Rijkswaterstaat: Institution for Dutch Ministry of Infrastructure and Environment.

1.1. Problem Definition

The construction sector takes a large share in the emission of carbon-dioxide, accounting for 39% of worldwide emissions in 2018, of which 11% comes directly from the production of construction materials including concrete and steel. (UN)[9] With the global effect of climate change in mind, the need for efficient design of civil engineering structures is increasing to meet both sustainable and economical demands. Non-linear finite element analysis is a numerical solution method that can provide such accurate assessment, and thereby, efficient design. However, the applicability has been questioned within the civil engineering community due to a lack of quantification of associated uncertainties.

With the publication of Hendriks et al. [3], a solution strategy for girder members was provided in order to minimize model uncertainties. This led to the possibility to better define uncertainties related to NLFEA for the given solution strategy. In combation with a proposed ductility index from Engen et al. [5], a better quantification of the uncertainties related to NLFEA is possible, leading to a more accurate and robust reliability model.

Classical methods like Monte Carlo simulation are unfeasible as computational times are large within NLFEA. Instead, a reliability model that can provide a quick estimate of the resistance is desired, while avoiding over prediction. Currently, three reliability methods are available from *fib* Model Code 2010 [2]. These methods have either shown to predict the ultimate resistance inaccurately due to large safety factors, or to lack robustness as failure modes are predicted incorrectly. The methods and their deficits are elucidated accordingly.

1. **Partial Resistance Factor (PRF):** Analysis is performed with very low partial material strengths, which may result in wrong failure mode prediction and structural instability. Serious concerns about its application are mentioned in *fib* Model Code 2010 [2].
2. **Global Resistance Factor (GRF):** Applies global safety factors after analysis with mean material parameters, which often leads to conservative results due to a relatively large safety factor without failure mode distinction.
3. **Estimation Coefficient of Variation (ECOV):** Based on interpolation between two analysis with mean and characteristic material strength parameters. The design resistance is assumed to be log-normal distributed, which only applies if both analysis have a similar failure mode. For optimised structures this may not be the case and method ECOV becomes unusable, which can be regarded as a lack of robustness.

In a comparative study of these reliability methods, Castaldo et al. [8] stated the following:

> *"This analysis implies that when the design ultimate resistance is estimated by means of a safety format, which does not take into account the actual distribution of the structural resistance as a function of the possible failure modes, the safety level is not adequately guaranteed." ... "a methodology able to capture the mechanical behaviour of the structure depending on the values assumed by material properties is necessary (i.e., failure mode sensitivity). At the same time, the methodology should be easy and with a limited required computational effort."*

This indicates that if the resistance is defined as a function of the failure mode, an improved reliability model that meets the required safety level could be established. As mentioned before, the failure mode can be determined objectively by means of a ductility index. (Engen et al.)[5] An improved reliability model can enhance the applicability of NLFEA within the design of reinforced concrete structures. The reliability method should require little computational time, while guaranteeing accuracy, robustness and safety.

Apart from the lack of proper quantification of uncertainties, attention should be paid to the fact that extracting towards the maximum capacity should be done with caution. Overestimation of the resistance is undesirable and should be clearly quantified in terms of an allowable probability of failure. Additionally, correct application of NLFEA requires extra effort and knowledge from the engineer.

1.2. Research Goal

As stated previously, the quantification of uncertainties related to design of reinforced concrete structures by NLFEA is lacking behind. Multiple research have investigated the effect of different solution strategies and led to suggestions on how to capture the failure mode objectively by a ductility index. With use of this knowledge, a better quantification of the uncertainties related to NLFEA is possible for the prescribed solution strategy, enabling an improved reliability method. Therefore, the goal of this research is to improve the quantification of uncertainties related to NLFEA and enhance its application in the design of reinforced concrete structures by defining a reliability model. Specifically, for simply supported reinforced concrete beam elements with and without shear reinforcement as part of a bridge superstructure. An accurate, robust and efficient reliability model is required to assess the design resistance of reinforced concrete beams by NLFEA. The main research question can be formulated as the following:

Can the quantification of uncertainties related to NLFEA be improved to enhance safe and efficient application for the design of reinforced concrete beam elements?

To answer the main research question, several sub-questions are specified. The sub-questions are specified with a short comment as follows:

1. **Can an efficient sampling strategy be applied to adequately describe the total space of design-related uncertainties?**
Uncertainties induced due to material heterogeneity, execution deviation and modelling choices should be considered to obtain a full view of the uncertainties associated with design by NLFEA. A large sample generally results in a better description of the uncertainties, but as computational times are large, an optimum for the number of samples and accuracy is desirable.

2. **Can the benchmarks be modelled efficiently in NLFEA according to a single solution strategy?**
Simplifications of the actual benchmarks are needed to limit the computational time. A single solution strategy is desirable to obtain a sufficiently large data-set by an automated process.

3. **What is the relation between the ductility index and the model uncertainty?**
The analysis is based on failure mode distinction by means of the ductility index. The ductility index boundary will be investigated, and the model uncertainty is evaluated with respect to the ductility index.

4. **Does distinction of the failure mode based on the ductility index enable a more accurate and robust reliability method?**
The proposed reliability model is compared to existing reliability methods (GRF,PRF,ECOV) to indicate their relative performance. Accuracy, robustness and efficiency are the assessment criteria.

5. **Can the NLFEA response of concrete beams be captured by a standalone model to be used for extensive analysis possibilities?**
A multivariate model may be able to capture the NLFEA response in a standalone model by means of a non-parametric Bayesian network, which can be used for extensive conditional analysis.

In the thesis outline (section 1.4), an overview is given for in which part the sub-questions are treated. The approach to answering the research questions is further elaborated in the methodology (chapter 3).

1.3. Scope

The research focuses on defining a reliability model for the ultimate limit state of an essential element of bridges: simply supported reinforced concrete beams. Available experimental tests from literature are used for calibration purposes. The test set-up of these experiments can be categorised in one- or two-point loading, and with or without shear reinforcement, as shown in Figure 1.1. All benchmarks are rectangular reinforced concrete beams with different material parameters for concrete and reinforcement and different layouts for span length, depth, width and reinforcement configuration. The beams are expected to experience a variety of failure mechanisms, either failing in a brittle or ductile manner. Full details of the 48 selected benchmarks are provided in Appendix A.

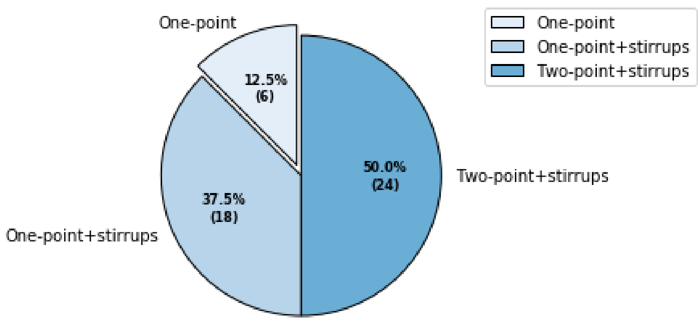

Figure 1.1: Overview of the experimental set-ups of the 48 selected benchmarks, of which six do not contain shear reinforcement.

Three types of uncertainties should be considered for determination of the resistance by NLFEA: Material properties, deviations in geometry and model uncertainties. Together they define the resistance as displayed in Figure 1.2. The model uncertainty implicitly contains all uncertainties that are not explicitly taken into account. In previous research, the model uncertainty has been quantified based on deterministic input variables. In this research, a full probabilistic approach is applied that explicitly accounts for material induced uncertainties besides the model uncertainty. Material properties such as concrete compressive strength and reinforcement yield strength are difficult to quantify exactly on forehand, and should therefore be evaluated with their prior known distributions from experiments. The model uncertainty can be assessed by calibration of the mean numerical resistance to the experimental resistance of the selected benchmarks.

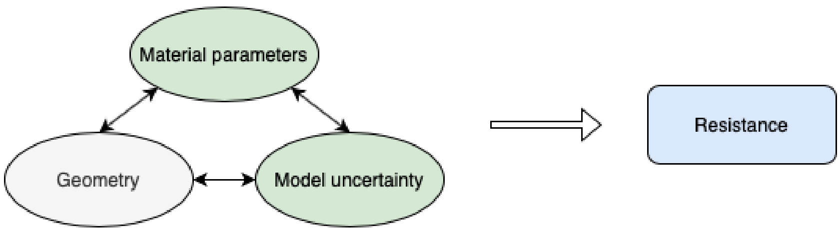

Figure 1.2: Combined resistance parameters that together define the design resistance. Uncertainties due to material parameters and modelling choices are explicitly taken into account.

Geometric uncertainties due to execution deviations are not considered in this research, as they may be identified after construction by quality control. This could eliminate the uncertainties due to execution deviations, and additional construction works can be carried out if found necessary. The magnitude of execution uncertainties is also very project-specific and was found insignificant compared to the material induced uncertainties for the selected benchmarks. For the selected benchmark experiments, the main geometric parameters, e.g. the effective depth, were measured with ± 1 millimeter accuracy. This corresponds to a coefficient of variation of 0.5%, which is negligible compared to the 30% of concrete mean compressive strength for example.

In non-linear finite element analysis, a large amount of modelling choices needs to be made. These engineering choices are accompanied by significant variations in results. In order to minimize model uncertainties and user factors, guidelines for NLFEA are followed from Rijkswaterstaat's document Hendriks et al.[3]. The research is not focused on comparing different modelling choices, but to quantify the design-related uncertainties for the prescribed solution strategy and to formulate a reliability model.

The research is carried out in non-linear finite element modelling software program Diana based on a total strain crack model and Von Mises plasticity. Different software may be based on different models and could give different outcomes. As computational times are significant in NLFEA, some simplifications were made. The benchmark reinforced concrete beams are numerically analysed on their maximum resistance in a 2D model, assuming plane stress. Furthermore, the problem is simplified by the use of symmetry boundary conditions. This simplification is valid under the assumption of a perfect symmetric experimental set-up, for which uncertainties for boundary and symmetry conditions are neglected. More on modelling choices is described in chapter 5. The used constitutive models, kinematic assumptions and equilibrium conditions are specified in Table 5.1.

1.4. Thesis Outline

The report consists of nine chapters in ascending order: Introduction, literature review, methodology, Latin hypercube sampling, non-linear finite element model, probabilistic analysis, comparison with existing models, non-parametric Bayesian network and a discussion. A diagram with the research questions and corresponding chapters is displayed in Figure 1.3. Subsequently, the content per chapter is described.

In **chapter 2**, a literature study is carried out. The relevant knowledge about reinforced concrete beam failure mechanisms, probabilistic analysis tools and modelling choices for non linear finite element analysis is addressed. This includes the theoretical background about Latin hypercube sampling, non-parametric Bayesian networks, non-linear finite element analysis and definitions of the ductility index and model uncertainty.

In **chapter 3**, the applied methodology to answer the research questions is described. This includes the sampling strategy, modelling choices and probabilistic analysis tools.

In **chapter 4**, the sampling strategy is described to answer sub-question (1). An Latin hypercube sampling strategy with spatial optimisation is applied to generate efficient samples that. In total, nine material parameters for concrete and reinforcement were included with their prior known distributions from Graubner and Brehm, Strauss et al.[10,11].

In **chapter 5**, sub-questions (2) and (3) are addressed. The applied constitutive, kinematic and equilibrium conditions are defined. The numerical output is compared to the experimental results and quantified by the model uncertainty. The ductility index boundary of $\chi = 0.6$ and the effect of geometry parameters on the model uncertainty are evaluated.

In **chapter 6**, sub-question (4) is answered. Distributions are fitted to the ductile and brittle failure modes based on the ductility index. From the fitted log-normal distributions, safety factors are derived to define a global reliability model. The empirical distributions of the resistance of both failure modes are discussed, and the sensitivity of the material parameters with respect to the model uncertainty is reviewed.

In **chapter 7**, a comparison of the proposed and existing reliability models is presented in addition to sub-question (4). A comparison is made based on accuracy and robustness with the methods PRF, GRF and ECOV.

In **chapter 8**, a non-parametric Bayesian network is constructed in correspondence with sub-question (5). The construction of the model is substantiated by physical logic. The model is validated based on a calibration score d-Cal. Furthermore, the model application is demonstrated for a random selection of input parameters and compared to the output of NLFEA.

In **chapter 9**, the discussion, conclusion and recommendations are addressed in order to discuss limitations, answer the research questions, and formulate recommendations for further research.

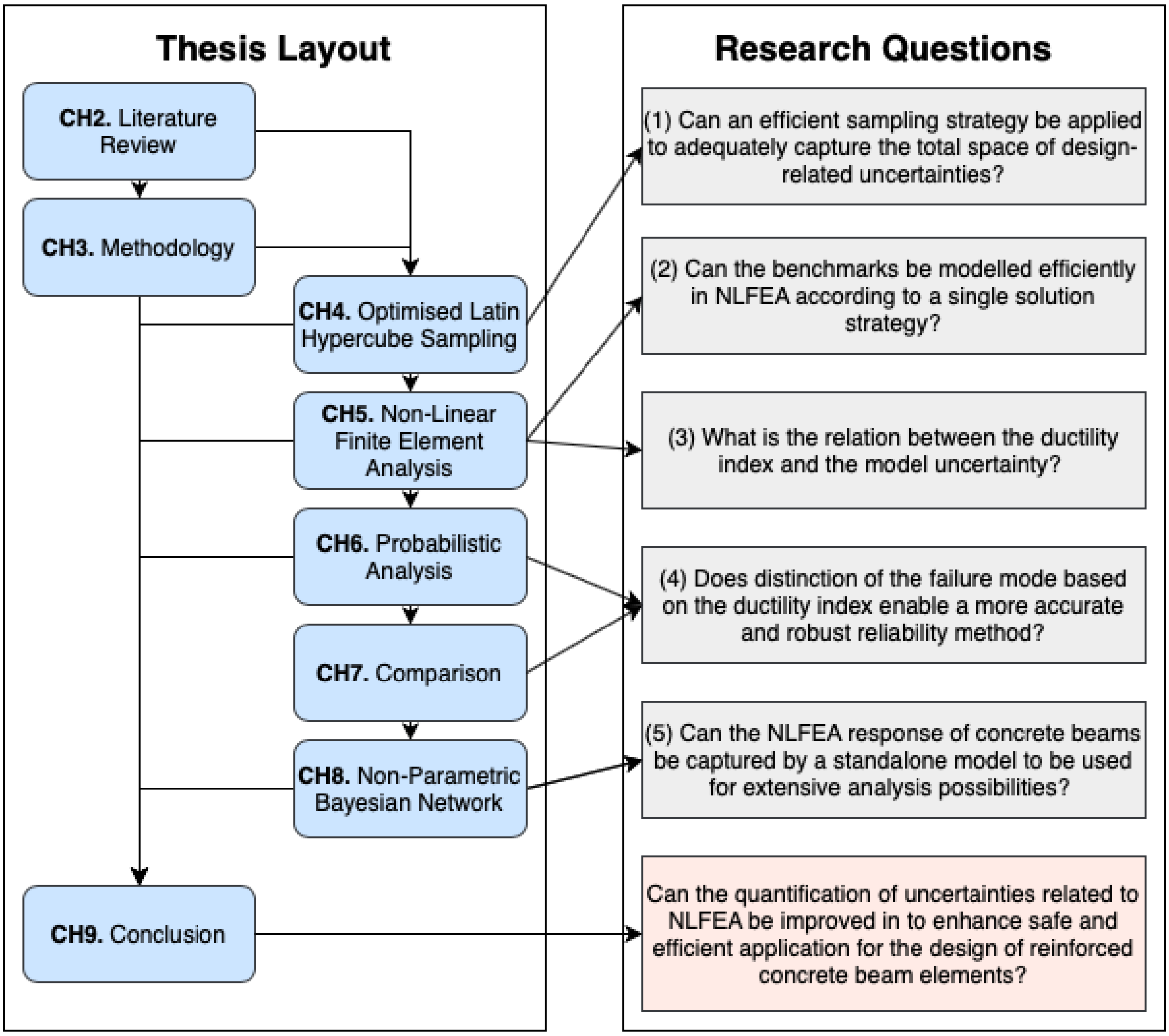

Figure 1.3: Thesis structure for answering the research questions.

2 | Literature Review

A literature review is carried out to address the knowledge and findings of other studies related to the scientific field of interest for this research. Three main categories of interest can be assigned: Beams failure mechanisms, non-linear finite element analysis and probabilistic analysis. Background information on these aspects is described consecutively.

2.1. Beams Failure Mechanisms

In this section, the main material behaviour of concrete and reinforcement is explained. Furthermore, the failure mechanisms for reinforced concrete beams are elaborated for transverse loading. This concerns ductile flexural failure and brittle shear failure. The analysis will focus on shear and bending moment resistance, which can suffer different types of failure mechanisms.

The relevant stress-strain (σ/ε) behaviour of reinforcing steel and concrete is shown in Figure 2.1. This material behaviour can be referred to as the constitutive model. Typical ultimate strains for reinforcement and concrete are $\varepsilon_{su} = 25‰$ and $\varepsilon_{cu} = 3.5‰$.

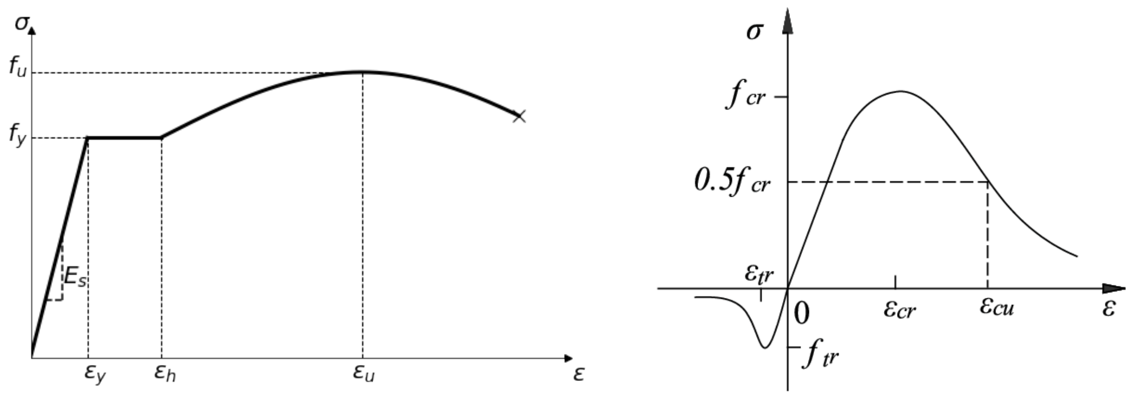

(a) Steel tensile.

(b) Concrete compression and tensile. (Xiao et al.)[12]

Figure 2.1: Stress-strain behaviour of (a) reinforcing steel and (b) concrete.

2.1.1. Ductile Failure

Ductile failure occurs for a bending moment that exceeds the bending moment resistance of the beam member. Three types of flexural failure can be addressed: tension failure, compression failure and balanced failure. The flexural capacity is determined by the reinforcement tensile strength with respect to the concrete compressive strength in the compressive zone. Flexural tension (FT) failure is a ductile failure that occurs If the bottom concrete undergoes flexural cracking and the reinforcement steel is activated, which may yield and deform plastically. The service limit state (SLS) is initialised before the ultimate limit state (ULS) is reached, and maintenance or replacement can be carried out. If the concrete strength is relatively low, the concrete under compression at the top can crush and may fail. The flexural compression (FC) failure type is a quasi-brittle failure mechanism accompanied with concrete crushing at the top and can be prevented in the design stage by limits of ρ_{max}, or by addition of top reinforcement. The last type is a balanced failure, where yielding of reinforcement and crushing of concrete occur simultaneously.

A quick estimate on the design bending moment for a distributed load can be obtained from well known mechanics by:

$$M_{Ed} = \frac{1}{8} q l^2 \qquad \text{where} \quad q = \psi_G q_G + \psi_Q q_Q \tag{2.1}$$

And for three point bending by:

$$M_{Ed} = \frac{1}{4}Fl \tag{2.2}$$

The bending moment resistance depends on the type of cross section and internal lever arms of the concrete compression force and tensile reinforcement force. (Walraven and Braam[13])

$$M_{Rd} = N_s * z_{leverarm}$$
$$\text{where } z_{leverarm} = d - c - \varnothing_{stirrup} - \frac{1}{2}\varnothing_l - \beta x_u \quad \textbf{or} \quad z \approx 0.9d \tag{2.3}$$

For the concrete and steel forces in the cross section it holds:

$$N_s = A_s f_{u,s}; \qquad N_c = \alpha b x_u f_{cd}$$
$$\text{where } \sum H = 0 \rightarrow N_c = N_s \tag{2.4}$$

with $\alpha = 0.75$ and $\beta = 0.39$ for concrete classes (CC) ≤C50/60, and $\gamma_G = 1.2$ for permanent loads, $\gamma_Q = 1.5$ for variable loads and $\gamma_P = 1.0$ for prestressing loads.

The bending moment resistance M_{Rd} is found from equilibrium of the cross section $\sum M = 0$ and $\sum H = 0$, either with or without prestressing. See Figure 2.2.

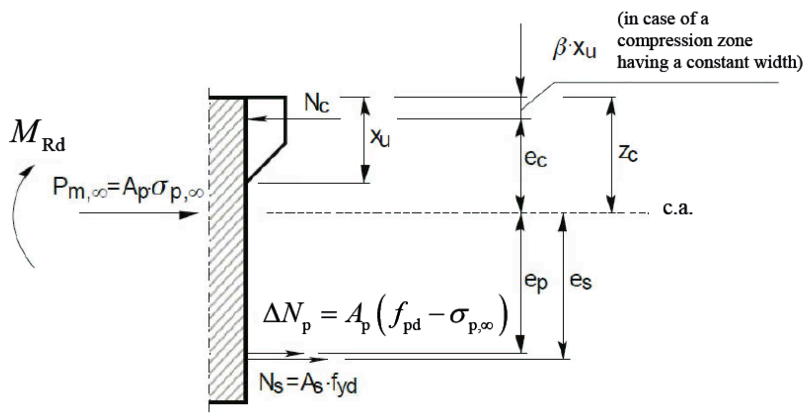

Figure 2.2: Forces acting on beam cross-section for equilibrium relations. (Walraven and Braam)[13]

2.1.2. Brittle Failure

Shear failure is a brittle failure mechanism. As this can lead to sudden failure, adequate measures should be taken during the design stage. Concrete cracking or crushing are the main concerns for loss of shear force capacity. The concrete material parameters are therefore normative, including concrete compressive strength, tensile strength, ultimate strain, Young's modulus and Poisson's ratio.

Within the constitutive models for concrete in NLFEA, the fracture energy G_f and compressive fracture energy G_c need to be specified, such that cracking and crushing of concrete can be modelled. These are a function of the (ultimate) strain, element size and concrete tensile strength. More on fracture energy is described in subsection 2.2.1.

For simply supported beams, the shear force under a distributed line load deviates linearly between the supports, being zero at mid-span. This can be described by:

$$V_{Ed} = q(\frac{1}{2}l - x) = \frac{1}{2}ql - qx \tag{2.5}$$

The normative shear force under four point loading test over the shear span a is defined as:

$$V_{Ed} = F \tag{2.6}$$

Shear resistance without stirrups is defined in EN 1992-1-1 [1] as:

$$V_{Rd,c} = \min \begin{cases} \left(C_{Rd,c} k 100 \rho_1 f_{ck}{}^{1/3} + k_1 \sigma_{cp}\right) b_w d \\ \left(v_{min} + k_1 \sigma_{cp}\right) b_w d \end{cases} \tag{2.7}$$

where

v_{min}	$= 0.035 k^{3/2} f_{ck}^{1/2}$	(Shear stress minimum)
k	$= 1 + \sqrt{\frac{200}{d}} \leq 2.0$	(Size effect)
ρ_l	$= \frac{A_{sl}}{b_w d} \leq 0.02$	(Longitudinal reinforcement ratio)
σ_{cp}	$= \frac{N_{Ed}}{A_c} < 0.2 f_{cd}$	(Axial compressive stress)

Different shear failure mechanisms are classified for slender and deep beams in ASCE-ACI [14]. Each failure mode has its own typical crack pattern, which is largely influenced by the slenderness of the beam (a/d-ratio). The crack patterns for the shear failure mechanisms are displayed in Figure 2.3.

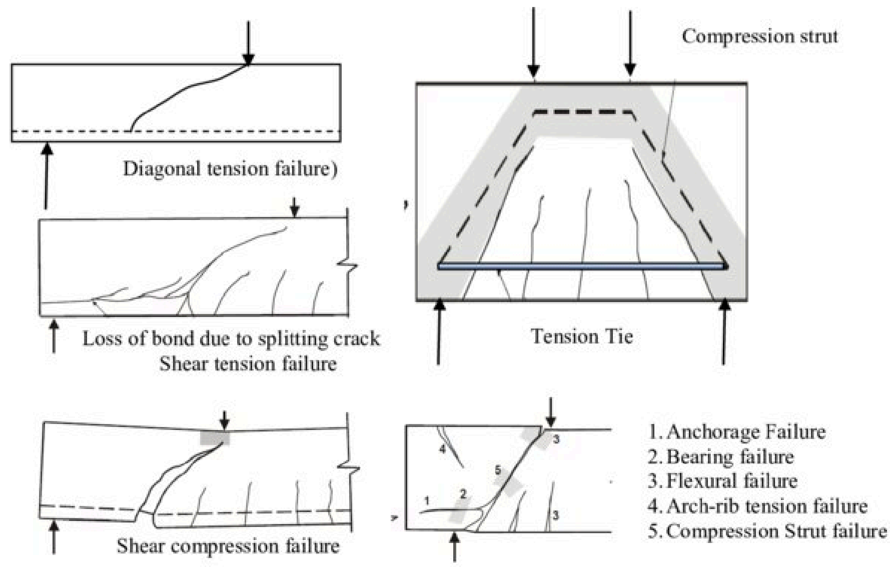

Figure 2.3: Crack patterns for different shear failure mechanisms and strut&tie model. (ASCE-ACI)[14]

Shear compression (VC) failure occurs when a crack is initialised and develops towards the top of the beam. The concrete compressive strength is exceeded and crushing near the tip of the crack at the beam top occurs. It is often observed for beams with large amounts of shear reinforcement and for $1.0 \geq a/d \leq 2.5$. Addition of top-reinforcement, lower longitudinal reinforcement ratio or higher concrete strength can prevent shear compression failure. Diagonal tension (DT) failure initiates with small diagonal cracks in the web, or flexural cracks on the bottom of the beam that propagate towards the loading point. A sudden failure occurs when the concrete fails in shear along the diagonal crack. Slender beams with $a/d \geq 2.5$ are prone to diagonal tension failure, which could be prevented with higher concrete strength or shear reinforcement. Shear tension failure occurs when the anchorage fails after diagonal or flexural cracks have propagated to horizontal cracks along the longitudinal reinforcement and the tensile transfer between reinforcement and concrete is inadequate. For deep beams with $a/d \leq 1.0$, the shear force is directly transferred to the supports and a arching type of failure can occur where the compressive strut fails.

2.1.3. Eurocode

The Eurocode is the leading guidance for construction works in the Netherlands. Three parts are of particular interest for design of reinforced concrete beams. In EN 1990 [15], principles are described regarding safety, usability and durability for constructions. EN 1992-1-1 [1] describes the design and calculations for concrete structures (bridges). Allowable inaccuracies for execution are described in NEN-EN 13670 [16].

In EN 1992-1-1 [1], design values are specified as:

- Concrete compressive design strength $f_{cd} = \alpha_{cc} f_{ck} / \gamma_C$.
- Concrete tensile design strength $f_{ctd} = \alpha_{ct} f_{ctk,0.05} / \gamma_C$.
- $\alpha_{cc,ct}$ coefficient for unfavourable long term effects on strength both equal to 1.0.
- $\gamma_c = 1.5$ partial safety factor concrete; $\gamma_s = 1.2$ partial safety factor steel.
- $\gamma_{Rd} = 1.15$ partial safety factor non-linear behaviour.

Loads on Constructions

The design loads are described by EN 1991-1-1 [17]. Three type of loads are to be considered: General loads, traffic loads and loads by cranes and machines. Partial safety factors are provided to account for any extreme loads and dynamic load effect due to vibrations.

- Point load F in [kN] with safety factor $\gamma_Q = 1.5$
- Variable line load q_Q in [kN/m] with safety factor $\gamma_Q = 1.5$
- Permanent line load q_G in [kN/m] with safety factor $\gamma_G = 1.2$

Service Limite State (SLS)

The limit state function for the SLS can be defined according to three principles given below.

1. Stress limits $\sigma_c \leq 0$ [-]
2. Crack width control $w_{crack} \leq s_0 \varepsilon_{stirrups}$ [mm]
3. Deformations $w_{max} \leq \frac{L}{250}$ [mm]

Ultimate Limite State (ULS)

The ULS can be checked according to three main criteria as well.

1. Moment capacity (bending stresses σ_{yy}) $\frac{M_{Ed}}{M_{Rd}} \leq 1$
2. Shear force (shear stresses σ_{xy}, σ_{yx}) $\frac{V_{Ed}}{V_{Rd}} \leq 1$
3. Normal force (normal stresses σ_{xx}) $\frac{N_{Ed}}{N_{Rd}} \leq 1$

Focus will be on shear and bending as no axial loads are applied to the benchmarks.

2.2. Finite Element Analysis

Finite element analysis (FEA) enables to design complex structures and to perform either linear or non-linear calculations. Discrete elements form a mesh along which stresses and deformations of the structure are described with respect to constitutive, kinematic and equilibrium relations. (Hartmann and Katz)[18] For shear and bending, the relevant degrees of freedom are vertical displacements w, horizontal displacements u and rotations φ. The accompanied stresses in a 2D plane are shear stresses $\sigma_{xy,yx}$, normal stresses σ_{xx} and bending stresses σ_{yy}.

For geometrically simple structures with limited deformations, linear FEA suffices to find stresses and deformations in the service limit state (SLS). However, as large deformations or difficult geometries are of concern, a linear analysis may be limited and give wrong results. Also an ultimate design resistance (ULS) cannot be found by LFEA, but can be through NLFEA.

A linear analysis simplifies the problem to linear elastic behaviour of materials to allow for fast computations, which can be accurate for structures with little deformations and simple geometry. In many other cases, large stress concentrations and wrong failure mechanism may be the result of linear analysis. Linear analysis does not allow for yielding of material, possibly resulting in unrealistically high stresses. Buckling or membrane state is not considered as such non-linear geometry is not allowed. The difference between linear and non-linear calculations is specified by the type of constitutive relations and respective stiffness matrices, but also comes with additional kinematic and equilibrium conditions.

The linear stress-strain relationship is described by Equation 2.8. These relations only describe the initial linear response of materials as can be seen for reinforcing steel and concrete in Figure 2.1. The real behaviour is simplified significantly, and cannot account for reinforcement yielding and concrete cracking or crushing. Yielding of reinforcement and cracking or crushing of concrete is not allowed for SLS, but can be used to find the ULS design resistance.

$$\begin{aligned} \varepsilon &= \frac{\partial u}{\partial x} = \frac{\Delta l}{l} \\ \sigma &= E\varepsilon \end{aligned} \tag{2.8}$$

Non-linear calculations in FEA can provide more realistic results in terms of deformations and stresses, but it also takes a lot more computational time and to some extent extra effort of the engineer. Three types of non-linear effects can be listed: Materials, geometry and contact. (Hartmann and Katz)[18]

1. Materials: Plastic deformations due to large stresses and/or cyclic loading.
2. Geometry: Large strains over 5‰, instability due to buckling.
3. Contact: Typically involves imposed boundary conditions which can cause large stress concentrations. E.g. point, line and surface contacts.

The materials type of non-linear induced effects is of particular interest for this research. By increasing the load to the maximum design resistance, the structure will pass the linear behaviour and exhibit non-linear behaviour until failure occurs. Cracks will develop in the concrete and steel reinforcement may deform plastically. To minimize the effect of user factors on the model uncertainty, the guidelines according to Hendriks et al.[3] combined with *fib* Model Code 2010[2] are followed. Prescriptions on application of constitutive models, kinematic assumptions and equilibrium conditions are discussed accordingly.

2.2.1. Constitutive Model

The constitutive model describes the stress-strain behaviour of the materials involved: Concrete, reinforcement and the support and loading plates. The constitutive model is intended to describe the actual behaviour of these material. The concrete model should include cracking and crushing behaviour, with consecutive local strength reduction and softening behaviour expressed by Poisson's ratio. Reinforcement should capture strain hardening behaviour beyond the yield stress, until an ultimate tensile stress is reached from which on the strain increases while incurring a loss of strength till ultimately rupture.

2.2.2. Concrete Constitutive Model

Different crack models can be applied to simulate concrete behaviour in NLFEA. A smeared crack approach or a discrete approach can be applied. Smeared crack models use an equivalent stiffness going to zero if the critical fracture energy G_f is exceeded. Therefore no visual discontinuity is present in the model. Alternatively, a discrete crack model can be used which is able to treat cracks as discontinuities in the model. Various studies have been performed to evaluate which method is more appropriate. (Rabczuk et al.)[19] For reinforced concrete, a smeared crack model has shown to have improved accuracy. Furthermore, fixed or rotating crack models can be applied. Rotating crack models are preferred for reinforced concrete beams with stirrups, as a fixed crack model could lead to large stress concentrations near the tip of a crack and cause convergence problems. In contrary, a fixed crack model has shown improved accuracy for beams without shear reinforcement. (de Putter)[7]

For NLFEA of reinforced concrete beams, it is advised to use a Hordijk tension softening curve and a parabolic compression curve for the concrete constitutive model.

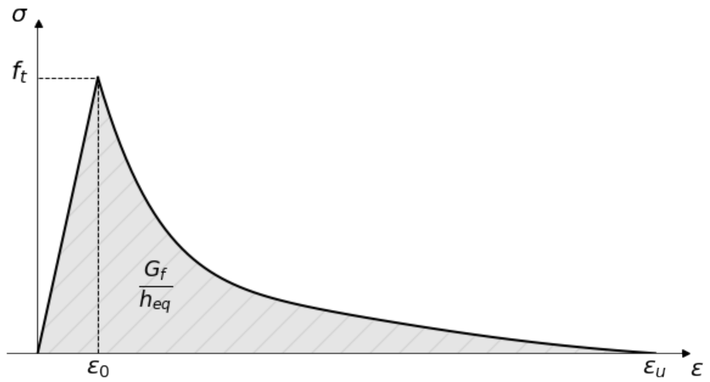

Figure 2.4: Hordijk's tension softening curve.

$$\sigma = \begin{cases} f_t\left(\left(1+\left(c_1\frac{\varepsilon^{cr}}{\varepsilon_u}\right)^3\right)\exp\left(-c_2\frac{\varepsilon^{cr}}{\varepsilon_u}\right)-\frac{\varepsilon^{cr}}{\varepsilon_u}(1+c_1^3)\exp(-c_2)\right) & 0 \leq \varepsilon^{cr} \leq \varepsilon_u \\ 0 & \varepsilon^{cr} > \varepsilon_u \end{cases} \tag{2.9}$$

where $c_1 = 3.0$, $c_2 = 6.93$ and the ultimate strain:

$$\varepsilon_u = 5.136\frac{G_F}{h_{eq}f_t} \tag{2.10}$$

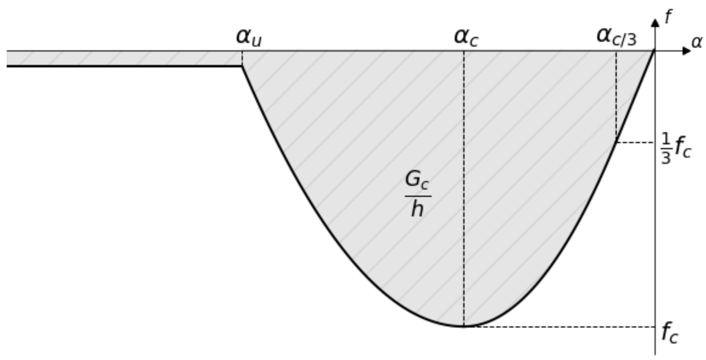

Figure 2.5: Concrete parabolic compression curve.

The compressive softening is based on the compressive fracture energy, which is derived from the tensile fracture energy according to Equation 2.14.

$$f = \begin{cases} -f_c\frac{1}{3}\frac{\alpha_j}{\alpha_{c/3}} & \alpha_{c/3} < \alpha_j \leq 0 \\ -f_c\frac{1}{3}\left(1+4\left(\frac{\alpha_j-\alpha_{c/3}}{\alpha_c-\alpha_{c/3}}\right)-2\left(\frac{\alpha_j-\alpha_{c/3}}{\alpha_c-\alpha_{c/3}}\right)^2\right) & \alpha_c < \alpha_j \leq \alpha_{c/3} \\ -f_c\left(1-\left(\frac{\alpha_j-\alpha_c}{\alpha_u-\alpha_c}\right)^2\right) & \alpha_u < \alpha_j \leq \alpha_c \\ 0 & \alpha_j \leq \alpha_u \end{cases} \tag{2.11}$$

here, α_j is the compressive strain for progressive compression part of:

$$\begin{cases} \alpha_{c/3} = -\frac{1}{3}\frac{f_c}{E} \\ \alpha_c = 5\alpha_{c/3} \\ \alpha_u = \alpha_c - \frac{3}{2}\frac{G_c}{hf_c} \end{cases} \tag{2.12}$$

Crack-band width

The crack bandwidth is a measure for the crack length depending on the type and distortion of elements. For an aspect ratio of 1:1, a Rots crack-band width suffices. For elongated elements a different crack band model may be needed to capture the softening stress-strain relationship in the constitutive model, for which Govindjee crack bandwidth is more appropriate. In Figure 2.6 various equivalent crack lengths are displayed for different elements and different crack orientations.

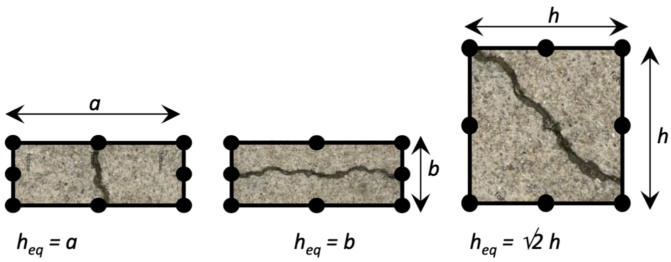

Figure 2.6: Equivalent crack lengths for different element dimensions and crack directions. (Hendriks et al. [3])

Softening Behaviour

The softening behaviour for concrete should be included to describe the crushing of concrete and to account for a strength reduction due to lateral tensile stresses. These are addressed as compression-compression to include the effect of confinement, and tension-compression for the effect of lateral cracking.

Compression-Compression

To be fully able to capture the non-linear behaviour of concrete, the effect of confinement is essential. It would be a conservative choice to not model it, but then the crushing of concrete is not adequately included. A suggested model for compression-compression behaviour is by Vecchio & Selby.

Tension-Compression

A reduction of the compressive strength of concrete due to lateral tensile stresses should be included. Due to cracks the compressive strength is reduced and ignoring it would not be conservative. This behaviour can be captured by a model of Vecchio & Collins (1993). For this application, a minimum reduction factor is defined as $\beta_{cr,min} = 0.4$.

Fracture Energy

The fracture energy is defined as the required energy for a tensile crack to propagate of a certain unit area. Within NLFEA the fracture energy G_f is used to specify the strains and stresses at which concrete cracks. This value is often determined by a concrete splitting test (three point bending on notched beam). It depends primarily on the water/cement ratio, maximum aggregate size and concrete age. (Strauss et al.)[11] This results in the fracture energy being very concrete specific. The formulation of the fracture energy therefore is still under debate. However, the proposed formula in Equation 2.14 was found to be accurate with a coefficient of variation of 20%. The mean estimates for concrete fracture energy, compressive fracture energy and Young's modulus can be specified as follows:

$$G_f = 73 f_{cm}^{0.18} \tag{2.13}$$

$$G_c = 250 G_f \tag{2.14}$$

$$E_{28\ days} = E_{c0}\left(\frac{f_{cm}}{10}\right)^{1/3} \tag{2.15}$$

$$\text{where } E_{c0} = 21.5\ [GPa] \tag{2.16}$$

2.2.3. Reinforcement Constitutive Model

Reinforcement can be modelled as fully bonded (embedded) or with slip-bond interaction. Although including slip-bond behaviour better approximates reality, assuming fully bonded reinforcement can suffice for the design stage. It is recommended to use an elasto-plastic constitutive model with hardening, for example by Von Mises criteria. The strain hardening of the reinforcement is captured in this way. If no hardening modulus is specified, $E_{har} = 0.02E_s$ can be used.

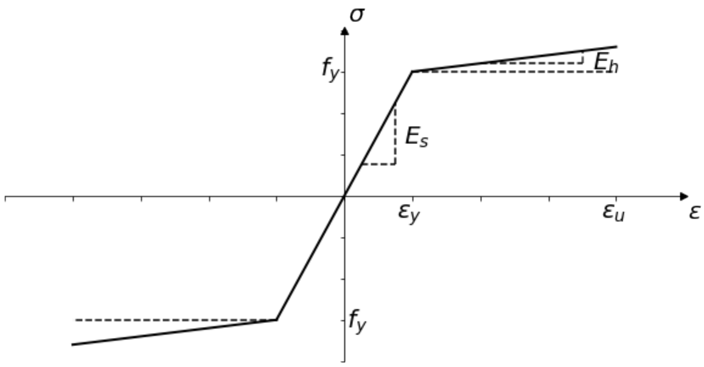

Figure 2.7: Bi-linear stress-strain reinforcement curve.

2.2.4. Kinematic Compatibility

Kinematic compatibility concerns element types and size, boundary conditions and connectivity (interfaces). In principle, a smaller mesh size improves the accuracy of the analysis. However, it is also comes at a cost of computational time. Typically an optimum should be reached for the relevant problem, while respecting the minimum element size as prescribed in Equation 2.17. An element size may be determined to be sufficiently accurate for the beams, and can be expressed as a fraction of the beam depth. Interpolation between elements may be linear or on shape. For the case of rectangular shaped beams it is irrelevant. Lastly, a rotating crack model is preferred as most of the considered beams contains shear reinforcement. A fixed crack model may lead to local stress accumulations which may lead to undesired non-convergence.

In Figure 2.8 an example of a linear and non-linear element is given. The left linear element has nodes at each corner and cannot deform along its axles. In other words, the axles will remain strait under any loading condition. Whereas the right non-linear element can deform along its axles to better approximate the real structural behaviour. A clear difference can be seen in the total number of nodes. By adding one node per axis, complexity of the problem increases significantly, resulting in larger computational time. Nonetheless, NLFEA is becoming more popular with improving computer capacity and improved methods for applying and assessing NLFEA.

Smaller element sizes generally provide better accuracy but calculation time increases approximately quadratic for smaller element sizes. (Hendriks et al.)[3] Maximum element sizes for beam structures are defined as:

$$\begin{aligned} 2D &: \min\left(\frac{l}{50}, \frac{h}{5}\right) \\ 3D &: \min\left(\frac{l}{50}, \frac{h}{5}, \frac{b}{5}\right) \end{aligned} \tag{2.17}$$

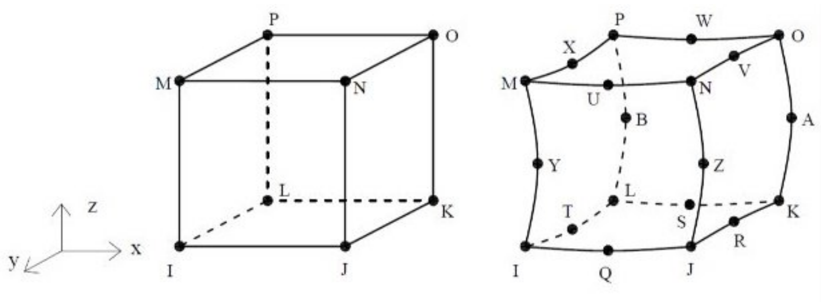

Figure 2.8: Example of linear 8-node quadrilateral element and non-linear 20-node hexahedral element. (Petrík and Ároch)[20]

Boundary Conditions
For simply supported beam elements at the support the bending moments and vertical displacements are equal to zero.

$$\begin{aligned} x(0) \rightarrow \quad M = 0 \text{ and } w = 0 \\ x(L) \rightarrow \quad M = 0 \text{ and } w = 0 \end{aligned} \tag{2.18}$$

The problem can be simplified to reduce computational time by means of symmetry conditions. The beam experiences its largest deformation at the center of the beam under symmetric loading, such that symmetry boundary conditions can be used for zero rotation and horizontal displacement. This results in:

$$x(\frac{1}{2}L) \rightarrow \; \varphi = 0 \text{ and } u = 0 \tag{2.19}$$

Interfaces
The connections for the loading and support plates can be modelled by interface conditions. The plates are used to redistribute the point loads to the concrete and to prevent preliminary local crushing of concrete. A low tangential stiffness of the interfaces is used to avoid the plates from contributing to the stiffness of the concrete beam. The following values can be used:

$$K_n = \frac{E_c}{h}, \quad (h = 1\ mm) \tag{2.20}$$

$$K_t = \frac{K_n}{1000} \tag{2.21}$$

The interface can be imagined as a fictitious interface of one millimeter thick concrete layer. This layer represents a normal stiffness of concrete Young's modulus divided by the virtual thickness of one millimeter. The tangential stiffness must be much lower in order to prevent a stiffness contribution to the beam, assuming that proper rollers were used in the experiments. A fictitious thickness of one meter concrete can represent the tangential stiffness, resulting in the normal stiffness divided by 1000. The following values are obtained: normal stiffness K_n=30000 N/mm^3 and the tangential stiffness K_t=30 N/mm^3. Interfaces between the reinforcement and concrete should also be modelled. For bond-slip interaction this has to be done manually. For this research, the reinforcement is assumed to be fully bonded (embedded), and the interface is generated automatically.

Bond Strength
The bond between reinforcement and the concrete concerns additional choices in modelling. The bond strength can be modelled as fully bonded, truss bonded or beam bonded. Again, various studies have shown advantageous and disadvantageous with respect to accuracy of the model. For assessment of the ULS, assuming fully bonded reinforcement suffices and is easier to implement. (Hendriks et al.)[3]

2.2.5. Equilibrium Conditions

Equilibrium conditions are related to the type of loading, load-steps, analysis control and convergence criteria. Either displacement or load controlled analysis can be performed. For displacement controlled analysis, a force balance and/or energy balance should be converged with respect to the convergence criteria. (Equation 2.22) An iteration scheme has to be selected, for which a maximum iteration number can be specified to avoid excessive loss of time due to non-convergence. A maximum number of iterations per step of 30 is often considered appropriate, but this depends on the kinematic compatibility.

Newton-Raphson

The Newton-Raphson algorithm is used for an iterative convergence of the partial differential equations. A first estimate is made for the displacements and forces at the nodes. A check is performed and the iteration continues until the result is sufficiently converged within a predefined allowable margin. Critical is the level of accuracy which comes at a cost in terms of computational time. A full Newton-Raphson algorithm is preferred.

A convergence tolerance for the Newton-Raphson method is defined by: Hendriks et al. [3], as:

$$\begin{gathered} L_2 = 0,01 \\ Energy\ norm = 0,0001 \end{gathered} \tag{2.22}$$

where L_2 is the norm for the unbalanced force. Using a force and energy norm leads to a displacement controlled loading scheme. An arc-length control and line search algorithm can enhance convergencence. In formula, the iteration process reads:

$$x_{n+1} = x_n - \frac{f(x_n)}{\frac{df(x_n)}{dx}} \tag{2.23}$$

The iteration is terminated if the maximum number of iterations is reached, or if the result is converged by:

$$|x_{n+1} - x_n| \ < \ L_x \tag{2.24}$$

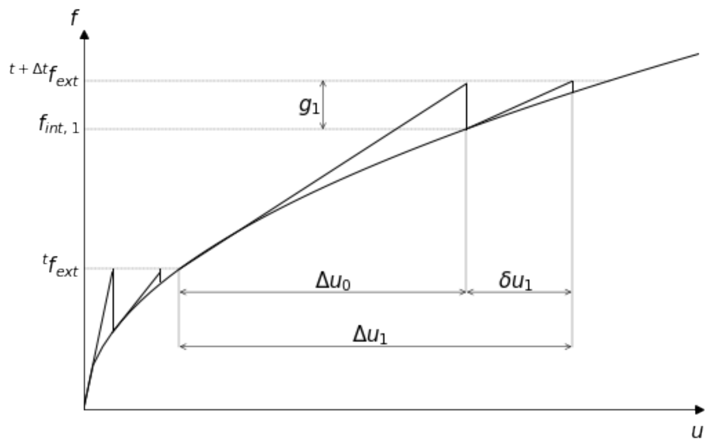

Figure 2.9: Full Newton-Raphson iteration procedure.

During the iteration the result can be converged, non-converged or divergent. In case the result is converged, a solution is found within the specified equilibrium conditions. If the result is non-converged, the equilibrium conditions are not met for the specific load-step. Non-converged steps are no concern as long as converged steps are present in the model near the desired output (e.g. at the maximum load). If divergence occurs, the iteration process is aborted and no solution could be found. Non-convergence and divergent problems can often be solved by reducing the element size, increasing the maximum number of iterations per step, or by adjusting the load-step. However, these actions are accompanied with an increase in computational time.

Arc-length Control + Line Search
To speed up the iteration process and improve convergence, an arc-length control and line search can be activated. Arc-length control is activated to continue iteration after a snap-through or snap-back, which is a change of direction in the load-displacement curve. A line search algorithm can be applied to improve the initial guess of the equilibrium forces and thereby increase the convergence rate.

Load-Step
Displacement controlled load step can be performed by setting a force and/or energy norm. For example, displacement steps of 1 millimeter can be applied for which an equilibrium force is iterated in each step. A smaller displacement step does not necessarily improve the convergence process, as a smaller displacement step means for each small step a new equilibrium must be found, which results in less smooth load-displacements curves and much more computational effort.

A displacement based load-step can be activated by setting energy and force equilibrium conditions, while for force based load steps energy and displacement based equilibrium conditions should be used. Depending on the stiffness of the beam and its expected failure mode, the magnitude of the load-step can be determined. A maximum displacement and a number of load-steps can be specified in Diana, as elaborated in subsection 5.2.1.

2.2.6. Design Verification

The SLS should be checked according to three principles. (*fib* Model Code 2010)[2]

1. Stress limits
2. Crack width control
3. Deformations

The deflection and stresses result directly from the NLFEA, while the crack opening control should be calculated according to Equation 2.25 where s_0 is the space between cracks [mm] and $\overline{\varepsilon_{stirrups}}$ is the average strain in the stirrups for shear stresses [-].

$$w = s_0 * \overline{\varepsilon_{stirrups}} \tag{2.25}$$

The ULS can be checked according to three reliability models (*fib* Model Code 2010)[2]

1. Global Resistance Factor method (GRF)
2. Partial Resistance Factor method (PRF)
3. Estimate of Coefficient of Variation method (ECOV)

GRF
The global resistance factor method is based on the assumption of the resistance being log-normal distributed and uses a global analysis for mean input variables. The global resistance is considered as a random variable for which uncertainties can be described by a global safety factor.

$$F_d \leq R_d, \quad R_d = \frac{R_m}{\gamma_R^* \gamma_{Rd}} \tag{2.26}$$

where F_d is the design value of actions, R_d the design resistance, R_m the mean value of resistance, $\gamma_R^* = 1.2$ a global resistance factor and $\gamma_{Rd} = 1.06$ a model uncertainty factor from *fib* Model Code 2010[2].

PRF
The partial resistance factor uses one analysis with design input parameters. The uncertainties are separated per variable by partial safety factors. The design input values are specified as:

$$
\begin{aligned}
f_{cd} &= \frac{f_{ck}}{\gamma_{Rd}\gamma_c} \\
f_{ctd} &= \frac{f_{ctk}}{\gamma_{Rd}\gamma_c} \\
f_{yd} &= \frac{f_{yk}}{\gamma_{Rd}\gamma_s} \\
G_{fd} &= G_{f0}\left(\frac{f_{cd}}{10}\right)^{0.7} \\
E_{cd} &= 22,000\left(\frac{f_{cd}}{10}\right)^{0.3}
\end{aligned}
\tag{2.27}
$$

Various safety factors are defined as γ_{Rd}=1.06, γ_c=1.5, γ_s=1.15, leading to the definition of the design resistance as:

$$P_d = P_u \tag{2.28}$$

It is stated that this method should not be on its own. Resistance parameters are very low, which may result in unrealistic types of failure mechanisms. (buckling modes)

ECOV
The method estimation of coefficient of variation relies on the assumption of a log-normal distributed resistance and involves two analysis to determine the design resistance.

$$P_d = \frac{P_{u,m}}{\gamma_{RD} * \gamma_R} \tag{2.29}$$

with γ_{RD}=1.06, γ_R=exp($0.8\beta V_R$), β=3.8 (lifetime), β=4.7 (one year) and the coeficient of variation defined as:

$$V_R = \frac{1}{1.65}\ln\left(\frac{P_{u,m}}{P_{u,c}}\right) \tag{2.30}$$

with $P_{u,c}$ the ultimate load obtained by using characteristic material properties and $P_{u,m}$ by mean material input.

Method ECOV uses a coefficient of variation based on the characteristic and mean design resistance for the respective resistance parameters, and estimates a safety factor based on the log-normal distribution. (Cervenka)[21] Method ECOV has shown to predict results accurately as long as failure modes are similar for both analysis. If not, the log-normal assumption is invalid and the method is inapplicable and therefore lacks robustness. An extensive description on the reliability methods is described in section 1.1.

2.2.7. Model Uncertainty
The model uncertainty θ is the main parameter used to quantify the numerical resistance with respect to the experimental resistance. Furthermore, a coefficient of variation V is used as ratio of the standard deviation and mean of the model uncertainty. Various research have been performed to quantify the model uncertainty within the NLFEA. Engen et al. [22] reported that the model uncertainty can be represented as a log-normal variable with mean $\mu_\theta = 1.1$ and standard deviation $\sigma_\theta = 0.12$, resulting in a coefficient of variation V of 11%.

$$\theta = \frac{R_{experimental}}{R_{numerical}} \tag{2.31}$$

$$V = \frac{\sigma_\theta}{\mu_\theta} \times 100\% \tag{2.32}$$

2.2.8. Ductility Index

A ductility index was introduced by Engen et al. [5] to objectively determine the failure mode for reinforced concrete beams. A value of $\chi_{ductility} = 0.6$ was found for the transition between a brittle and ductile failure mode, hence, shear and bending failure. The ductility index is formulated as the ratio of the plastic dissipated energy of the steel reinforcement with respect to the total plastic dissipated energy in the system:

$$\chi_{ductility} = \frac{W_{pl,s}}{W_{pl,sys}} \tag{2.33}$$

For a ductility factor going towards one (>0.6), most of the plastic energy is taken by the reinforcement indicating a ductile failure mechanism. When the ductility index tends towards zero (<0.6), the reinforcement has not contributed little to the total plastic energy dissipated in the system and the concrete must have failed prematurely, indicating a brittle shear failure mechanism. In Figure 2.10, the ductility index is displayed against the model uncertainty. The boundary between brittle and ductile failure mechanism is clearly indicated. Furthermore, it can be seen that the model uncertainty exhibits a larger variance for the brittle failure mechanism than for the ductile failure mechanism.

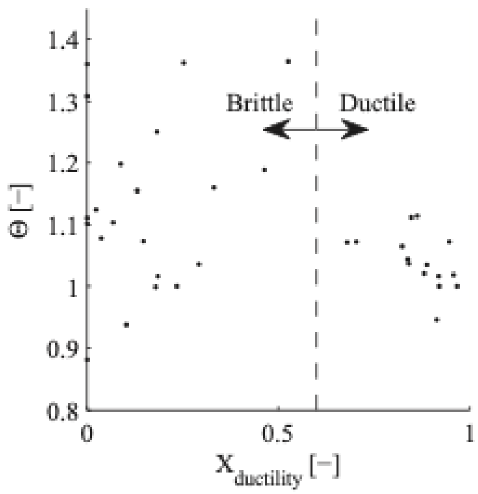

Figure 2.10: Model uncertainty as function of the ductility index. A boundary at $X_{ductility} = 0.6$ indicates a division between brittle and ductile failure mode. (Engen et al. [5])

The total dissipated energy in the system $W_{pl,sys}$ can be derived from the load-displacement curve. It is represented as the total area under the curve as the structure is unloaded after reaching its maximum capacity.

The total dissipated energy in the reinforcing steel, $W_{pl,s}$, can be calculated according to Equation 2.34.

$$W_{pl,s} = \left\{ \sum_{1}^{N} \frac{1}{2} (\sigma_{n-1} - \sigma_n)(\varepsilon_{n-1} - \varepsilon_n) - W_{el,s} \right\} * V_{int} \tag{2.34}$$

where the reinforcement elastic energy is equal to $W_{el,s} = \frac{1}{2} * f_y * \varepsilon_y$ and V_{int} is the volume per integration point of the reinforcement, equivalent to the number of nodes in the reinforcement.

2.3. Probabilistic Model

As computational time is generally large for non-linear finite element analysis (NLFEA), a classical method like Monte Carlo simulation is unfeasible. Instead a Latin hypercube sampling (LHS) strategy can be used as proposed by Tran et al. [23], by which a much smaller sample size can result in a clear distribution of the design resistance. By using representative combinations, a distribution on the design resistance can be well defined. From the found distribution the respective resistance and failure probabilities can be found. For more information on probabilistic methods is referred to Jonkman et al.[24].

Reliability Levels

The different types of reliability levels are specified as:

Level O	Deterministic, global safety factor (GRF)
Level I	Semi-probabilistic, partial safety factors (PRF)
Level II	Approximation (FORM, SORM, ECOV)
Level III	Numerical, full probabilistic (MCS, LHS, NPBN)
Level IV	Risk based

Accuracy of the probabilistic model can improve for higher reliability levels. GRF assumes a global safety factor for all variables, and PRF may distinguish safety factors for different parameters. ECOV uses an estimation on the distribution of the design value based on mean and characteristic material properties. The opted model would be level III reliability level, for which the probability of failure can be obtained through numerical integration. (Jonkman et al.)[24]

Limit State Functions

Limit state functions can be used to assess the probability of failure for empirical design formula's. These limit state functions can be defined by safety rules as described in EN 1992-1-1[1]. Again a difference is made between the SLS and ULS limit state functions. Limit state functions can be split into resistance and load parts defined as:

$$Z = R - S \tag{2.35}$$

in which

Z<0:	Failure
Z=0:	Limit State
Z>0:	No failure

The limit state functions for SLS are defined as combination of:

$$Z = \begin{cases} s_0 * \varepsilon_{stirrups} - w_{crack} & [mm] \\ 0 - \sigma_x & [N/mm^2] \\ 10 \ - w_{max} & [mm] \end{cases} \tag{2.36}$$

The limit state functions for ULS are defined as combination of:

$$Z = \begin{cases} M_{Rd} - M_{Ed} & [kNm] \\ V_{Rd} - V_{Ed} & [kN] \\ N_{Rd} - N_{Ed} & [kN] \end{cases} \tag{2.37}$$

2.3.1. Univariate Analysis

A univariate analysis is used to define the distribution of each variable and to analyse the distribution of the results on the design resistances. In literature, it is found that the resistances are well described by a log-normal distribution. (Graubner and Brehm)[10] For small variations, e.g. execution deviations, a normal distribution may fit as well. Both cases would enable further multivariate analysis on the assumption of the Gaussian copula. If X is log-normal distributed, then $Y = \ln(X)$ is normal distributed. For results on X it may be used that $X = \exp(Y)$.

2.3.2. Bivariate Analysis

For the resistance, multiple parameters can be addressed for both concrete and reinforcement. These parameters may be correlated and their joint distribution can be included by a Cholesky decomposition by using the covariance matrix. This procedure is further explained in section 4.3.

A copula can describe the joint distribution of two variables. A copula C is defined as the description of the joint distribution of two random variables X and Y. This copula is a distribution on the unit square [u,v] ∈ $[0,1]^d$ with uniform marginal distributions on [0,1]. Every continuous bivariate distribution can be represented by a copula. Moreover, an unique copula can be found which best describes the joint continuous distribution according to:

$$F_{XY}(x,y) = C(F(x), F(y)) \tag{2.38}$$

Dependency between the variables can be expressed by Spearman's rank correlation coefficient ρ_n, which is Pearson's correlation coefficient but then applied on the rank of two random variables. (Genest and Favre)[25] An attractive feature of the rank copula model is that the rank correlation coefficients are preserved under any monotonic transformation. For example, the correlation coefficient of the ranks is similar for $\rho(X,Y)$ and $\rho(X^2,Y^2)$ for the strictly positive data set. Pearson's correlation coefficient is defined as:

$$\rho(X,Y) = \frac{E[XY] - E[X]E[Y]}{\sigma_X \sigma_Y} \tag{2.39}$$

With F_X and F_Y being the cumulative distribution functions of X and Y, Spearman's rank correlation is defined as:

$$r(X,Y) = \rho\,[F_X(X), F_Y(Y)] \tag{2.40}$$

2.3.3. Non-Parametric Bayesian Network

One way to represent complex interdependent relations is by means of a non-parametric Bayesian network (NPBN). It is a tool for multivariate analysis, which represents dependencies between the nodes (variables) which are connected through arcs in an acyclic graph. (Ickstadt et al.)[26] The data can be used to construct relations between variables through arcs that represent the rank correlation (Spearman's ρ). By a NPBN, clear relations can be visualised and reviewed for a large number of variables. Also, the NPBN can be easily updated or adapted if new information becomes available. (Marcot and Penman)[27] The probabilities in the NPBN are defined by the factorization formula in which $pa(v)$ is the set of parents of v:

$$p(x) = \prod_{v \in V} p\left(x_v | x_{pa(v)}\right) \tag{2.41}$$

In order to construct the NPBN, sufficient data for each variable is needed where a minimum sample size of 1000 seems reasonable. The Gaussian copula enables for fast computations for large networks. However, the data may not always be Gaussian distributed which could enhance errors. Other distributions may be used, but this slows computational speed drastically. The underlying Gaussian normal copula is formulated in Equation 2.42. (Genest and Favre)[25]

$$\Phi_\rho(x_1,x_2) = \int_{-\infty}^{x_2}\int_{-\infty}^{x_1} \frac{1}{2\pi\sigma_1\sigma_2\sqrt{1-\rho^2}} \mathrm{e}^{\frac{\left(\frac{s_1-\mu_1}{\sigma_1}\right)^2 - \left(\frac{2\rho(s_1-\mu_1)(s_2-\mu_2)}{\sigma_1\sigma_2}\right) + \left(\frac{s_2-\mu_2}{\sigma_2}\right)^2}{2(1-\rho^2)}} \mathrm{d}s_1 \mathrm{d}s_2 \tag{2.42}$$

The NPBN can be validated based on a calibration score d-Cal or through the determinants of the correlation matrices. The determinants of the correlation matrices are compared to a confidence interval of 90%. The d-Cal is a measure for the 'distance' between the correlation matrix and the empirical data, empirical normal data and samples of the constructed NPBN. No clear consensus about the minimum required sample size of the d-Cal exists, but a higher sample indicates a better description of the dependencies.

2.3.4. Sampling Strategy

Monte Carlo simulation is based on drawing a large number of random samples from predetermined distributions. A sufficiently large data-set is needed to evaluate small probabilities of failure. The failure probability can be obtained as:

$$P_f = \frac{n_f}{N} \tag{2.43}$$

in which N is the total number of generations, and n_f is the total number of structural failures defined by the limit state function. Monte Carlo simulation in NLFEA is unfeasible due to large computational times per simulation in finite element analysis. Therefore, an alternative sampling strategy is considered: Latin hypercube sampling.

2.3.5. Latin Hypercube Sampling

As mentioned before, an efficient sampling strategy is needed due to large computational times in NLFEA. A Latin hypercube sampling (LHS) strategy can be applied, which is an efficient form of Monte Carlo simulation. Different variants of the classical LHS exist, which are intended to attain optimal spatial variability or randomness. These two properties can directly be optimized by means of maximizing the minimum distance, or to minimize the correlation between sample points for each subset.

First, the total space is split in sections of equal probability density $P_{i,j} = \frac{1}{N}$. Samples are generated from an uniform distribution with $X_{i,j} \in [0,1]$. Only one sample point is used in each row and each column as displayed in Figure 2.11. An iterative scheme is applied to optimise the spread amongst the variables by minimizing correlation between samples, or to optimise spatial variability by maximizing the minimum distance between the sampled points. The generated random uniform samples can then be transformed to the known marginal distributions of the parameters. For this research, spatial variability was selected as optimisation criterion, which corresponds with the following optimisation rule for maximizing the minimum distance between sample points:

$$\max\left\{\min\left\{d(X_i, X_j)\right\}\right\} \tag{2.44}$$

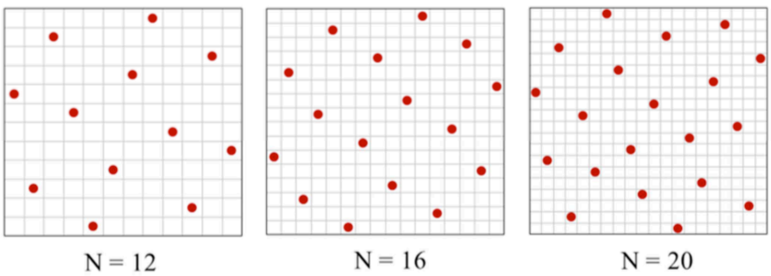

Figure 2.11: Example of Latin hypercube sampling with near perfect spatial and correlation characteristics. (Tran et al.)[23]

3 | Methodology

In this chapter, a description of the methodology is presented. The approach to answering the research questions is substantiated, and an objective is formulated per sub-question. The reason behind choices and the emerging benefits and limitations are discussed.

In chapter 2, a literature review has been performed to analyse all relevant aspects to the topic of this research. The literature review has resulted in a collection of knowledge about reinforced concrete beams failure mechanisms, modelling choices in NLFEA, and probabilistic sampling and assessment tools. The model uncertainty and ductility index are essential parameters for the analysis.

The structure of the research is presented such that the research questions are answered in different chapters as shown in Figure 1.3. After the literature review, data was collected for benchmark reinforced concrete beams. For these benchmarks, an optimized Latin hypercube sampling strategy is used to generate input samples of selected material parameters. NLFEA is executed to obtain the output response in terms of the ultimate load and ductility index. The results are evaluated by a probabilistic analysis. Distribution fitting is used to define a reliability model, which is compared to existing reliability methods. Furthermore, a complex multivariate model is established by means of a non-parametric Bayesian network. These methods together are used **to accomplish the research goal to better quantify uncertainties related to NLFEA to enhance its application for safe and efficient determination of the ultimate limit state of reinforced concrete beams.** In addition, a secondary objective is to develop a transparent and efficient format which can be adapted to analyse different types of reinforced concrete structures.

3.1. Data Collection

The numerical results are calibrated to experimental results to quantify the model uncertainty. Conducting own laboratory tests is not feasible as a large sample of benchmarks of existential size are desirable, which can be both time consuming and costly. Therefore, benchmarks were selected from other experimental research. This included data concerning material properties, geometry and maximum load. A part of a collection of experiments by de Putter [7] was used. In total 48 symmetrical simply supported beams were selected, of which 42 contained shear reinforcement. A detailed description of the experiments and input parameters can be found in Appendix A.

It is inevitable that differences in testing procedures for the benchmarks are present. This could lead to slightly biased results as the benchmarks originate from four different studies of which not all details are fully described. Details concerning concrete mixture and drying for example, are not identical for all experiments. It was supposed that these deviations were negligible compared to the other imposed uncertainties, as large coefficients of variation for concrete parameters.

Symmetrical benchmarks were selected, as non-symmetrical beams would take approximately twice the computational time. Prestressed beams are excluded as this would induce additional uncertainty by consideration of prestressing losses. To ensure feasibility, it was opted to exclude prestressed and non-symmetrical beams.

3.2. Sampling Strategy

Generally, a larger sample size results in a better description of the uncertainties. However, as computational times within NLFEA are substantial, an efficient sampling strategy is needed. A more efficient form of the classical Monte Carlo simulation is the optimized Latin hypercube sampling strategy. Random samples with similar statistics to a classical Monte Carlo simulation can be generated, but much less samples are needed due to the spatial optimisation of the samples. The entire sampling space is covered whereas for Monte Carlo simulation clustering may occur.

The optimized Latin hypercube sampling method is fully elaborated in section 4.3. The sampling strategy will be performed in *Python*[1] and is illustrated in Appendix B. Uniform random samples are created, which can be adjusted to the marginal log-normal distributions of the variables. The joint distribution of variables can be applied through a Cholesky decomposition by a predefined correlation matrix. Representative random samples are obtained from the resistance parameters to be used in the analysis.

As explained in the scope (section 1.3), the focus will be on quantifying model and material induced uncertainties. A probabilistic guideline for distributions of concrete and reinforcement material parameters is followed from Graubner and Brehm [10]. The distribution type for concrete fracture energy was taken from Strauss et al. [11]. The included material parameters are displayed in Table 3.1.

Table 3.1: Description of selected material input parameters for concrete and reinforcement.

Concrete		**Reinforcement**	
Compressive mean strength	f_{cm}	Yield strength	f_y
Tensile mean strength	f_{ctm}	Ultimate strength	f_u
Elasticity modulus	E_c	Elasticity modulus	E_s
Fracture energy	G_f	Poisson ratio	ν_s
		Ultimate strain	ε_{su}

The coefficient of variation is given as measure for the material uncertainties. The coefficients of variations are based on the strength of a wide variety of material types, and could be reduced significantly if the specific type of concrete and reinforcement are known. The geometry input was measured with a ± 1 millimeter accuracy in most studies, due to which these uncertainties were insignificant compared to those of the material parameters. (CoV 0.5% against 3-30%) Therefore, the geometry was considered as deterministic input. A sample size of $N = 20$ per benchmark was chosen, such that in total a data-set of approximately 1000 samples would be obtained. This was a trade-off between accuracy and time efficiency, and based on the statement from Tran et al. [23] that an accurate description of the design resistance could be obtained for a sample size of $N = 10$ by Latin hypercube sampling.

3.3. Non-Linear Finite Element Analysis

Non-linear finite element models for the reinforced concrete beams are created by software program *Diana*[2]. The analysis based on a total strain crack model, and contains useful features as logging of the ductility index and analysis control by a Python interface. The model is made such that the different geometries of beams and combinations of resistance parameters can be assessed. To create the model, Rijkswaterstaat's guidelines are followed for the constitutive, kinematic and equilibrium conditions. (Hendriks et al.)[3] The modelling choices were kept constant as much as possible to avoid deviations inflicted by these modelling choices.

The benchmarks were modelled in a 2D plane with use of symmetry conditions. Even with these simplifications, a single analysis could take up to 10 minutes. A displacement controlled analysis was applied, for which different load-steps were used depending on the magnitude of displacements and whether convergence was reached. (section C.1) This resulted in 20 samples for each of 48 benchmarks, in total 960 analysis. Existing reliability methods (PRF,GRF and ECOV) were also evaluated to compare the respective performance. An additional 144 analysis were obtained, which resulted in a total data set of 1104 analysis. A full example of the used Python script to run in Diana is attached in Appendix B.

[1] Python: used for sampling and probabilistic analysis
[2] Diana 10.4: Software used for NLFEA

Three output files were obtained per analysis: The NLFEA model (*.dnb*), an Excel file (*.xlsx*) and a logging file (*.out*). The Excel file was used to store the maximum applied external point load for each load-step. From this file the maximum load was retrieved. The logging file was used to evaluate the convergence per load-step and to obtain the ductility index at the maximum load-step. The solution was accepted if convergence occurred near the maximum applied load. If not, the analysis was redone with a smaller load-step.

Another simplification concerns the modelling of reinforcement. The reinforcement was assumed to be fully bonded and modelled as line elements in accordance with Hendriks et al. [3]. This holds as advantage that the anchorage of the reinforcement does not need to be modelled in detail and could be used as most benchmarks contained externally anchored reinforcement. However, the transfer of stresses between the reinforcement and concrete is thereby idealised, and Poisson's effect for reinforcement is also disregarded. This could induce a slight overestimate of the resistance. Bond-slip interaction models do exist, e.g. Shima, but this requires modelling of interfaces and additional uncertainties which were unfeasible for the opted large amount of analysis to be performed.

The uncertainties for concrete were taken into account by prior known marginal distributions from literature. Concrete however, is eminently a heterogeneous material and shows inconsistencies along the beam. The anisotropic character of concrete could be taken into account by spatial variability along the beam, which could reduce the variance of the model uncertainty. For simplicity however, concrete was modelled as an isotropic material per single analysis. As a consequence, the results should be used with caution for larger beams as no size effect was incorporated. The size effect could induce a strength reduction for larger structures.

3.4. Probabilistic Analysis

A probabilistic analysis is used to evaluate the obtained results. The probabilistic analysis consists of a univariate analysis by distribution fitting and statistical hypothesis test. Distribution fitting is used to obtain distributions for the model uncertainty, which can be compared to findings from other research. This could lead directly to safety factors and propositions for a reliability model.

In literature it is found that resistance can typically be fitted by either a normal or log-normal distribution. The brittle and ductile failure mechanisms are separated by the ductility index. For both, a normal and log-normal distribution are fitted by a probability density function (PDF) and cumulative distribution function (CDF) to give a visual representation. The goodness of fit is quantified by a Kolmogorov-Smirnov test (KS-test) for a prescribed confidence level. The KS-test verifies if the sample originates from the fitted distribution for the specified confidence level by comparing the distance between the empirical and fitted distribution. If no proper fit would be obtained, different types of distributions and verification methods could be considered.

Welch's test can be used to indicate whether the separated failure mechanisms indeed are from two different distributions. For both failure mechanisms the fitted distributions may result in safety factors for a given reliability level, $\alpha = 0.8$ and $\beta = 3.8$ for a 50 year lifetime.

3.5. Comparison with Existing Models

The proposed model, based on the ductility index, will be compared to existing reliability models to underline its performance in terms of accuracy and robustness. The benchmarks will be analysed with the methods PRF,GRF and ECOV. The respective performances are quantified by the mean and coefficient of variation of the model uncertainty. Robustness is difficult to quantify, but comments are made whether the methods dysfunction as failure modes are predicted incorrectly.

3.6. Non-Parametric Bayesian Network

A NPBN is a powerful tool that enables fast computation of conditional probabilities given specification of input parameters. The standalone multivariate NPBN was constructed in *Uninet*[3]. An user-friendly interface enables clear visualisation of the variables and relations. Only the Gaussian copula is available, such that it needs to be validated whether the data can be represented by the Gaussian copula. The most important parameters were included in the model. The dependence between variables was based on physical logic. The parameters of concrete, reinforcement and geometry were assumed independent, but were all related to the output of maximum load and ductility index.

To validate the NPBN, a *Matlab*[4] toolbox was used. The model can be validated through comparing the empirical data, empirical normal data and the simulated Bayesian network data. The validation could be performed based on the determinants of the respective correlation matrices, but this is known to be a sensitive indicator. (Hanea et al.)[28] Instead, the model can be validated based on a calibration distance score, d-Cal. No clear consensus exists about the magnitude of the calibration for validation, but generally a larger value implies a better model.

The model will also be tested to a random selection of input parameters that are captured within the data-set. Three virtual beams could indicate if the order of magnitude of the standalone NPBN agrees with the numerical output by NLFEA.

[3]Uninet: Software used for constructing NPBN
[4]Matlab: used for validation of NPBN by toolbox BANSHEE

4 | Latin Hypercube Sampling

In this chapter the sampling strategy is described. First, the marginal distributions of the material properties are described. Secondly, correlation between certain variables is described by means of a correlation matrix. The optimised Latin hypercube sampling strategy is applied and explained in detail, including the Python script in Appendix B. The sampling strategy includes transformations from the uniform to log-normal samples, and correlation is included by a Cholesky decomposition with the correlation matrix. A sample size of $N = 20$ per benchmark with combinations of nine material parameters was attained. The types of distributions and correlation matrices are taken from probabilistic code Graubner and Brehm [10]. The distribution for concrete fracture energy was taken from Strauss et al. [11].

4.1. Marginal Distributions

In literature, resistance parameters are found to be well described by normal or log-normal distributions. The mean input values are used from the selected benchmarks when possible. However, not all parameters were tested and therefore also not specified. For concrete, often cubic compressive tests were performed from which only the mean concrete compressive strength was measured. For reinforcement testing was also limited, and often only the yield strength was specified. The mean input for other concrete parameters were then derived from the mean concrete compressive strength and reinforcement yield strength (f_{cm} and f_y) as shown in Table 4.1.

Table 4.1: Design formula's for mean input variables of concrete and reinforcement. (*fib* Model Code 2010)[2]

Parameter	Formula	Condition
Concrete characteristic compressive strength	f_{ck}	
Concrete mean compressive strength	$f_{cm} = f_{ck} + 8$	
Concrete mean tensile strength	$f_{ctm} = \begin{cases} 0.30 f_{ck}^{2/3} \\ 2.12 \ln(1 + f_{cm}/10) \end{cases}$	for CC $\leq$ C50 for CC $>$ C50
Concrete Young's modulus	$E_c = 21{,}500(f_{cm}/10)^{1/3}$	
Concrete Poisson ratio	$\nu_c = 0.20$	
Concrete fracture energy	$G_f = 73 f_{cm}^{0.18}$	
Concrete compressive fracture energy	$G_c = 250 G_f$	
Reinforcement yield strength	f_y	
Reinforcement ultimate strength	f_u	
Steel Young's modulus	E_s	
Steel Poisson ratio	$\nu_s = 0.3$	
Steel ultimate strain	$\varepsilon_{su} = 25‰$	

The marginal distributions of the material parameters are specified in Table 4.2. The coefficient of variation (CoV) is specified and shall not be mistaken as the covariance (COV). The coefficient of variation is related to the standard deviation σ and mean value μ as:

$$CoV = \frac{\sigma}{\mu} \, (\times 100\%) \tag{4.1}$$

Table 4.2: Description of the used material parameters with their marginal distributions. (Graubner and Brehm, Strauss et al.)[10,11]

Parameter description	Symbol	Distribution	Mean	CoV
Concrete				
Compressive mean strength	f_{cm}	LN	1.0	0.06
Tensile mean strength	f_{ctm}	LN	1.0	0.30
Elasticity modulus	E_c	LN	1.0	0.15
Fracture energy	G_f	LN	1.0	0.20
Reinforcement				
Yield strength	f_y	LN	$f_{ysp}\alpha \exp(-uv) * C$	0.07
Ultimate strength	f_u	LN	$B * E[f_u]$	0.04
Elasticity modulus	E_s	LN	E_{sp}	0.03
Poisson ratio	ν_s	LN	ν_{sp}	0.03
Ultimate strain	ε_{su}	LN	ε_{usp}	0.06

where

α = 1.0, spatial position factor
u = ∈ [-1.5; -2.0], factor for distance between nominal and mean value
C = 20 MPa, reduction difference yield strength mill test and static
B = 1.5 for structural carbon steel

The used coefficients of variation are relatively large as they account for a broad type of concrete mixture and reinforcing steel. Significant reductions on the coefficients of variation can be obtained if specific types of concrete and reinforcement are known. For example, in Strauss et al.[11] a maximum coefficient of variation for concrete tensile strength of 16.8% was found instead of the applied 30% from Graubner and Brehm[10].

4.2. Correlated Variables

Some of the reinforcement parameters are correlated, as are reinforcement yield and ultimate strength (f_y and f_u). The correlation is specified by means of a correlation matrix. The marginal samples are first generated, after which correlation can be added by a Cholesky decomposition. The correlation matrix for reinforcement is specified below for the order of parameters $f_y, f_u, E_s, \nu_s, \varepsilon_s$.

$$R = \begin{bmatrix} 1 & 0.75 & 0 & 0 & -0.45 \\ & 1 & 0 & 0 & -0.60 \\ & & 1 & 0 & 0 \\ & & & 1 & 0 \\ & & & & 1 \end{bmatrix} \quad (4.2)$$

The following relation is used to convert the correlation matrix to the covariance matrix:

$$COV(X,Y) = \rho_{XY} * \sigma_X * \sigma_Y \quad (4.3)$$

which can be described in matrix notation as:

$$S = D_\sigma * R * D_\sigma = L * L^T \quad (4.4)$$

where S is the covariance matrix, D is the diagonal matrix of standard deviation and R is the correlation matrix. By applying the Cholesky decomposition, the covariance matrix S can be written as the product of a lower triangular matrix L and the transposed matrix L^T. The desired correlated samples can be obtained by multiplying the Cholesky decomposed lower triangular covariance matrix L with the standard normal sample matrix.

For the concrete parameters no correlation is specified in Graubner and Brehm [10], but the mean values are derived from the concrete mean compressive strength according to Table 4.1. The concrete parameters are not necessarily uncorrelated, but one clear definition is difficult to specify as it is not possible to perform tensile splitting tests and compressive tests on the same specimen. Furthermore, different micro-scale aspects contribute to concrete behaviour. This includes: aggregate mixture, water/cement-ratio, curing conditions, cement type and additives. The aggregate size for example is of large influence on the concrete tensile strength. This is difficult to incorporate due to a lack of information and would result in an excessive analysis. Therefore, the mean concrete parameters were derived from design formula's and their marginal distributions were assumed independent.

4.3. Sampling Procedure

An optimized Latin hypercube sampling strategy has been applied, for which the Python script is attached in Appendix B. Initially, random samples were generated from a uniform distribution $U \sim (0,1)$ with Latin hypercube conditions. Spatial optimisation was applied by 10,000 iterations per subset, as described in subsection 2.3.5. These random samples $X \in [0,1]$ were then transformed to a random normal sample Y_N by the inverse of the normal cumulative distribution function.

$$
\begin{aligned}
Y_N &= F^{-1}(X) \\
F(X;\mu_Y;\sigma_Y) &= \frac{1}{\sigma\sqrt{2\pi}} \int_{-\infty}^{x} \exp\left(\frac{(t-\mu)^2}{2\sigma^2}\right) dt
\end{aligned} \tag{4.5}
$$

The mean value and standard deviation for the normal distribution were converted from the specified log-normal distribution $LN \sim (\mu_Z, \sigma_Z)$ by:

$$
\begin{aligned}
\mu_Y &= \ln\left(\frac{\mu_Z}{\sqrt{\sigma_Z^2 + \mu_Z^2}}\right) \\
\sigma_Y &= \sqrt{\ln\left(1 + \frac{\sigma_Z^2}{\mu_Z^2}\right)}
\end{aligned} \tag{4.6}
$$

The obtained normal distribution is then transformed to the desired log-normal distribution by:

$$
Z_{LN} = \exp(Y_N) \tag{4.7}
$$

An example for this transformation to obtain the uncorrelated concrete parameters f_{cm} and f_{ctm} is shown in Figure 4.1.

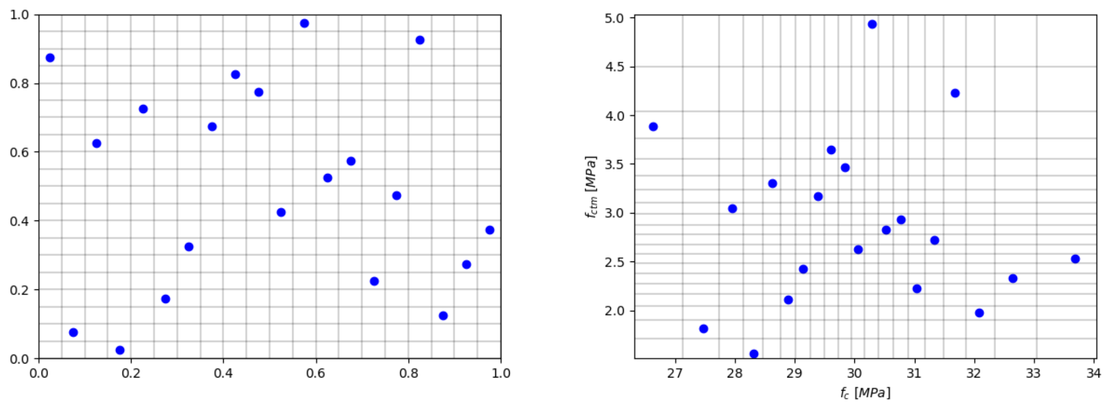

(a) Uniform random samples $U \sim (0,1)$.

(b) Transformed log-normal random samples $LN \sim (\mu_Z, \sigma_Z)$.

Figure 4.1: Transformation of $N = 20$ random uniform samples to random log-normal samples that suffice the marginal distributions of f_{cm} and f_{ctm}.

The reinforcement parameters are sampled in a similar way, but also includes correlation between parameters. An additional transformation by Cholesky decomposition was required. The standard normal random samples were transformed to normal correlated samples, after which they were transformed to the desired correlated log-normal parameters. The correlation matrix of a random sample is depicted in Equation 4.8, which despite some deviations caused by the small sample size ($N = 20$), shows resemblance with the correlation matrix in Equation 4.2.

$$R_{sample} = \begin{bmatrix} 1.00 & 0.76 & 0.05 & 0.24 & -0.41 \\ 0.76 & 1.00 & 0.11 & 0.28 & -0.70 \\ 0.05 & 0.11 & 1.00 & 0.09 & -0.03 \\ 0.24 & 0.28 & 0.09 & 1.00 & 0.09 \\ -0.41 & -0.70 & -0.03 & 0.09 & 1.00 \end{bmatrix} \tag{4.8}$$

The Cholesky decomposition is performed on the standard normal $N \sim (0, 1)$ samples. After which they were transformed to the desired normal distribution with converted mean and sigma $N \sim (\mu_Y, \sigma_Y)$.

$$Y_N = \sigma_Y * X + \mu_Y \tag{4.9}$$

The resulting samples are shown in Figure 4.2. The positive correlated, negative correlated and uncorrelated samples are clearly visible. In these figures, the axes are not transformed.

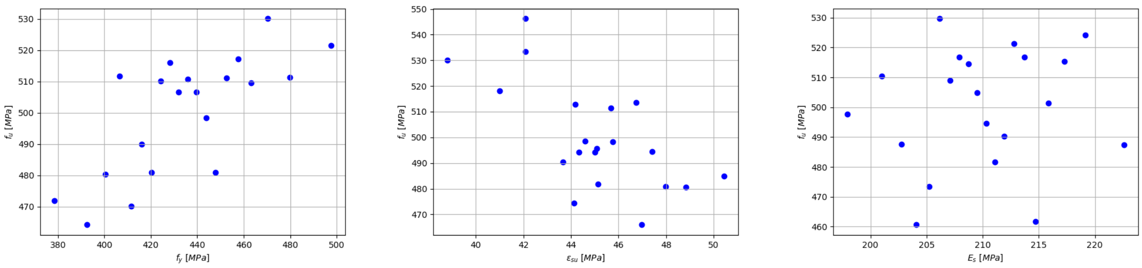

(a) Positive correlated f_y and f_u

(b) Negative correlated ϵ_{su} and f_u

(c) Uncorrelated E_s and f_u

Figure 4.2: Reinforcement samples obtained after Cholesky decomposition to correlated random samples for $N = 20$. In (a) positive correlation of $\rho = 0.75$, in (b) negative correlation of $\rho = -0.60$ and in (c) no correlation.

4.4. Summary

Representative combinations of nine material parameters for concrete and reinforcement were obtained through an optimized Latin hypercube sampling strategy. For each of 48 benchmarks, 20 random combinations of parameters were used, resulting in 960 analysis with 8640 different material parameters.

The distribution types were taken from Graubner and Brehm, Strauss et al. [10,11], and the mean input parameters were derived through design formula's from *fib* Model Code 2010 [2]. Due to unspecified characteristics for concrete and reinforcement types, relatively large coefficients of variation were taken into account. The variation could be reduced significantly if specific material types and their distributions would be used.

The samples were generated on the uniform space with Latin hypercube conditions and spatial optimisation was implemented through an iterative procedure of 10.000 iterations per sampling layer. The uniform samples were transformed to the log-normal marginal distributions of concrete parameters. For reinforcement, the samples were transformed to normal standard variables in advance of the Cholesky decomposition to include correlation. These correlated standard normal samples could then be transformed to the desired log-normal correlated samples.

The optimized Latin hypercube sampling strategy has shown to result in stratified samples which can be used as input for the NLFEA. The statistical properties and marginal distributions of random samples for concrete and the correlated samples for reinforcement are well represented in the samples.

5 | Non-Linear Finite Element Model

In this chapter, a description is given on how the benchmark beams are modelled within NLFEA. First, the geometry and loading conditions of the beams are described including the mechanical schemes for shear and bending. Furthermore, the choices regarding constitutive, kinematic and equilibrium relations are elaborated. At last, the numerical and experimental failure modes are compared by evaluation of crack patterns of the numerical model and by assessment of the ductility index.

5.1. Benchmark Beams

The benchmarks were either tested in one- or two-point loading. Typically, the one-point loading configuration was used for benchmark expected to fail in shear, while the two-point bending was used for benchmarks expected to fail in bending. The four-point bending test exerts a constant bending moment along the mid-span, whereas the three-point bending test exerts a constant shear force over the span. In Figure 5.1, a schematic overview of the benchmark test-set up with dimensions and shear and bending diagrams is displayed. The bending and shear diagrams display the contribution of external loads only, and do not include the effect due to self-weight of the beam. The configuration of shear reinforcement is not displayed as it varied per benchmark. For the full details of benchmarks is referred to Appendix A.

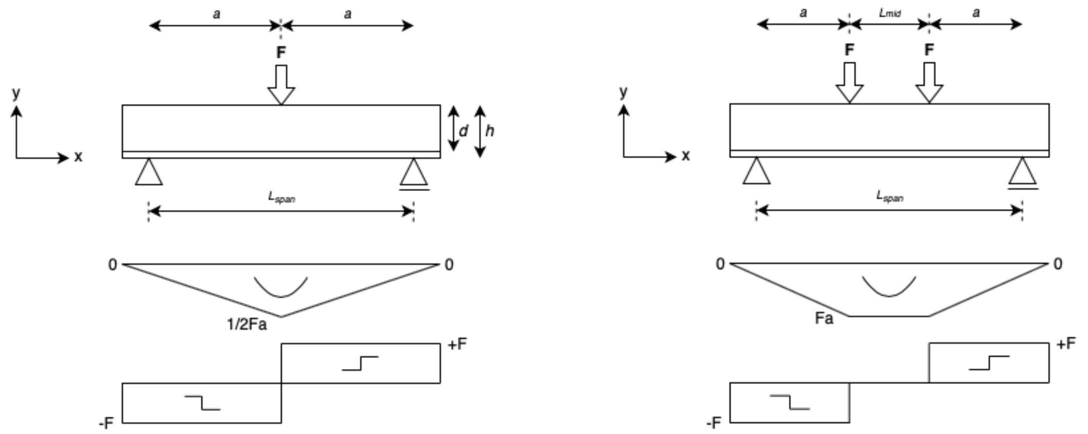

(a) One-point loading.

(b) Two-point loading.

Figure 5.1: Test arrangement with bending moment and shear force diagrams for three- and four-point bending.

The following parameters can be listed as geometry input of the model:

b_w	Beam width	[mm]
h	Beam height	[mm]
d	Beam effective depth	[mm]
a/d	Shear over depth ratio	[-]
ρ_l, ρ_s	Ratio longitudinal/shear reinforcement	[%]
s	Horizontal spacing of web reinforcement	[mm]
A_{plate}	Area loading/support plate	[mm^2]

where

$$\rho = \frac{A}{b_w d} \ (\times 100\%) \tag{5.1}$$

$$A_{plate} = l * w \ \ [mm^2] \tag{5.2}$$

5.2. Modelling Choices

The benchmarks were modelled in a 2D plane in software program Diana. By using a 2D simulation, the needed calculation time can be decreased significantly. Although in 3D the actual problem can be fully replicated, a 2D analysis can give accurate results for the subjected geometries and for the purpose of this research.

Symmetry of the beams was used to further reduce computational time per analysis. Using symmetry at the middle of the beam gives similar results as for analysing the full length of the beam, given that the loading and geometry conditions are perfectly symmetrical. A correct symmetry condition should be put in place. This symmetry condition yields that the horizontal displacement is restricted ($u_h = 0$) and the rotation should be zero ($\phi = 0$). In Figure 5.2, a 2D model of a four-point bending test is displayed with use of symmetry conditions. The beam is vertically supported with a roll support at the left support plate. Horizontal and rotational restriction are imposed by a line support as symmetry conditions at the mid-span of the beam. By reviewing half of the problem, also the applied load should be divided by two.

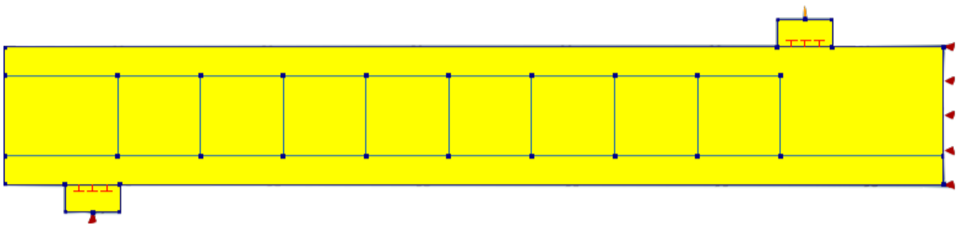

(a) 2D model of four-point bending with symmetry conditions.

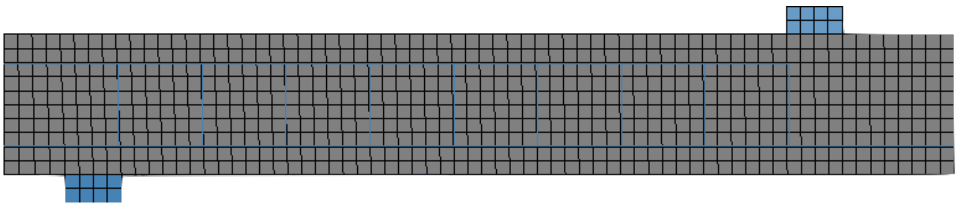

(b) Mesh layout for element size equal to $h/10$.

Figure 5.2: Example of NLFEA model for benchmark B-H2 from Ashour [29].

Modelling choices were kept constant as much as possible to prevent bias in the results. This includes for example the reinforcement and concrete constitutive models, element size $h/10$, convergence norms and maximum number of iterations. A full overview of the used constitutive, kinematic and equilibrium relations is displayed in Table 5.1. The modelling choices were made based on Hendriks et al. [3] as discussed in section 2.2. To enable an automated process for a large sample of analysis, some simplifications were made. These simplifications and limitations are mentioned accordingly.

The reinforcement is modelled as 2D line elements with an equivalent area for weight purposes. Hereby, only axial strains and stresses are taken into account. The effect of transverse strain within the reinforcement, Poisson's effect, is neglected. The reinforcement is assumed to be fully bonded and is embedded within the concrete. The advantage comprises that a detailed anchorage and interfaces for the bond-slip behaviour between reinforcement and concrete do not need to be modelled. As a consequence, the transfer of stresses between the reinforcement and concrete is idealised, which could induce a slight overestimation of the actual strength.

Information about the support and loading plates was not always specified. For some benchmarks, the dimensions were assumed to be equal to the beam width and a length of 150 millimeters if unspecified in the research. The loading and support plates were modelled as linear elastic stiff elements to redistribute the stresses from the applied point load and point support to the concrete. The connection between the plates and concrete was modelled by an interface that contained a high normal stiffness with respect to the local axis to transfer the vertical stresses. A low shear stiffness was used to avoid the plates from contributing to the stiffness of the beam, which could yield a higher overall strength.

For uncracked concrete, a constant Poisson's ratio equal to $\nu_c = 0.20$ was assumed. For higher concrete strengths (CC ≥ 50), Poisson's ratio could typically reduce to $\nu_c = 0.10 - 0.15$. This can be regarded a conservative assumption as the tensile transverse strain and stresses for high concrete class may be overestimated, which causes concrete cracking and ultimately failure. For cracked concrete, a Poisson's ratio of zero is applied amidst the softening behaviour. Furthermore, constant values for the specific weights of concrete and reinforcement were assumed constant as ρ_c = 2400 kg/m^3 and ρ_s = 7800 kg/m^3. A full example of the Python script used to perform the NLFEA in Diana 10.4 is attached in Appendix B.

5.2.1. Load-Step & Convergence

Displacement-controlled loading was used for the analysis, similar to the testing procedure of most benchmarks. The load-step is inserted as $xx(yy)$, where xx represents the magnitude of the displacement per step, and yy is the total number of loading steps to be performed. Per step, a maximum number of iterations was set equal to 40 to avoid excessive iterations and time consumption. This may lead to non-converged steps, which is not an issue as long as convergence is reached for critical load-steps. A check is performed in Python to see the status of the three steps before and after the maximum load. In case of converged results near the maximum load, the resulting maximum load was accepted. If non-convergence occurred, a smaller increment with a larger total of load-steps was selected to redo the analysis. The non-convergence can be explained by the fact that the maximum load often comes with a deflection of the load-displacement curve due to concrete cracking, which takes additional effort to find equilibrium for. At the sime time, an optimal load-step and maximum number of iterations are desired to limit the computational time. The applied load-steps per beam are displayed in section C.1.

Table 5.1: The applied solution strategy including constitutive models, kinematic assumptions, equilibrium conditions and interfaces.

Concrete Constitutive Model	
Material model	Total strain crack model
Crack orientation	Rotating
Element type	Quadratic (CQ16M)
Tensile curve	Hordijk
Crack bandwidth	Govindjee
Tensile reduction model	Damage based
Minimum reduction factor	β_{cr} = 0.4
Residual tensile strength	0 MPa
Compression curve	Parabolic
Compression reduction model	Vecchio and Collins (1993)
Residual compressive strength	0 MPa
Confinement model	Selby and Vecchio
Density	2400 kg/m^3
Reinforcement Constitutive Model	
Material model	Von Mises plasticity
Bond type	Embedded
Material model	Elasto-plastic with hardening
Element type	Truss element
Density	7800 kg/m^3
Kinematic Compatibility	
Element class	Regular plane stress
Integration scheme	Gaussian 3x3
Mesh order	Quadratic
Mid-side node location	Linear interpolation
Element size	$h/10$
Aspect ratio	1:1 (where possible)
Equilibrium Conditions	
Type	Displacement-controlled
Load-step	Variable
Analysis control	Arc-length + line search
Iteration scheme	Full Newton-Raphson
Energy norm	0.0001
Force norm	0.01
Max. iteration	40
Interfaces	
Element type	Linear elastic
Element type	2D line (CL12I)
Integration scheme	4 point Newton-Cotes
Interpolation type	Quadratic
Shear stiffness	30000 N/mm^3
Normal stiffness	30 N/mm^3

5.3. Numerical Output

The numerical output to determine the model uncertainty and failure mode is retrieved as the maximum external load and the ductility index. Other parameters like the displacement, crack widths, strains and stresses are also logged, but only used for indirect analysis.

P_u	Ultimate load (ULS)	[kN]
χ	Ductility index	[-]

The mean numerical load and the experimental maximum load are displayed in Figure 5.3. The brittle (red) and ductile (blue) failure mechanisms are objectively determined by the ductility index boundary $\chi = 0.6$. Results above the black dotted line indicate a numerical overestimation, and beneath indicates underestimation. The gray shaded area indicates 20% over- or underprediction. It can be observed that the ductile failure mechanism is estimated with higher accuracy, but in some cases also over-predicts the ultimate limit state capacity. The mean model uncertainty and coefficient of variation for the 48 benchmarks can be expressed as $\mu_\theta = 1.16$ and $CoV = 0.144$.

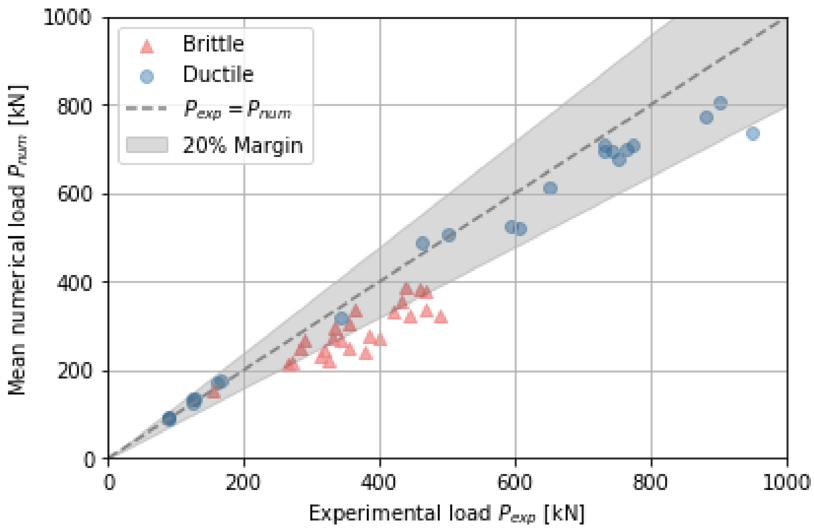

Figure 5.3: Mean numerical load displayed against the experimental load for 48 benchmarks. Markers under the dotted line represent numerical underestimation, and above indicate overestimation.

5.3.1. Model Uncertainty & Ductility Index

The model uncertainty is a measure for the accuracy of the numerical resistance with respect to the experimental resistance. The ductility index is formulated as the ratio of the plastic dissipated energy in the reinforcement over the total dissipated energy in the system, as rephrased in Equation 5.3.

$$\theta = \frac{R_{exp}}{R_{num}} \quad ; \quad \chi = \frac{W_{steel}}{W_{system}} \tag{5.3}$$

The ductility index can be logged in the output file. Logging can be activated by *'Analysis/Logging'* → *'Add energy'*. The output files were then used to retrieve the ductility index per load-step and were selected at the load-step where the maximum load occurred. A validation for the implementation of the ductility index in Diana was performed by de Putter[7].

The ductility index was retrieved at the maximum load-step, but it can be argued whether it should be derived some load-step(s) behind the maximum load as the beam would then have truly failed. However, in case of a brittle failure mode the concrete fails and the reinforcement plastic energy would increase, which then could indicate an erroneous ductile failure mode. In case of a ductile failure, the opposite would occur and a wrong brittle failure mechanism could be assigned. The derivative of the ductility index shows agreement with the failure modes, and could be used as indicator of the failure mode by the relative change of the ductility index between the maximum load-step and some load-step(s) afterwards. This relation is further discussed and displayed in section C.2.

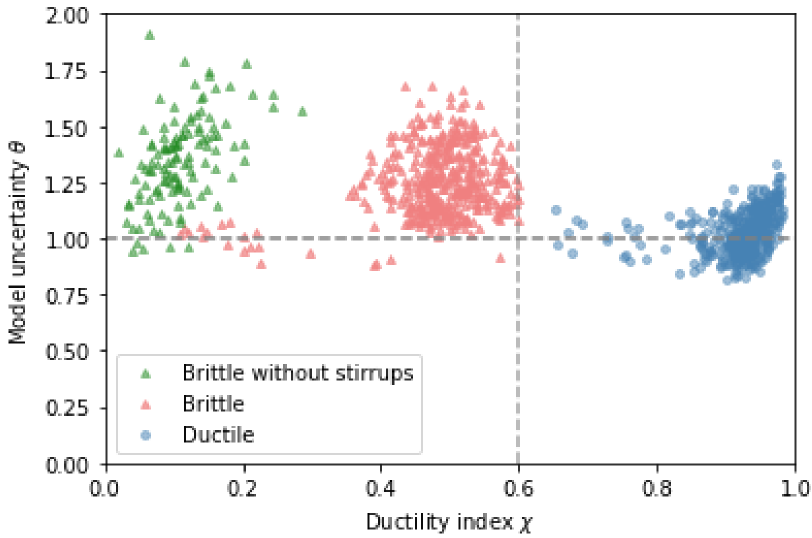

Figure 5.4: Scatter plot of the model uncertainty against the ductility index for 960 analysis. Ductile and brittle failure modes are distinguished by ductility index boundary $\chi = 0.6$.

In Figure 5.4, a scatter plot of the model uncertainty against the ductility index for 960 samples is shown. The proposed boundary of $\chi = 0.6$ is used as distinction between a ductile and brittle failure mode. Furthermore, a distinction is made for beams without shear reinforcement (green). From the graph, an higher model uncertainty and variance can be observed for the brittle failure mechanism (red&green). Generally, the brittle failure mechanism is more difficult to predict, and as concrete failure is the main cause of brittle failure, the larger variance can be explained by the heterogeneity of concrete and accompanying larger coefficients of variation. The ductile failure mechanism (blue) shows a much smaller variance and higher accuracy, although the resistance is also overestimated more often.

5.3.2. Ductility Index Boundary

The numerical failure mode can be determined subjectively by evaluating the crack patterns, stresses within the reinforcement and the deformed state. Beside, the ductility index can be used as an objective measure for the failure mode. A comparison between the subjective visual failure mode based on the deformed finite element model and the objective failure mode based on the ductility index is given below. Separate sections were appointed for which random selected samples were visually inspected.

A first distinction can be observed for $\boldsymbol{\chi \leq 0.3}$. Most of these results can be explained by the layout of the beams as they do not contain shear reinforcement. This includes beams numbers: 20,21,22,30,31 and 32 (green). The variance is slightly larger and the model uncertainty higher, which can be supported by findings from de Putter [7] that a fixed crack model might be more suitable for beams without shear reinforcement. The typical failure mechanism observed is a diagonal shear failure, as shown in Figure 5.5, where $\chi = 0.13$. One exception involves beam index 8: This beam can be appointed as an over-reinforced beam with a very high concrete strength. The low ductility index may have been caused by discretization problems near the loading plate, as relatively large elements accompanied with a small concrete compressive zone could have induced a spike in the plastic dissipated energy by the concrete. It was found later that this issue could be resolved by a smaller element size ($h/20$).

Secondly, the brittle failure mechanism for $\boldsymbol{0.3 < \chi \leq 0.6}$ is reviewed. The crack pattern for the brittle failure mode is displayed in Figure 5.6. Several diagonal shear cracks have developed between the

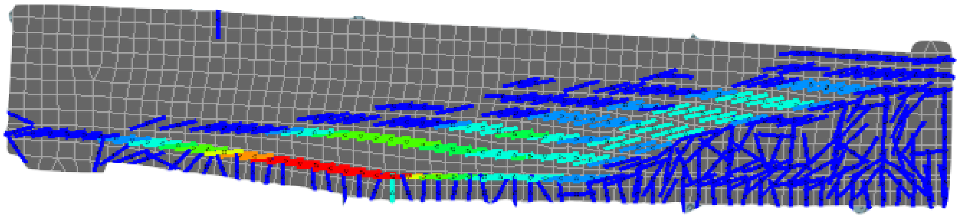

Figure 5.5: Crack strain for beam index 20 (BS-OA3) without shear reinforcement and $\chi = 0.13$, showing diagonal shear failure.

shear reinforcement. The concrete strength is too low to absorb the transverse tensile stresses in the concrete compressive struts. Although it is appointed as a brittle failure mode, warnings before failure are given by crack development along the shear reinforcement.

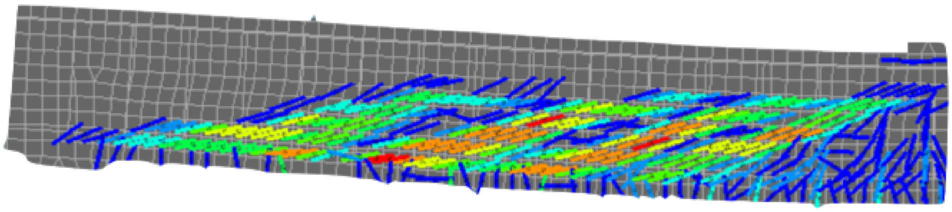

Figure 5.6: Crack strain for beam index 17 (BS-C3) with shear reinforcement and $\chi = 0.50$, showing diagonal shear failure.

A visual inspection for failure mechanisms between $\mathbf{0.60 < \chi \leq 0.65}$ is performed to substantiate the correctness of the failure mode boundary. Especially from an engineering point of view, it is undesirable to overlook a brittle failure mechanism as this could lead to sudden failure. In Figure 5.7, the deformed model and crack strains are displayed at the maximum load in (a) and one load-step afterwards in (b). A brittle diagonal shear failure can be observed, while the ductility index varies from $\chi = 0.647$ at the maximum load to $\chi = 0.590$ at one load-step afterwards. The reinforcement had not reached the yield strength. In Table 5.2 other benchmarks are evaluated to further investigate the failure modes. From the observations, brittle failure mechanisms would still occur up till $\chi = 0.652$, indicating that a higher boundary could be more appropriate. Some contradicting results are obtained as a ductile failure mode was observed for $\chi = 0.656$ and brittle again for $\chi = 0.670$. The numerical observed failure modes indicate a boundary between $\mathbf{0.65 < \chi \leq 0.67}$, which is higher than proposed by Engen et al. [5]. A better definition of the ductility index boundary might be obtained by distinction of the longitudinal and shear reinforcement, or by evaluating the relative change of the ductility index after occurrence of the maximum load.

Table 5.2: Visual inspected failure mechanisms for benchmarks with a ductility index between $0.60 \leq \chi \leq 0.68$.

Sample id.	χ	Visual Failure Mechanism
41_18	0.631	Brittle, diagonal shear failure
36_18	0.633	Brittle, diagonal shear failure
8_7	0.638	Quasi-brittle, concrete crushing
36_5	0.647	Quasi-brittle, concrete crushing
44_16	0.652	Brittle, diagonal shear failure
5_0	0.656	Ductile, yielding reinforcement
40_13	0.670	Brittle, diagonal shear failure
8_17	0.676	Ductile, yielding reinforcement

At last, a ductile failure mode is shown in Figure 5.8 for $\boldsymbol{X > 0.65}$. Flexural cracks can be observed and

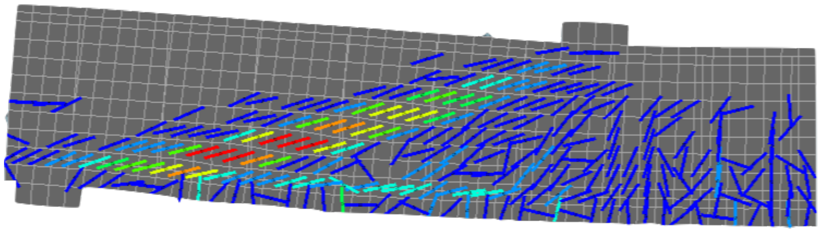

(a) At the maximum load. (χ = 0.647)

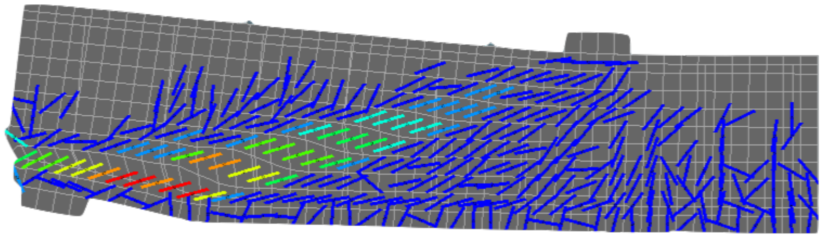

(b) At one load-step behind maximum load. (χ = 0.590)

Figure 5.7: Crack strain for beam index 36 (B311) with shear reinforcement, showing diagonal shear failure.

the reinforcement yields till its ultimate strength is reached and failure occurs. The ductility index at the maximum load equals $\chi = 0.94$.

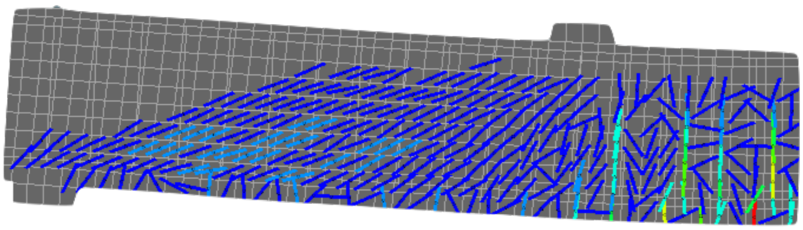

Figure 5.8: Crack strain for beam index 37 (B312) with shear reinforcement and χ = 0.94, showing flexural tension failure.

5.3.3. Failure Mode Prediction

An important aspect of the analysis is whether the experimental failure mechanism is captured by the numerical predicted failure mode. A comparison of the objective numerical failure mode and experimental failure mode is given in Table 5.3. A distinction was made based on the brittle or ductile failure mode for $\chi = 0.6$. Furthermore, the numerical load-displacement curve is compared to the available experimental load-displacement curves in section C.3, as this also could be used as indication to whether the numerical model describes the experimental behaviour properly.

Some deviations of the predicted failure mode may occur as material uncertainties could lead to a different failure mode than the one observed experimentally. As the total space for material uncertainties was used as input, the actual failure mode should be observed ate least once in the predicted failure modes.

From Table 5.3, it can be observed that the majority of predicted failure modes agree with the experimental failure mode. All samples do capture the correct failure mode within the 20 samples at least once. Three beams however, can be appointed to have an excess of the wrong failure mode. This

Table 5.3: Comparison of experimental failure mode with the numerical failure modes based on $\chi = 0.6$.

# Beam	Ductile	Brittle	Experimental	# Beam	Ductile	Brittle	Experimental
0	20	0	Ductile	24	0	20	Brittle
1	20	0	Ductile	25	0	20	Brittle
2	20	0	Ductile	26	0	20	Brittle
3	20	0	Ductile	27	0	20	Brittle
4	20	0	Ductile	28	0	20	Brittle
5	18	2	Ductile	29	1	19	Brittle
6	20	0	Ductile	30	0	20	Brittle
7	16	4	Ductile	31	0	20	Brittle
8	6	14	Ductile	32	0	20	Brittle
9	0	20	Brittle	33	20	0	Ductile
10	0	20	Brittle	34	20	0	Ductile
11	0	20	Brittle	35	20	0	Ductile
12	0	20	Brittle	36	18	2	Ductile
13	0	20	Brittle	37	20	0	Ductile
14	0	20	Brittle	38	20	0	Ductile
15	0	20	Brittle	39	20	0	Ductile
16	0	20	Brittle	40	20	0	Ductile
17	0	20	Brittle	41	3	17	Ductile
18	0	20	Brittle	42	20	0	Ductile
19	0	20	Brittle	43	20	0	Ductile
20	0	20	Brittle	44	15	5	Ductile
21	0	20	Brittle	45	5	15	Ductile
22	0	20	Brittle	46	20	0	Ductile
23	0	20	Brittle	47	20	0	Ductile

holds for beam index 8, 41 and 45. For all three, most numerical failure modes were categorised as brittle while a ductile failure mode was expected. Furthermore, it can be seen that for the brittle failure modes (beams 9-32) almost all numerical failure modes correspond to the experimental brittle failure mode, except one for beam 29. For the beams failing in a ductile manner, the number of correct predicted failure modes was much lower. (beams 0-9 and 33-47)

In total 54 shear failures were predicted where ductile failure mechanisms were expected. On the opposite, only one ductile failure mode was predicted where experimental shear failure occurred. A correct prediction of 94.3% was obtained for $\chi = 0.6$. The boundary of $\chi = 0.65$ better agreed with the numerical observed failure mode as discussed in subsection 5.3.2, but it would result in a decrease of the correct predicted experimental failure mode to 91.8%. Therefore, the boundary of $\chi = 0.6$ was maintained.

Several explanations are possible for the excess of wrong predicted ductile failure modes. As can be seen from Figure 5.4, the brittle failure mechanisms shows on average an higher model uncertainty and a larger variance. This is caused by the difficulty of shear failure prediction, as different crack patterns can occur for which new equilibrium must be found with stress concentrations near crack tips. In contrary, the assumption of fully bonded reinforcement yields an higher model uncertainty and overestimates the resistance more often. As a consequence, a numerical shear failure may be predicted while a brittle experimental failure was observed.

The configuration of the benchmarks also affects the prediction of the numerical failure mode for the different input parameters. The larger coefficients of variation for concrete might impose a larger variety in failure modes. Furthermore, the implementation of a higher boundary of $\chi = 0.65$ did not improve the accuracy of the predicted failure modes. The systematic underestimation of shear capacity enhances a wrong prediction of the numerical failure mode. This effect is deteriorated for a higher boundary, even though this boundary better agrees with the visual observed numerical failure mode. On the contrary, the experimental failure mode prediction would improve for a lower ductility index boundary towards $\chi = 0.55$. As these are two contradicting values for the ductility index boundary, the original boundary of $\chi = 0.6$ was maintained, given that awareness should be paid for the failure mode in case of a ductility index between $0.55 \leq \chi \leq 0.65$.

5.3.4. Relation Geometry and Model Uncertainty

The effect of the main geometric input variables on the model uncertainty is investigated to establish statements on the usability related to beams of different size. Concrete is a heterogeneous composite for which larger size structures show a relative strength reduction due to the increased chance of imperfections, known as size effect. Dimensions of a structure and even the maximum aggregate size are known to affect the relative strength. (Bazant and Planas)[30] No explicit reduction of strength is included in NLFEA for this size effect, while it is included in the design formula for shear resistance in Equation 2.7. In NLFEA, the fracture energy is defined as the energy needed to form cracks per unit area, but this does not necessarily translate to the size of a structure. Therefore, it is investigated whether the model uncertainty shows correlation to the main geometric parameters.

In Figure 5.9, the mean model uncertainty for 48 benchmarks is displayed relative to six relevant geometric parameters: shear span over depth ratio, span length, effective depth, stirrups diameter, beam width and longitudinal reinforcement ratio. A distinction is made between beams with and without shear reinforcement, as it was observed in subsection 5.3.1 that the mean model uncertainty and variance for beams without shear reinforcement is much larger. The six beams without shear reinforcement are indicated with blue markers and the remaining 42 beams with shear reinforcement with black markers. For each geometric input variable the observed and expected relations are commented on accordingly.

- a/d: A slender beam is more likely to fail in a flexural ductile manner. Therefore, the shear span over depth ratio is expected to have a negative effect on the model uncertainty. For the current benchmarks, this trend is not clearly visible even if the blue samples are disregarded.
- L_{span}: An increased span length could induce a bending failure if the beams become relatively more slender. The model uncertainty would than be expected to decrease for an increasing span length. However, if the height increases in a similar extent, a size effect in the real experiment could lead to a higher model uncertainty.
- d: If the effective depth increases, the beam is more likely to fail in shear. A shear failure is associated with a higher model uncertainty which is clearly visible within the data.
- s_d: A clear distinction of a higher model uncertainty for the blue samples without shear reinforcement is visible, in line with findings from subsection 5.3.1.
- b_w: As the benchmarks are modelled in a 2D plane, the beam width is not expected to affect the model uncertainty. It can be observed that no clear relation is present within the data-set.
- ρ_l: The longitudinal reinforcement ratio is a measure for the strength of the reinforcement relative to the concrete. For an increased reinforcement ratio, the concrete depth should decrease or the amount of reinforcement should increase. Both are expected to have a negative relation on the model uncertainty as is also observed in the data.

Based on the previous observations, no concise relations for all geometry parameters and the model uncertainty could be appointed. However, it is noted that the obtained results should not be straightforward applied to beams that exceed the size of those evaluated in this research. The model uncertainty increases with the effective depth, which could be enlarged for deep beams. Furthermore, it may be more appropriate to model beams without shear reinforcement with a fixed crack model instead of a rotating crack model, because the variance and model uncertainty are found to be relatively large. (de Putter)[7] Additional safety factors or experiments should be considered for beams of higher depths, hence, deep beams.

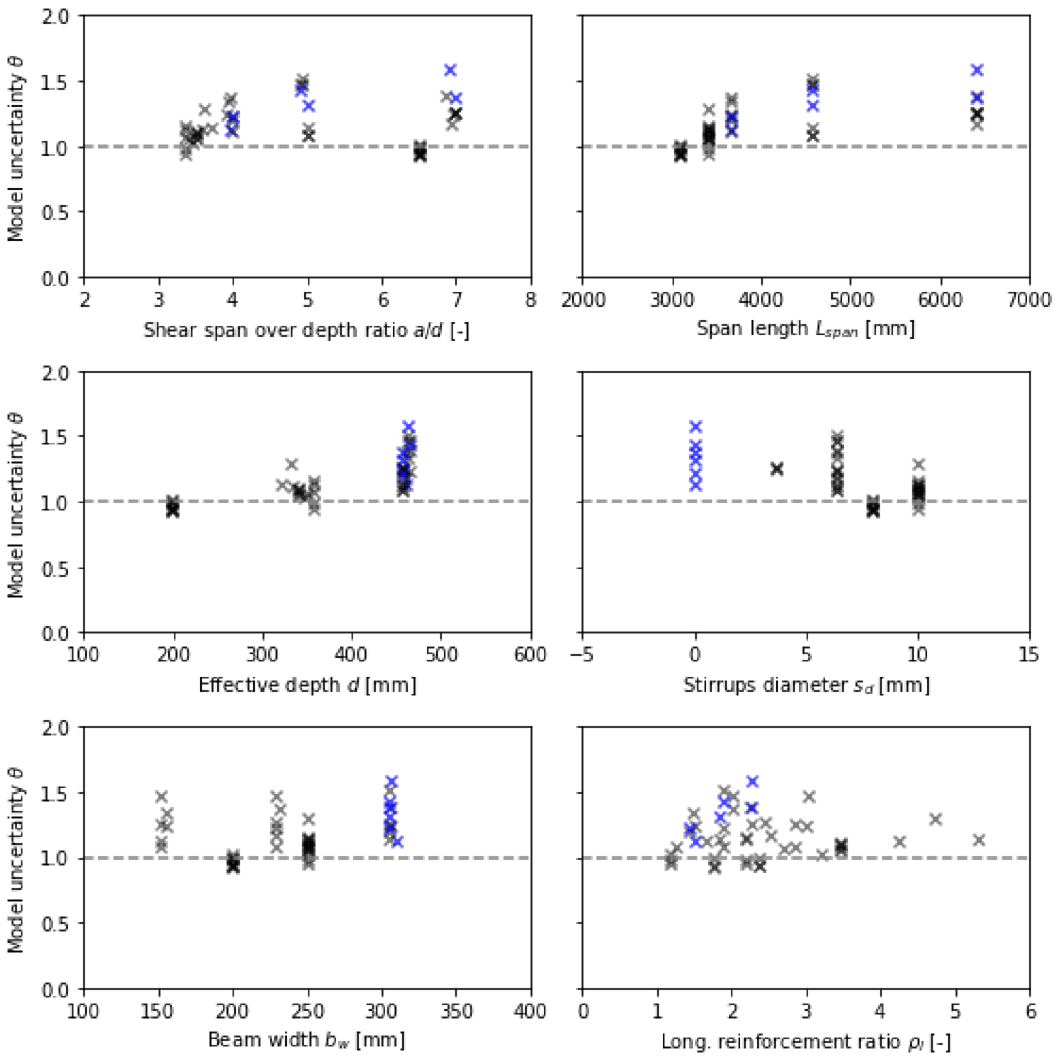

Figure 5.9: Relation between mean model uncertaintiy and six geometry parameters.

5.4. Summary

In this chapter, the modelling choices and initial results on the model uncertainty and ductility index have been described. For the 48 benchmarks, the mean model uncertainty and coefficient of variation could be described as $\mu_\theta = 1.16$ and $CoV = 0.144$. However, distinction based on the ductility index showed that for the brittle failure mode a higher variance and model uncertainty are observed than for the ductile failure mode. By dividing failure modes based on ductility index, a better description of both distributions may be acquired.

The correctness of defining the ductility index at the maximum load with the proposed boundary of $\chi = 0.6$ has been thoroughly investigated. It was observed that the numerical failure mode better agreed with a boundary of $\chi = 0.65$. However, shifting of the boundary did not improve the prediction of the numerical failure mode with respect to the experimental failure mode. Under this consideration, the boundary of $\chi = 0.6$ was found valid for practical use. By defining the ductility at the maximum load, a correct prediction of 94.3% was achieved. It was noted that most of incorrect failure mode predictions were caused by a systematic underestimation of the shear capacity. Random samples were checked to evaluate whether different failure mechanisms could be captured for different ranges of the ductility index, but no clear tendency was observed.

The effect of the main geometry parameters on the model uncertainty was evaluated. Not for all parameters clear relations could be appointed. However, two clear relations could be observed: 1) For a larger effective depth, the model uncertainty increased accompanied with a higher variance and 2) The model uncertainty and variance reduced for beams with shear reinforcement. This indicates that the derived model should not straightforward be applied to beams of larger depth, hence, deep beams. The beams without shear reinforcement exerted a relatively high model uncertainty and variance, which consents with findings from de Putter [7] that a fixed crack model may be more appropriate to estimate the ultimate limit state for beams without shear reinforcement.

In Appendix C the ductility index was displayed as a function of the load-step and the change of ductility index was analysed. The relative change of the ductility index between the maximum load and one step afterwards showed agreement with the expected failure mode. The relative change of the ductility index could be a good measure to define whether the numerical model exerted a ductile or brittle failure, but also depends on the used load-step. Furthermore, the numerical load-displacement curves were compared to the experimental load-displacement curves. The ductile numerical failure mode almost exactly replicated the experimental load-displacement curve. The brittle numerical failure showed premature failure and did not replicate the load-displacement curve as good. Especially the beams without shear reinforcement differentiated substantially, underpinning earlier statements about an underestimation of shear capacity and an incorrect crack model for beams without shear reinforcement.

6 | Probabilistic Analysis

In this chapter, a univariate probabilistic analysis is performed by distribution fitting. Safety factors are derived and a sensitivity analysis is performed. The model uncertainty is quantified for brittle and ductile failure modes based on the ductility index, from which a reliability model is defined. Initially, the total data is reviewed and thereafter the separated data based on the ductility index boundary $\chi = 0.6$.

The results on the model uncertainty of 48 benchmarks with a sample size of $N = 20$ per beam are displayed in Figure 6.1. The mean model uncertainty is displayed with a bandwidth for the minimum and maximum observed model uncertainties. Values above one indicate underestimation and below one overestimate the experimental maximum load. Ductile failure was typically observed for beams 0-8 and 33-47 (light-gray), whereas brittle failure was observed for beams 9-32 (dark-gray).

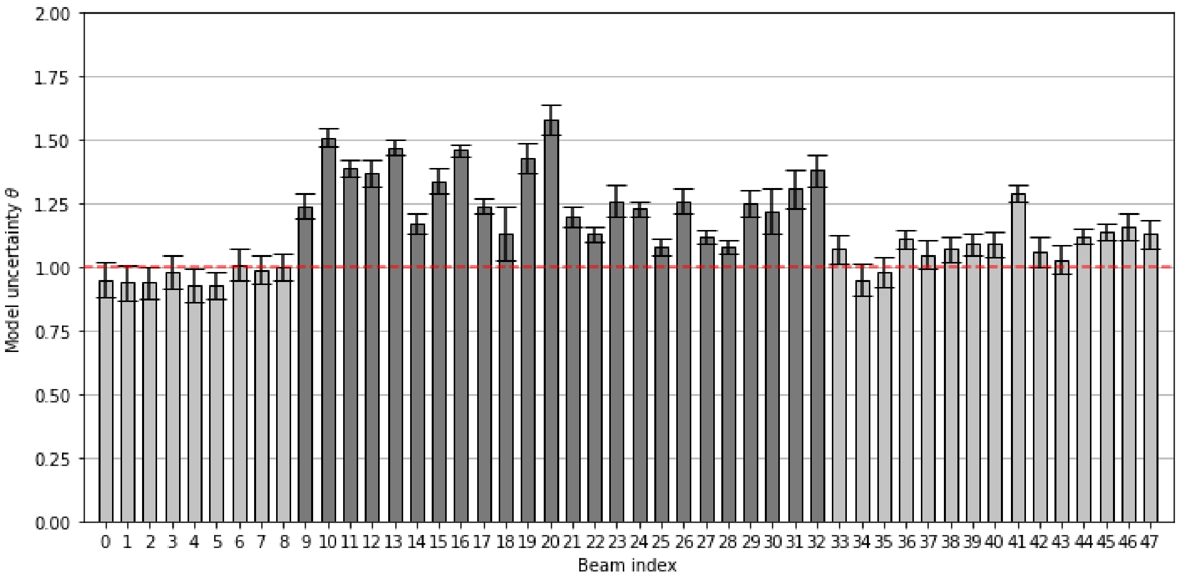

Figure 6.1: Histogram displaying the mean model uncertainty for 48 beams with 20 samples per beam. The range of the minimum and maximum observed model uncertainty is displayed by the error bars. Beams failing in bending are displayed in light-gray, and shear beams in dark-gray.

6.1. Combined Design Resistance

The probability density functions for brittle and ductile are displayed together in Figure 6.2. The two colors indicate the difference based on ductility index boundary at $\chi = 0.6$. The brittle data (red) shows a large variance and tends to under predict the design resistance. For the ductile data (blue) a lower variance can be observed with a more accurate mean estimate of the design resistance. The brittle failure mode is typically more difficult to predict as distortions along the beam occur due to crack formation. Furthermore, concrete is a heterogeneous material for which its parameters exhibit larger coefficients of variation.

The total data could be represented by a log-normal distribution, but that would imply a very large standard deviation. Therefore, a two-sided statistical Welch's t-test is performed to test the hypothesis that both populations have the same mean, and therefore originate from the same distribution. It is more robust than student's t-test, because Welch's t-test can be applied to samples of unequal size

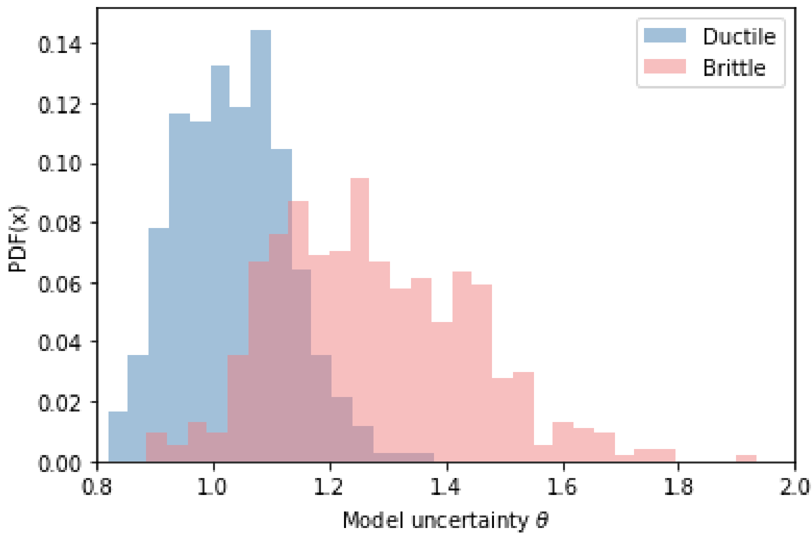

Figure 6.2: Probability density functions of the model uncertainty of both the ductile and brittle failure mode. Separation based on ductility index boundary $\chi = 0.6$.

and unequal variance. Welch's test preliminary assumes that the data is independent, approximately normal distributed and does not contain significant outliers, which are all satisfied.

$$t\text{-statistic} = 27.97996387433144$$
$$p\text{-value} = 1.0698007222820207e - 123$$

The p-value rejects the null-hypothesis against a significance level of $\alpha = 5\%$, from which it can be concluded that the means of both groups are significantly different. Therefore, the analysis will further focus on quantifying the model uncertainties for both ductile and brittle failure mechanisms separately. Only for comparative purposes, a normal and log-normal are fitted to the full data as displayed in Table 6.1. From the p-values, obtained by Kolmogorov-Smirnov test, it can be seen that both the normal and log-normal fits are rejected at a 5% significance level for the combined data.

Table 6.1: Normal and log-normal fit to the model uncertainty of the full data-set.

	μ	σ	$. V$	p-value
Normal	1.17	0.18	0.15	4.21e-14
Log-normal	1.15	0.15	0.15	6.19e-03

The parameters for the log-normal distribution do not directly translate to the mean and standard deviation of the variable itself. The relations are given in Equation 6.1 - Equation 6.3.

$$E[X] = \exp\left(\mu + \frac{\sigma^2}{2}\right) \tag{6.1}$$

$$Var(X) = \exp\left(2\mu + \sigma^2\right)\left(\exp\left(\sigma^2\right) - 1\right) \tag{6.2}$$

$$V = \sqrt{e^{\sigma^2} - 1} \tag{6.3}$$

6.2. Bending Design Resistance

As stated before, the brittle and ductile failure mechanisms are statistically rejected to have the same mean value. If the brittle and ductile failure mechanisms are treated separately, a better fit can be obtained. The probability density function (PDF) and cumulative distribution function (CDF) for the ductile failure mode are displayed in Figure 6.3 and Figure 6.4 respectively.

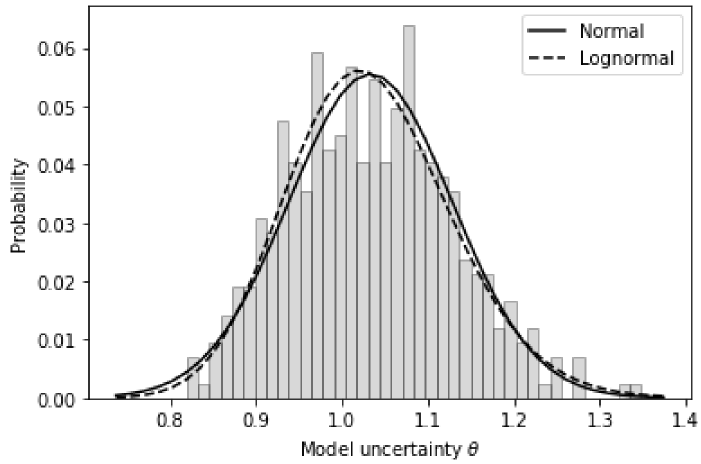

Figure 6.3: Probability density function for ductile failure mode with normal and log-normal fit.

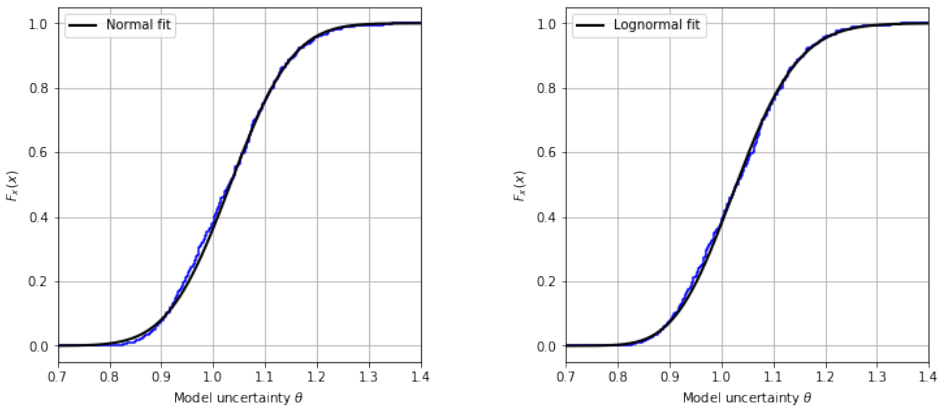

Figure 6.4: Cumulative distribution function for ductile failure mode with normal fit (left) and log-normal fit (right).

From Figure 6.4, it can be observed that the log-normal distributions fits the empirical cumulative distribution function slightly better than the normal distribution. The results for the normal and log-normal fitted parameters are displayed in Table 6.2. The goodness of fit is determined by a Kolmogorov-Smirnov test which is based on a measure of the distance between the empirical data and the fitted distribution. The result is again translated in a p-value which is tested against a 95% confidence level for whether the data could originate from the fitted distribution. Both the normal and log-normal fitted distributions are accepted for the ductile date as $p \geq 0.05$, but the log-normal fit is superior.

Similar results were found in Engen et al., de Putter [5,7], where the ductile model uncertainty was found to be well represented by a log-normal distribution with a mean $\mu_\theta = 1.0/1.045$ and coefficient of variation $V = 0.10/0.10$ respectively. In these research, different benchmarks were used and the model uncertainty was approximated by use of deterministic input parameters. This however, does not guarantee reliability levels as important uncertainties related to material and geometry are not considered.

Table 6.2: Normal and log-normal fit to the model uncertainty of the ductile data.

	μ	σ	V	p-value
Normal	1.03	0.10	0.10	0.065
Log-normal	1.02	0.09	0.09	0.478

(Strauss et al.)[11] In this research, a full probabilistic approach was adapted that took into account material induced uncertainties. To obtain similar results is promising and indicates that a correct approach has been applied.

6.3. Shear Design Resistance

The probability density function (PDF) and cumulative distribution function (CDF) for the brittle failure mechanism are displayed in Figure 6.5 and Figure 6.6. Again, the log-normal distribution seems to fit the data slightly better, although the normal fit performs good as well. The derived parameters for the fitted normal and log-normal distributions are shown in Table 6.3.

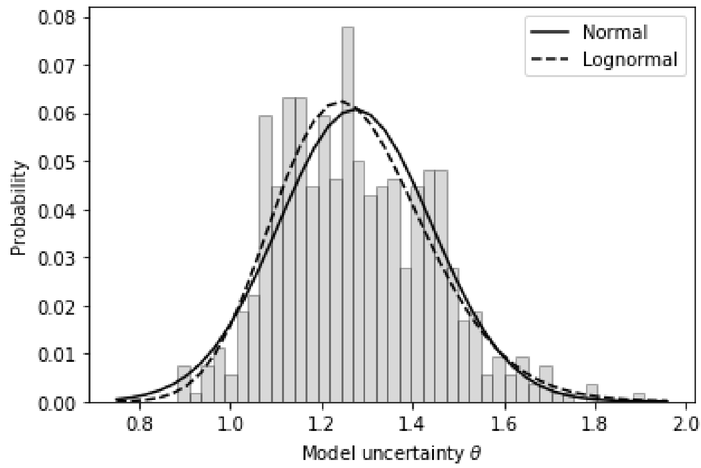

Figure 6.5: Probability density function for brittle failure mode with normal and log-normal fit.

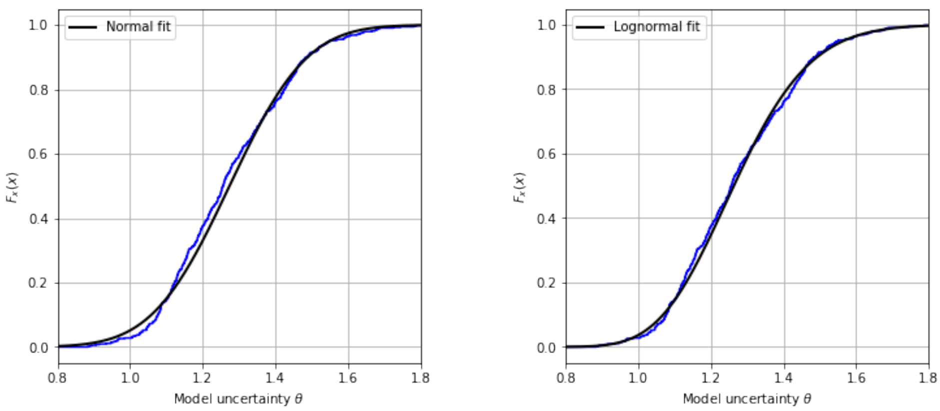

Figure 6.6: Cumulative distribution function for brittle failure mode with normal fit (left) and log-normal fit (right).

Table 6.3: Normal and log-normal fit to the model uncertainty of the brittle data.

	μ	σ	V	p-value
Normal	1.27	0.17	0.13	4.31e-04
Log-normal	1.26	0.13	0.13	0.352

From Table 6.3, the p-values indicate that only the log-normal distribution has a proper fit for a 95% confidence level. The results can be compared to other research from Engen et al., de Putter[5,7], where similar parameters were found for the brittle failure mode: $\mu_\theta = 1.2/1.131$ and $V = 0.15/0.16$. The lower mean value found in de Putter[7] can be explained by the application of a different solution strategy for beams failing in a brittle manner. The most evident difference is that a fixed crack model was applied for beams without shear reinforcement. Furthermore, the six beams without shear reinforcement are also considered within the data and this induces a higher average model uncertainty.

6.4. Proposed Reliability Model per Failure Mode

From the previous sections, parameters for a log-normal distributions were obtained that satisfied the goodness of fit by a Kolmogorov-Smirnov test. These distributions are used to define safety factors for a global reliability model, similar to Global Resistance Factor (GRF). The resistance of both failure modes can be represented by a log-normal distribution, such that the following equations can be used to derive safety factors and define the reliability model.

$$R_d = \frac{R_{num}(f_{cm}, f_{ym}, a_{nom})}{\gamma_R} \tag{6.4}$$

$$\gamma_R = \frac{\exp(\alpha_R \beta V_R)}{\theta_m} \tag{6.5}$$

$$V_R = \sqrt{V_g^2 + V_m^2 + V_f^2} \tag{6.6}$$

where the coefficient of variation accounts for the combined effect of geometry, model, and material related uncertainties. For reasons mentioned in section 1.3, the geometry related uncertainties were not explicitly included in the analysis. EN 1990[15] suggests values for $\alpha_R = 0.8$ and $\beta = 3.8$ for a 50 year design lifetime. This method however, does not consider the amount of samples used. A more extensive approach by Bayes inference could provide more favourable safety factors, since reduction factor for the number of samples is taken into account. (Engen et al.)[5] Following Equation 6.4-Equation 6.6, a reliability method for simply supported reinforced concrete beams is defined as:

$$R_d = \begin{cases} \dfrac{R_{num}(f_{cm}, f_{ym}, a_{nom})}{\gamma_{brittle}} & \chi \leq 0.6\ (brittle) \\[2ex] \dfrac{R_{num}(f_{cm}, f_{ym}, a_{nom})}{\gamma_{ductile}} & \chi > 0.6\ (ductile) \end{cases} \tag{6.7}$$

combined with $\gamma_{brittle} = 1.17$ and $\gamma_{ductile} = 1.27$. A significant difference between the safety factor for the ductile and brittle failure mode is obtained. The safety factor for the brittle failure mode differs from the suggested safety factor by GRF, $\gamma_{Rd} = 1.27$. The used coefficients of variation were relatively large and could be reduced to obtain more efficient safety factors that are also reliable. The aforementioned Bayes inference could also result in a reduction of safety factors. A full comparison between the proposed model and existing reliability models is presented in chapter 7.

The empirical distribution functions of the individual benchmarks are displayed in Figure 6.7 and can be compared to the fitted log-normal distribution. The individual benchmarks follow the same shape as the fitted distribution function, only differences for the mean model uncertainty are observed. A higher accuracy and lower variance of the model uncertainty can be observed for the ductile failure mode in (a) with respect to the brittle failure mode in (b).

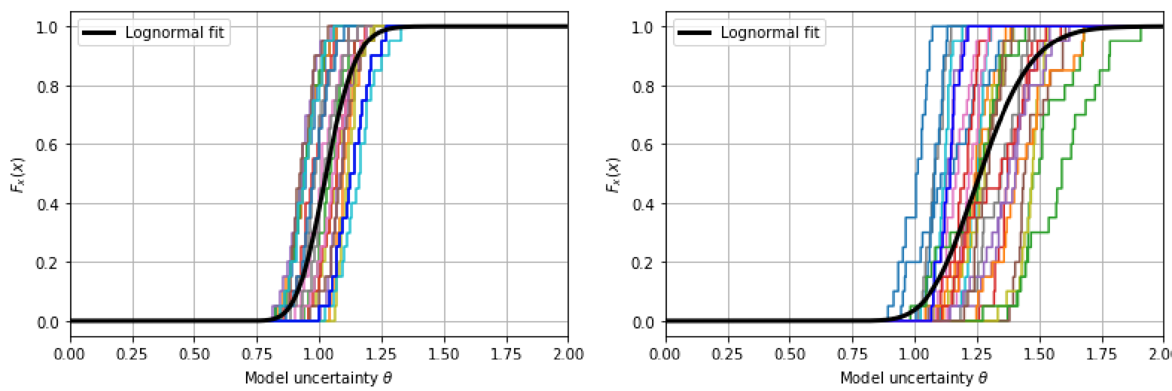

(a) Ductile failure mode.

(b) Brittle failure mode.

Figure 6.7: Empirical distribution functions of the 48 benchmarks displayed with respect to the fitted log-normal distributions.

6.5. Sensitivity Analysis

The relation between the model uncertainty and the material parameters is reviewed to investigate the relative importance of the individual material parameters on the resistance. (Figure 6.8) The sensitivity of the parameters on the model uncertainty could indicate where potentially the largest benefits can be obtained if these parameters would be measured with higher accuracy. A distinction for the failure mode based on $\chi = 0.6$ was made, such that the brittle data is displayed in red and the ductile data in blue.

Apart from the influence of geometry on the failure mode, the benchmarks are most likely to fail in bending if the reinforcement is relatively weak compared to the concrete. Meanwhile, the beam is most likely to fail in shear if the concrete is relatively weak compared to the reinforcement. Therefore, the ductile failure mode is expected to be highly correlated to the reinforcement yield strength and ultimate strength, whereas the brittle failure mode will be correlated to concrete compressive and tensile strength.

The ductile failure mode (blue) shows clear correlation with the yield strength and the ultimate strength. This makes sense, as a ductile failure mode is paired with yielding of reinforcement. A near perfect negative correlation is reviewed, indicating that the variation of yield strength per benchmark dominates the numerical response. A slight positive correlation can be observed for the ultimate strain of reinforcement. An higher ultimate strain results in delayed yielding of reinforcement, which could result in additional strains and cracks in concrete which increases the model uncertainty. Steel Young's modulus only affects the linear response and therefore does not affect the model uncertainty. Furthermore, no correlation is observed for the ductile failure mode with respect to the concrete parameters.

For the brittle failure mode (red), lower parameters of concrete strength are translated into an higher model uncertainty. This makes sense, as lower concrete strength makes the beam vulnerable to brittle shear failure. For concrete tensile strength, Young's modulus and fracture energy, a negative correlation with the model uncertainty is noted. A positive relation for the brittle failure mode can be observed for the model uncertainty and reinforcement yield strength, ultimate strength and Young's modulus, which also can be explained due to the beam being more likely to fail in shear if the reinforcement is relatively strong. The Poisson's ratio of reinforcement shows zero correlation as expected, because the reinforcement is modelled as one dimensional line elements and therefore only accounts for axial stresses.

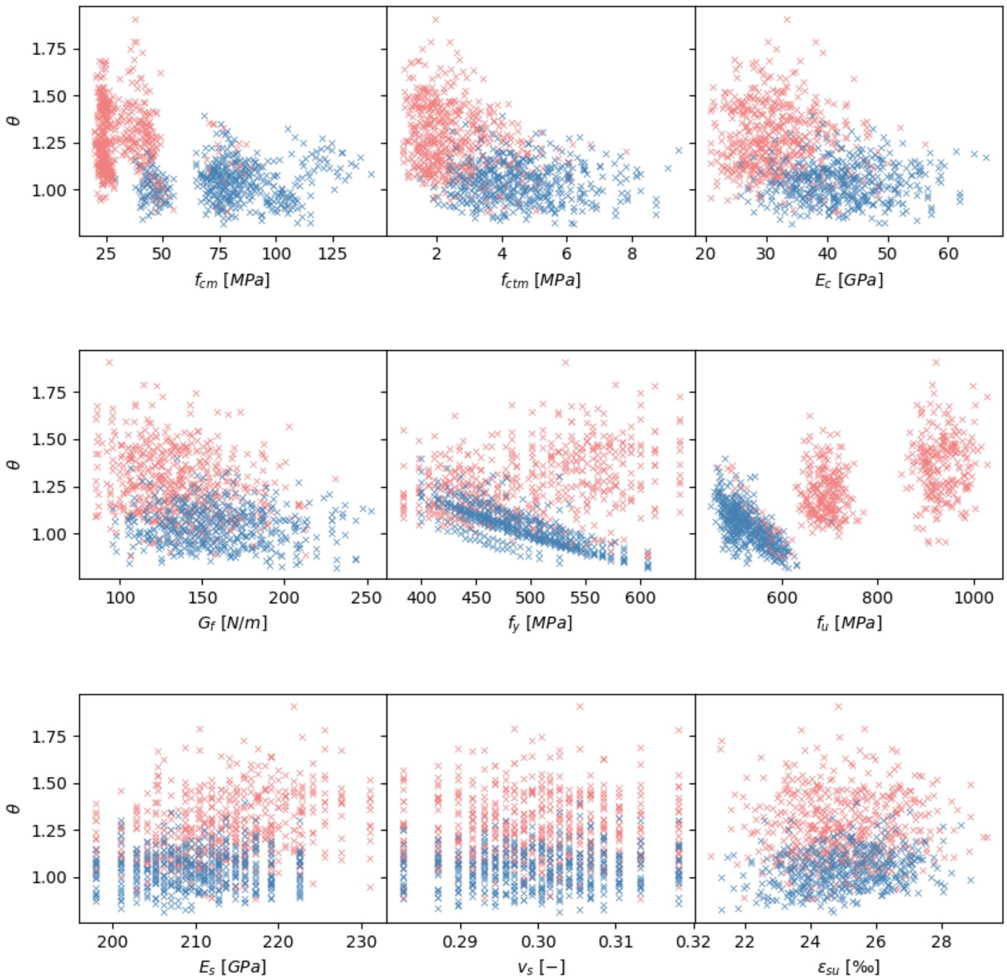

Figure 6.8: Relationship between material parameters and model uncertainty.

In general, the model uncertainty reduces for higher concrete strength parameters. Conversely, higher reinforcement strength parameters tend to increase the model uncertainty. The negative correlation of the yield and ultimate strength for the ductile failure mode (blue) indicate a near linear response of the resistance and model uncertainty to these parameters. The model uncertainty of the ductile failure mode can be reduced most by an improved determination of the coefficient of variation of the yield strength. For the brittle failure mode, all four concrete parameters seem to have quite a similar response on the model uncertainty. However, the used coefficient of variation could relatively be reduced the most for the concrete mean tensile strength for specific types of concrete, according to Strauss et al. [11].

6.6. Summary

The model uncertainty was evaluated for the total data-set. The mean model uncertainty and coefficient of variation for the 48 benchmarks could be expressed as $\mu_\theta = 1.16$ and $CoV = 0.144$. Nonetheless, a clear distinction could be observed in the probability density function of both populations. A statistical Welch's test indicated that both samples do not have a same mean, and therefore do not originate from the same distribution. The goodness of fit tests (KS-test) also rejected both a normal and log-normal distribution for the total data-set.

Subsequently, the resistances of the brittle and ductile failure mode were separated based on the ductility index boundary $\chi = 0.6$. Both the normal and log-normal distribution were accepted for the ductile failure mode, although the log-normal distribution showed a better fit. For the brittle failure mode, only the log-normal distribution was accepted against a 5% significance level. The resulting parameters and a comparison with parameters found in two other research is displayed in table Table 6.4.

Table 6.4: Comparison of the model uncertainty with other research.

	Ductile		Brittle	
	Mean	CoV	Mean	CoV
This research	1.03	0.09	1.27	0.13
Engen et al. [5]	1.00	0.10	1.20	0.15
de Putter [7]	1.05	0.10	1.13	0.16

A full probabilistic approach was applied contrary to the semi-probabilistic approach with deterministic input of the comparative research. Nevertheless, similar magnitudes were found for the mean and coefficient of variation of the model uncertainty with minor explainable differences. This confirms a correct application of the applied methodology. These results are promising and indicate that the model uncertainty can be improved substantially if smaller coefficients of variation are used for specific types of concrete and reinforcement.

From the log-normal distributions, safety factors were derived to establish a reliability model. The safety factors were defined for a 50 year design lifetime with a sensitivity factor $\alpha = 0.8$ and reliability index $\beta = 3.8$. The resulting reliability method relies on a global approach of one simulation with mean input parameters to obtain the design resistance of simply supported reinforced concrete beams by:

$$R_d = \begin{cases} \dfrac{R_{num}(f_{cm}, f_{ym}, a_{nom})}{\gamma_{brittle}} & \chi \leq 0.6 \qquad \gamma_{brittle} = 1.17 \\ \dfrac{R_{num}(f_{cm}, f_{ym}, a_{nom})}{\gamma_{ductile}} & \chi > 0.6 \qquad \gamma_{ductile} = 1.27 \end{cases} \tag{6.8}$$

At last, a sensitivity analysis was performed to investigate which parameters could most enhance accuracy. The reinforcement parameters for the ductile failure mode showed a low mean model uncertainty and low variance. The brittle failure mode had much larger variance and model uncertainty for each of concrete parameters. The variation of the brittle failure mode can be reduced significantly by a better quantification of the concrete tensile strength, while for the ductile failure mode the yield strength was found most relevant with a near linear response.

7 | Comparison with Existing Models

The performance of the proposed and existing reliability models is evaluated based on their accuracy and robustness. First, accuracy of the models can be quantified by the magnitude of the mean estimate and the coefficient of variation. Secondly, robustness is a qualitative measure which addresses to what extent models are applicable for different type of problems.

The proposed reliability model is applied as defined in Equation 6.8. A single global analysis is performed with deterministic input variables, after which a safety factor is applied depending on the type of failure mode. For a brittle failure mode ($\chi \leq 0.6$), the mean numerical resistance is divided by a safety factor $\gamma_{brittle} = 1.17$. For a ductile failure mode ($\chi > 0.6$), the mean numerical resistance is divided by a safety factor $\gamma_{brittle} = 1.27$. The reliability method results in a design resistance, which can be compared to the experimental observed load as defined by the unity check (UC):

$$\text{UC} = \frac{R_d}{R_{exp}} \quad (\times 100\%) \tag{7.1}$$

7.1. Accuracy

Accuracy can be quantified by the estimate of the mean value (μ) and the coefficient of variation (CoV). Both quantities are displayed at the bottom of Table 7.1 for the proposed model and existing reliability models. Based on the full comparison, the following statements can be made.

For all reliability models, no overestimation of the design resistance is observed. The highest unity check observed is equal to 89% for method ECOV beam index 0. Furthermore, method PRF has the lowest prediction of the design resistance with an average unity check of 61%. Subsequently are method ECOV and GRF with a unity check equal to 66% and 69% respectively. The proposed model shows for the ductile failure mode and brittle failure mode a mean unity check of 77% and 67% respectively. Furthermore, the coefficient of variation of the proposed model is reduced compared to the other existing reliability models. This can also be observed within the range of the minimum and maximum values.

Remarkably, method ECOV seems to estimate the ductile failure modes with relatively high accuracy, while the brittle failure modes are underestimated significantly compared to the proposed model and method GRF. The combined effect results in a lower efficiency. This can also be observed as method ECOV has the highest coefficient of variation and contains both the lowest and highest prediction of the unity check.

It can be concluded that distinction of the failure mode by means of the ductility index allows for different safety factors and can result in a higher mean unity check and lower coefficients of variation, while guaranteeing safety levels. The unity check for ductile failure modes shows a mean unity check equal to 77% and a coefficient of variation of 8%. The brittle failure modes exhibit a mean unity check of 67% and a coefficient of variation of 13%. From this perspective, it is stimulated to design a ductile failure mode not only to avoid sudden failure, but also to design more efficiently.

Table 7.1: Comparison of the model uncertainty between the proposed and existing reliability models. (GRF, PRF, ECOV)

	Proposed Model		GRF		PRF		ECOV		
Beam #	$UC_{ductile}$	$UC_{brittle}$	UC_{GRF}	χ_{GRF}	UC_{PRF}	χ_{PRF}	UC_{ECOV}	$\chi_{ECOV,m}$	$\chi_{ECOV,k}$
0	0.84	-	0.84	0.94	0.79	0.92	0.89	0.94	0.93
1	0.84	-	0.84	0.93	0.79	0.92	0.85	0.93	0.93
2	0.84	-	0.84	0.93	0.79	0.91	0.88	0.93	0.93
3	0.81	-	0.81	0.93	0.76	0.90	0.84	0.93	0.93
4	0.86	-	0.85	0.92	0.79	0.90	0.86	0.92	0.91
5	0.85	-	0.85	0.89	0.79	0.87	0.86	0.89	0.89
6	0.78	-	0.78	0.90	0.71	0.88	0.78	0.90	0.84
7	0.80	-	0.81	0.86	0.72	0.55	0.79	0.86	0.84
8	-	0.85	0.79	0.15	0.68	0.05	0.82	0.15	0.14
9	-	0.69	0.64	0.40	0.48	0.42	0.47	0.40	0.39
10	-	0.54	0.50	0.46	0.45	0.44	0.42	0.46	0.46
11	-	0.61	0.56	0.52	0.52	0.46	0.55	0.52	0.50
12	-	0.62	0.57	0.42	0.46	0.44	0.47	0.42	0.44
13	-	0.59	0.55	0.48	0.44	0.44	0.47	0.48	0.48
14	-	0.69	0.64	0.54	0.59	0.46	0.65	0.54	0.50
15	-	0.62	0.57	0.48	0.52	0.46	0.57	0.48	0.50
16	-	0.56	0.51	0.50	0.43	0.41	0.44	0.50	0.49
17	-	0.69	0.64	0.54	0.55	0.42	0.61	0.54	0.48
18	-	0.82	0.76	0.08	0.41	0.11	0.33	0.08	0.10
19	-	0.62	0.57	0.11	0.36	0.13	0.39	0.11	0.11
20	-	0.48	0.44	0.26	0.42	0.08	0.54	0.26	0.33
21	-	0.72	0.66	0.45	0.56	0.37	0.50	0.45	0.44
22	-	0.74	0.68	0.49	0.60	0.39	0.64	0.49	0.45
23	-	0.66	0.61	0.52	0.57	0.43	0.65	0.52	0.48
24	-	0.67	0.62	0.48	0.51	0.30	0.56	0.48	0.44
25	-	0.76	0.69	0.49	0.60	0.34	0.65	0.49	0.43
26	-	0.69	0.64	0.56	0.64	0.50	0.66	0.56	0.50
27	-	0.76	0.70	0.47	0.55	0.20	0.56	0.47	0.35
28	-	0.79	0.73	0.46	0.56	0.31	0.58	0.46	0.36
29	-	0.68	0.63	0.57	0.61	0.49	0.68	0.57	0.51
30	-	0.62	0.57	0.08	0.39	0.12	0.53	0.08	0.08
31	-	0.74	0.68	0.13	0.44	0.15	0.38	0.13	0.15
32	-	0.49	0.45	0.09	0.46	0.08	0.56	0.09	0.27
33	0.74	-	0.74	0.95	0.69	0.95	0.75	0.95	0.94
34	0.83	-	0.83	0.91	0.77	0.88	0.84	0.91	0.91
35	0.80	-	0.81	0.96	0.76	0.95	0.83	0.96	0.95
36	0.73	-	0.73	0.92	0.68	0.91	0.74	0.92	0.91
37	0.75	-	0.75	0.93	0.70	0.89	0.76	0.93	0.92
38	0.74	-	0.74	0.92	0.68	0.89	0.75	0.92	0.91
39	0.73	-	0.73	0.93	0.68	0.93	0.75	0.93	0.94
40	0.72	-	0.72	0.92	0.69	0.93	0.74	0.92	0.92
41	-	0.67	0.62	0.56	0.58	0.45	0.66	0.56	0.52
42	0.74	-	0.74	0.95	0.70	0.94	0.77	0.95	0.95
43	0.77	-	0.77	0.94	0.72	0.92	0.79	0.94	0.94
44	0.71	-	0.71	0.64	0.68	0.88	0.77	0.64	0.90
45	-	0.74	0.68	0.59	0.65	0.47	0.78	0.59	0.54
46	0.68	-	0.68	0.97	0.65	0.96	0.71	0.97	0.96
47	0.70	-	0.69	0.97	0.67	0.96	0.74	0.97	0.96
Mean	0.77	0.67	0.69	0.63	0.61	0.58	0.66	0.63	0.62
CoV	0.08	0.13	0.16	0.46	0.20	0.53	0.23	0.46	0.47
Min.	0.68	0.48	0.44	0.08	0.36	0.05	0.33	0.08	0.08
Max.	0.86	0.85	0.85	0.97	0.79	0.96	0.89	0.97	0.96

7.2. Robustness

A second important feature is the robustness of a reliability model. Both the proposed model and method GRF rely on a single global analysis with mean input parameters, which ensures robustness. Only for the proposed model, analysis with a ductility index near the boundary of $\chi = 0.6$ require attention as was discussed in subsection 5.3.2. In the sample, beams 8, 41 and 45 predict a wrong failure mode based on the ductility index χ_{GRF}. Beam 8 was found to experience discretization issues near the loading plate, causing a very low ductility index as discussed in subsection 5.3.2. Beams 41 and 45 exerted a ductility index of 0.56 and 0.59, indicating that for translation to the experimental failure mode the ductility index boundary might be lower than 0.6. On the contrary, a boundary of 0.65 showed better agreement based on the numerical visual failure mode.

Method PRF on average results very low design resistances and has an increased wrong prediction of the experimental failure modes based on the ductility index. The findings substantiate the concerns related to method PRF mentioned in *fib* Model Code 2010 [2]. Furthermore, method ECOV is advised to be applied only if both analysis show the same failure mode. Most benchmarks were either expected to fail in shear or bending, but still this can be questioned for beams 26, 29, and 45 based on the ductility index. Method ECOV does not show improved results compared to method GRF, and costs extra effort as two analysis need to be performed.

7.3. Summary

A comparison between the proposed model and existing reliability methods was conducted. The comparison showed the relative performance of the different reliability methods and elucidated shortcomings. The proposed model included an objective distinction of the failure mode by the ductility index boundary $\chi = 0.6$, which resulted in noticeable improvements.

It was observed in Table 7.1, that none of the reliability methods overestimated the resistance of the evaluated benchmarks. The proposed method showed on average the highest prediction of the unity check and the lowest coefficients of variation by distinction of the failure mode. The mean unity check for ductile and brittle failure mode was found to be 77% and 66% respectively. The respective coefficients of variation were found as 8% and 13%. The range of unity checks for the ductile failure mode varied from 68% to 85%, and for the brittle failure mode between 48% to 85%. A significant improvement was found respective to the similar method GRF where a mean unity check of 69% was found with a coefficient of variation of 16%. This affirms that it can be more efficient to distinguish per failure mode. Design for a ductile failure mode by NLFEA was found most efficient, which is also desirable from a safety point of view.

From the existing models, method GRF was found most efficient and robust. This was followed up by method ECOV and the least favourable was method PRF. This substantiated the discouragement of method PRF in *fib* Model Code 2010 [2]. Method ECOV lacks robustness if different failure modes occur and takes additional effort as two analysis need to be conducted. Method ECOV showed to predict the ductile failure modes accurately, but performed badly on brittle failure modes. Method GRF showed on average the best prediction and assures robustness as only one global analysis needs to be performed. Based on these findings, a global analysis approach seems most efficient and can be improved by failure modes distinction as was included in the proposed reliability method. (Equation 6.8)

8 | Non-Parametric Bayesian Network

In this chapter, a description of a multivariate non-parametric Bayesian network (NPBN) for reinforced concrete beams is given. The choices for creation of the model are explained, and the model is validated. The model can be used independently for quick estimation of the resistance for the input of material and geometry parameters. Furthermore, conditional probabilities can be assessed if certain material parameters or design loads are known. The establishment, validation and usability are treated accordingly.

8.1. Construction of the Model

The NPBN was constructed in software program Uninet. The input and output variables of the non-linear finite element analysis are represented by nodes, and grouped into four main categories. The different categories can be listed accordingly: Concrete (gray), reinforcement (turquoise), geometry (beige) and output variables (green). The nodes are connected through arcs to represent their dependency by rank correlation. Arcs were drawn between nodes if the variables were assumed to be dependent based on physical logic. The order in which arcs are drawn was also considered, as this influences the order of the conditional probability, and hence, the correlation matrix of the NPBN.

The full model, consisting of 16 nodes and 72 arcs, is displayed in Figure 8.1. The concrete, reinforcement and geometry parameters are set independent of each other. The relation with the response is complex, and therefore, arcs are considered to each output node. The concrete variables were assumed to be dependent and in the following order of importance: mean compressive strength f_{cm}, mean tensile strength f_{ctm}, fracture energy G_f and Young's modulus E_c. The mean compressive strength was used as input for the other three variables according to design formula's. (See Table 4.2) For reinforcement, the order of importance was set as: yield strength f_y, ultimate strength f_u, Young's modulus E_s and ultimate strain ε_s. At last, the geometry values were connected in order of: span length L_{span}, effective depth d, beam width b_w and area of longitudinal reinforcement A_{long}.

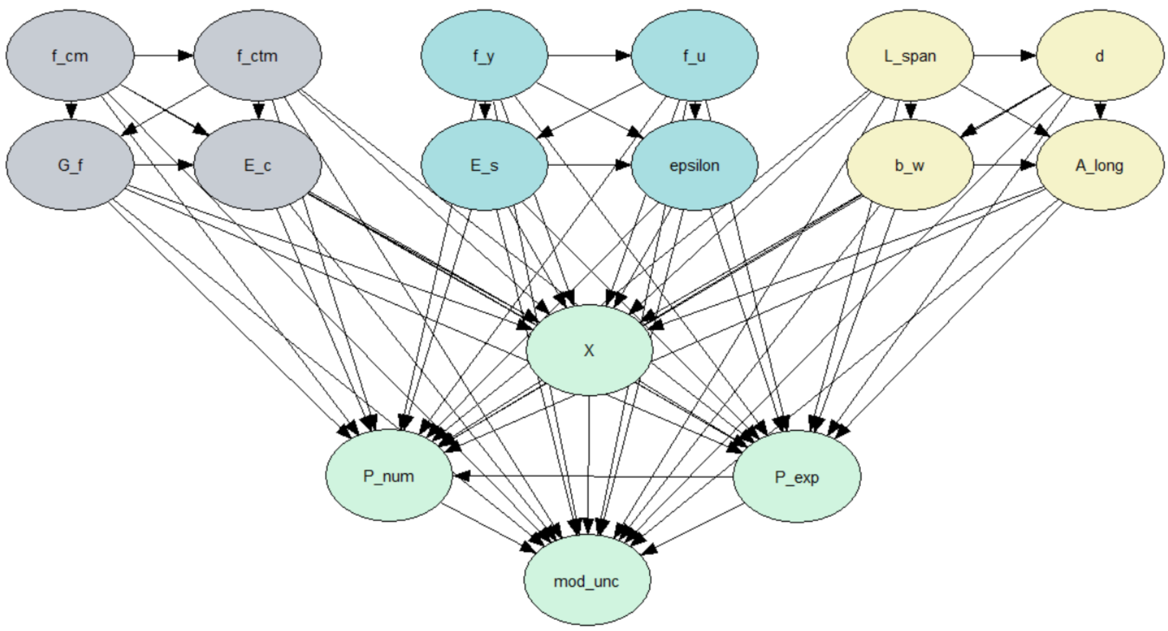

Figure 8.1: Proposed NPBN for the NLFEA response of reinforced concrete beams.

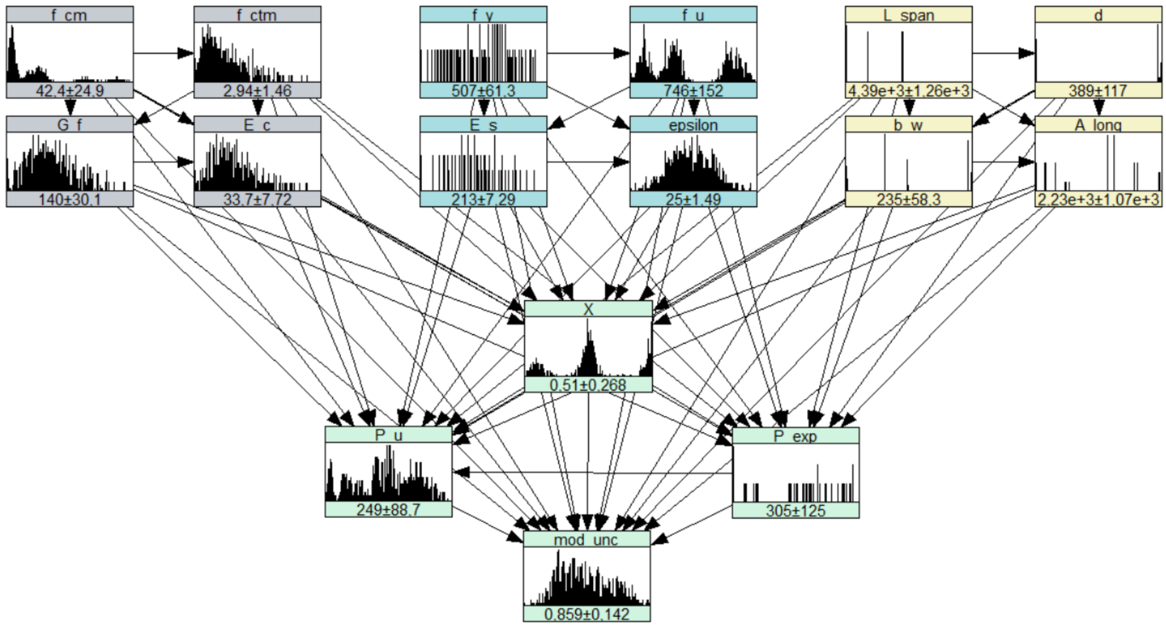

Figure 8.2: Proposed NPBN the showing distribution per variable by histograms.

The number of geometry parameters is limited within the proposed model. Relevant missing geometry parameters are related to the shear reinforcement configuration and the type of loading. These parameters were not included as perfect correlation between several parameters existed due to the arrangement of experiments and the assumption of deterministic geometry variables. Furthermore, the beams without shear reinforcement would have multiple zero values for the shear reinforcement parameters, which caused errors in evaluating the model.

Moreover, the correlation between geometry variables is physically less substantiated than for the material parameters, as an engineer will make sensible choices for the combination of geometry parameters. For the selected range of benchmarks however, the geometry parameter were chosen such that a certain failure mechanism was to be expected due to which the geometry parameters were strongly related to a specific research. Therefore, correlation was assumed between the geometry nodes for the used data-set. For different random combinations of geometry input this assumption may not be valid, and representing the geometry variables as independent can be more appropriate. Furthermore, the geometry nodes are discrete variables, whereas the other nodes represent continuous variables as can be seen in Figure 8.2. The discrete nodes limit the possibilities of conditional assessment, and the range of benchmarks also caused some deficits as will be elucidated in section 8.3.

At last, all input nodes were connected to the output nodes (green), resulting in 48 arcs. The output nodes were connected to each other by the assumed order as will be explained accordingly. Hierarchy in the output nodes is used to show the order in which the nodes were connected. First, the input variables were assumed to affect the ductility index χ and thereby, the failure mode and distribution type as discussed in chapter 6. The ductility index was connected to the remaining three output nodes. The experimental load P_{exp} was assumed to be dependent on all input variables and the ductility index. In succession, the experimental load affects the numerical load P_{num} and the model uncertainty θ, and the model uncertainty is simply a division of the experimental load with the numerical load.

8.2. Validation Model

The constructed model should describe the actual dependencies observed within the data-set. Two aspects need to be verified: 1) whether the assumption of the Gaussian copula for the data-set is valid and 2) if the constructed NPBN represents enough dependence. The validation process can either be based on a comparison of the determinants of the correlation matrices of the empirical data (EC), the empirical normal data (ENC) and the Bayesian network (BNC), or by means of a calibration score that is a measure of the distance between the aforementioned correlation matrices. Both methods can be reviewed by use of a Matlab toolbox: BANSHEE. (Paprotny et al.)[31]

Validation based on the determinants of the respective correlation matrices is known to be a sensitive indicator to the number of variables, as the determinant will tend to zero if the number of variables exceeds the number of samples or discrete states per node. (Hanea et al.)[28] As this is the case for the span length, an alternative validation procedure is used by means of the dependence calibration score d-Cal. This method is less sensitive to the number of nodes and discrete states, and is defined as:

$$d(\Sigma_1, \Sigma_2) = 1 - \sqrt{1 - \eta(\Sigma_1, \Sigma_2)} \tag{8.1}$$

$$\eta(\Sigma_1, \Sigma_2) = \frac{\det(\Sigma_1)^{1/4}\det(\Sigma_2)^{1/4}}{\det(\frac{1}{2}\Sigma_1 + \frac{1}{2}\Sigma_2)^{1/2}} \tag{8.2}$$

where Σ_1 and Σ_1 are the correlation matrices of compared empirical, empirical normal or Bayesian net data respectively. The dependence score will tend towards one if the respective matrices show similarity, and towards zero if the correlation matrices are significantly different. (Mendoza-Lugo et al.)[32] A sample size needs to be selected and is generated for a number of times. Generally, a large sample indicates a good performance of the model in terms of describing the dependencies. Although, there is no consensus yet about what the minimum sample size would need to be.

The validation of the d-score is displayed in Figure 8.3. In (a) the empirical rank correlation is compared to the distribution of the normal rank correlation, and lies within the 90% confidence interval for a large sample equal to 4000, generated a 1000 times. This confirms that the Gaussian copula is applicable to the data. In (b), the normal rank correlation matrix is compared to the distribution of the rank correlation matrix of the NPBN. A sample of 205 generated a 1000 times indicates that the constructed NPBN is valid, but could be improved to better describe the dependency. As mentioned before, the geometry variables could be expanded to continuous parameters, addition of shear reinforcement parameters, addition of loading type and perhaps independent geometry parameters.

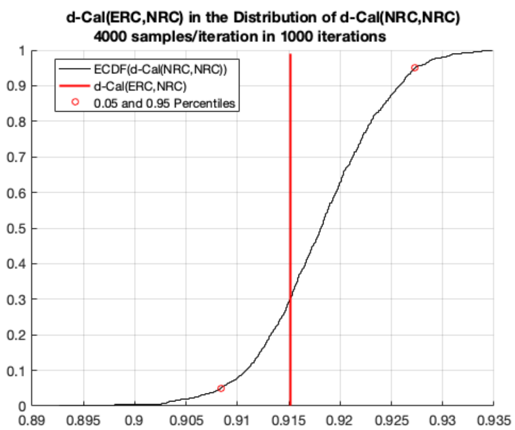

(a) Empirical rank correlation in distribution of empirical normal rank correlation.

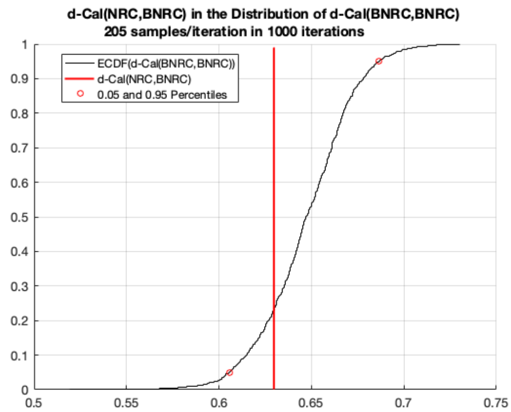

(b) Empirical normal rank correlation in distribution of Bayesian network correlation.

Figure 8.3: Validation of the proposed NPBN based on the calibration score d-Cal for total data-set. (960 samples)

After reviewing both tests, the Gaussian copula was found valid to describe the data-set, but the NPBN could be improved in terms of describing the dependencies. Generally, a larger data-set could be expected to improve the model. However, it was opted to exclude the six beams without shear reinforcement as it was shown in chapter 5 that the solution strategy and response was significantly different. Six beams, accountable for 120 samples, were excluded from the data-set. The remaining data-set of 840 samples only included beams with shear reinforcement. The validation based on the d-Cal is displayed in Figure 8.4.

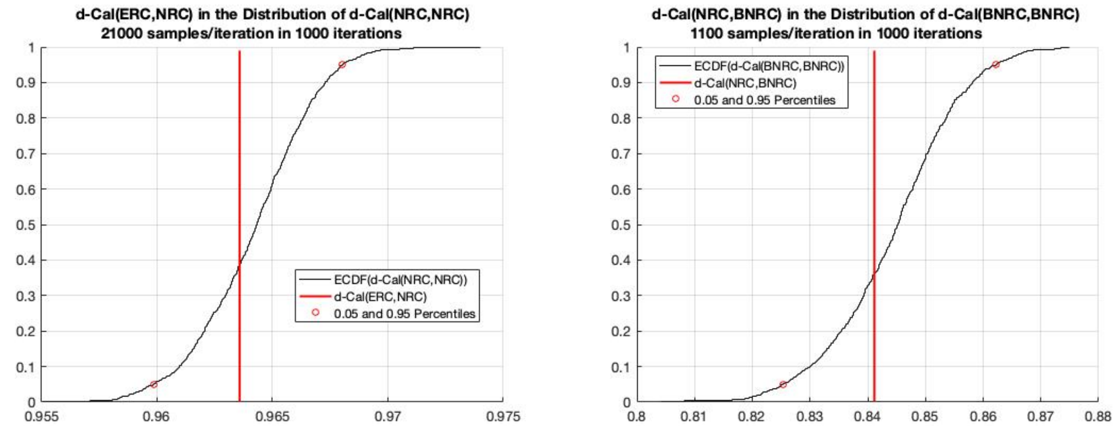

(a) Empirical rank correlation in distribution of empirical normal rank correlation.

(b) Empirical normal rank correlation in distribution of Bayesian network correlation.

Figure 8.4: Validation of the proposed NPBN based on the calibration score d-Cal for beams with shear reinforcement only. (840 samples)

From Figure 8.4, it can be observed that (a) the calibration score for the empirical and empirical normal correlation matrices is validated for a very large number of samples equal to 21000. In (b), the validation score of the empirical normal falls within the 90% confidence interval of the correlation matrix of the proposed Bayesian network with a relatively large sample of 1100. Based on the results from Figure 8.3 and Figure 8.4, the choice to exclude the six beams without shear reinforcement improves the quality of the NPBN, meaning that the response is better described. The capabilities of the proposed NPBN on the beams with shear reinforcement (840 samples) will be further discussed in section 8.3.

8.3. Model Application

In this section, the application of the NPBN is demonstrated by two examples. In example 1, the numerical resistance is evaluated for different combinations of concrete and reinforcement strength. In example 2, a reversed analysis is performed, in which the effect on the concrete compressive strength is shown for a desired design resistance.

8.3.1. Example 1: Conditional Material Strength

The response of different conditional concrete and reinforcement material strengths on the numerical resistance is shown for a beam of dimensions similar to B321 from Rashid and Mansur [33]. The input dimensions are displayed in Equation 8.3. The material strengths are defined through the concrete compressive strength and reinforcement yield strength in percentiles of 0-25% (Low), 25-75% (Medium) and 75-100% (High), as displayed in Table 8.1.

$$L_{span} = 3400\ mm, \quad b_w = 250\ mm, \quad d = 340\ mm, \quad A_{long} = 2945\ mm^2 \tag{8.3}$$

The obtained conditional resistances for significance levels of 5%, 50% and 95% are displayed in Table 8.2. The mean numerical response of NLFEA is displayed in the right column based on the percentiles 12.5%, 50% and 87.5%, which should more or less correspond to the mean estimates of the NPBN.

Table 8.1: Definition of the low, medium and high conditional input for concrete compressive strength and reinforcement yield strength.

Input Node	Lower Bound	Upper Bound	Label
	20.06	27.34	Low
f_{cm} [MPa]	27.34	79.87	Med
	79.87	141.68	High
	383.59	449.83	Low
f_y [MPa]	449.83	535.74	Med
	535.74	634.95	High

Table 8.2: Numerical resistance for 5%, 50% and 95% significance level, conditional on different combinations of concrete and reinforcement strength.

Case #	f_{cm}	f_y	$P_{num}^{5\%}$	$P_{num}^{50\%}$	$P_{num}^{95\%}$	P_{num}^{NLFEA}
1	Low	Low	250	516	767	391
2	Low	Med	153	352	726	391
3	Low	High	99	276	587	391
4	Med	Low	264	654	790	570
5	Med	Med	199	388	750	570
6	Med	High	135	326	702	570
7	High	Low	274	702	822	560
8	High	Med	215	510	781	630
9	High	High	149	346	734	720
Unconditional			95	330	763	570

The results in Table 8.2 can be used to assess the resistance for a desired significance level. For example, $P_{num}^{5\%}$ is the resistance corresponding to a 5% significance level. Suppose we want to assess the probability of failure of reinforced concrete beams as part of a bridge superstructure. After inspection, the current status of concrete strength and reinforcement yield strength are both identified as 'Medium', belonging to case 5. The mean expected resistance equals 388 kN, and the resistance corresponding to a 5% significance level is equal to 199 kN.

Depending on the expected loads on the bridge, a Monte Carlo Simulation can be performed based on a limit state function:

$$Z = R - S \tag{8.4}$$

where in this case, R is the numerical resistance derived by the NPBN for a large number of samples, e.g. 5 million. S is the expected load which can be a single value, or defined as for example a normal distribution based on measured vehicle weights. The large conditional sample can be tested against this design load. Failure occurs if $Z < 0$, and the number of failures n_f with respect to the total number of samples N defines the probability of failure:

$$P_f = \frac{n_f}{N} \tag{8.5}$$

Small probabilities of failure can now be assessed quickly due to the ability of generating large representative samples by the NPBN. No excessive amounts of time consuming analysis would be needed to derive probabilities of failure with magnitudes $P_f < 10^{-3}$.

8.3.2. Example 2: Conditional Resistance

Example 2 illustrates a reversed analysis, were the conditional effect on the concrete strength is displayed. In Table 8.3, two cases are defined for a desired range of the ultimate resistance P_u, the ductility index χ for a ductile failure mode and the span length L_{span}. A visual example with the change of distributions of the NPBN due to conditional parameters is attached in Appendix D.

Table 8.3: Two cases for demonstration of reversed analysis by the NPBN.

Case #	P_u	χ	L_{span}
Case 1	[100; 130]	[0.85; 0.90]	3080 mm
Case 2	[200; 300]	[0.85; 0.90]	3080 mm

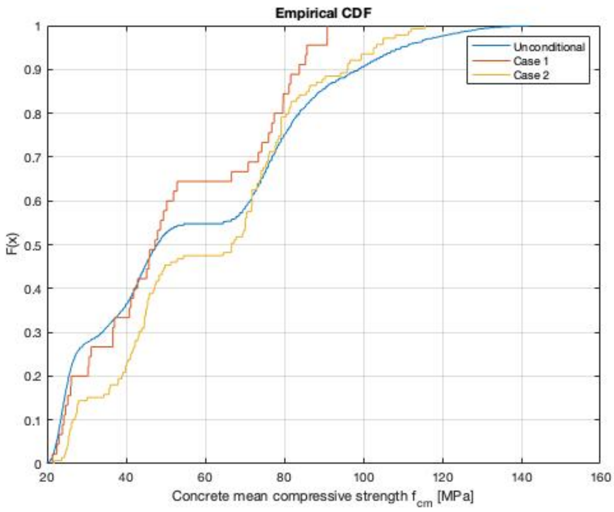

Figure 8.5: Empirical cumulative distribution function of the concrete strength based on conditional resistance, ductility index and span length.

The conditional response on the concrete strength is displayed in Figure 8.5 by the empirical cumulative distribution functions of the unconditional sample and the two cases. The probability of exceedance is displayed on the vertical axis. For a mean estimate of 50%, it can be observed that the concrete strength for the unconditional sample and case 1 are nearly identical, being approximately 47 MPa. For case 2 with a higher desired resistance, a higher concrete strength is observed equal to 67 MPa. A quick estimates of needed type of concrete or reinforcement strength can be obtained for a particular design load. In this case, it is advised to perform a design process for the derived parameters.

The two examples illustrate how the model can be used. A lot more different combinations are possible. The described conditional resistances for example 1 can be particularly useful if the quality of concrete or reinforcement is questioned. The model output can be directly compared to the expected design loads and used to define a probability of failure by Monte Carlo Simulation. Application can be useful to quickly assess the probability of failure for existing structures, or if after construction the quality of materials is questioned.

In Table 8.2, the model predictions are roughly compared to the resistance found by NLFEA. The mean estimates do not always agree, and the conditional resistance exhibits a very large standard deviation. Some limitations of the model have been addressed in section 8.1. Most of the model deficits can be assigned to the discrete geometry parameters instead of being continuous variables. Due to perfect correlation between the discrete geometry parameters within the data-set, not all geometry parameters could be included within the NPBN. Essential parameters related to shear reinforcement configuration and the load application are not considered. The limitations of the model are further discussed in chapter 9.

8.4. Summary

A NPBN was constructed that included four parameters for each category of concrete, reinforcement, geometry and output. These sixteen parameters were represented by nodes and connected through arcs to include dependency based on physical logic. The model was validated based on a distance calibration score d-Cal for the similarity between the empirical rank correlation (ERC), empirical normal (NRC) and Bayesian net (BNRC) rank correlation matrices. Furthermore, two examples of the model application were given along with a comparison to the output of NLFEA.

First, the assumption of the Gaussian copula was validated. The test on d-Cal felt within the 90% confidence interval for a large sample of 4000, from which it could be concluded that the data can be represented by the Gaussian copula. Secondly, the constructed NPBN is tested to the normal data to indicate whether the NPBN could describe sufficient dependency. The d-Cal score validated the model, but did insinuate that the NPBN can be improved as the number of samples was on the lower side, equal to 205.

To improve the model validation, it was opted to exclude the 120 samples related to the beams without shear reinforcement as these beams exhibit a different mechanical response. For the remaining 840 samples, the same model was found to improve substantially. The assumption of the Gaussian copula was validated by a very high d-Cal equal to 21000 samples. For the d-Cal score on the empirical normal and Bayesian network correlation matrices, a relatively large sample of 1100 was attained. This showed that the proposed NPBN is better defined for beams with shear reinforcement only.

Deficits of the model response were pointed out by demonstrating the model application in subsection 8.3.1. The limitations were presumed to originate mostly from the description of the geometry parameters. The geometry variables could be extended by addition of the shear reinforcement variables including the horizontal spacing, bar diameter and yield strength. By considering the geometry as deterministic input variables, the model is limited to the exact geometric values as collected from the benchmarks. The NPBN could be improved significantly by input of geometry parameters as continuous instead of discrete and by addition of shear reinforcement parameters.

Furthermore, the response of the NPBN was observed to be largely influenced by the composition of the benchmarks within the data-set. One specific research for example considered one deterministic span length with high reinforcement strengths. Incorrect or wide estimates of the conditional resistance could occur if for this span length low concrete strengths were assigned. This issue can be resolved by extending the data-set of benchmarks, and by addition of analysis that include continuous overlapping geometry and material parameters.

9 | Discussion, Conclusions and Recommendations

This chapter contains the discussion, conclusion and recommendations. In the discussion, the limitations of the applied methodology will be discussed, and the results will be interpreted and compared to other research. After the discussion on the methodology and results, conclusions will be drawn by answering the research questions. At last, recommendations are presented for further research.

9.1. Discussion on Methodology

For implementation of NLFEA in the design of reinforced concrete structures, a better quantification of uncertainties is required to establish a reliability method that is both safe and efficient. To achieve this, a full probabilistic approach was applied with use of failure mode distinction based on the ductility index. The research resulted in a reliability method based on a global approach. Furthermore, a complex standalone multivariate NPBN was developed that can be used for extensive analysis possibilities. As NLFEA can be time-consuming and a large sample size was desirable, some assumptions and simplifications were made that could affect the results. These limitations on the methodology are discussed accordingly.

Full Probabilistic Approach

A full probabilistic approach was used that considered material induced uncertainties and the model uncertainty in NLFEA for a particular solution strategy. For feasibility and reasons mentioned in section 1.3, the uncertainties inflicted by deviations in geometry and boundary conditions were not explicitly taken into account. In general, these aspects should not be overlooked in the design phase. A perfect symmetrical test procedure was assumed along with geometric variables that were measured with high accuracy. Therefore, not explicitly taking into account these aspects was found justifiable for the selected benchmarks and for the purpose of this research.

To generate efficient samples of material parameters that governed the total space of reinforcement and concrete uncertainties, an optimized Latin hypercube sampling strategy was used. In Tran et al. [23], it was shown that for a similar problem the results converged for a sample size $N = 10$ per benchmark. The used sample size $N = 20$ therefore was a sensible choice considering time efficiency.

The distribution types for material parameters were taken according to Graubner and Brehm, Strauss et al. [10,11], which were derived for a wide variety of concrete and reinforcement. No specific types of concrete and reinforcement with their marginal distributions were identified. A reduced variance could be obtained by testing of specimens, resulting in a more precise description of the design resistance.

Solution Strategy NLFEA

It was aimed to apply one consistent solution strategy to all benchmarks, to avoid bias in the results from different modelling choices. A solution strategy was chosen in line with Hendriks et al. [3], as defined in Table 5.1. Nonetheless, it was observed that the solution strategy was not necessarily appropriate for all benchmarks.

It became evident that the opted solution strategy provided an adequate numerical response for beams with shear reinforcement, but less for beams without shear reinforcement. A clear distinction in mean model uncertainty and coefficient of variation was observed in Figure 5.4. Only six of 48 beams did not contain shear reinforcement, by which the proposed reliability method mostly applies to beams with shear reinforcement. It could have been more appropriate to exclude beams without shear reinforcement, as shear reinforcement is a requirement according to EN 1992-1-1 [1].

Ductility Index

The ductility index was used as an objective way to distinguish between a ductile and brittle failure mode, based on the suggested boundary $\chi = 0.6$ from Engen et al. [5]. This boundary could be used to assign the numerical failure mode for a large number of analysis. However, robustness of the boundary itself can be improved.

Contradicting results on the numerical and experimental failure mode were obtained in subsection 5.3.2 and subsection 5.3.3. The numerical failure mode showed better correspondence with a boundary $\chi = 0.65$, while the experimental failure mode suggested a lower boundary up till $\chi = 0.55$. As this was inconclusive, it was decided to proceed the analysis with the suggested boundary of $\chi = 0.6$ from Engen et al.[5]. For a ductility index within the aforementioned range, it is advised to perform an additional visual inspection of the numerical failure mode.

Construction of Non-Parametric Bayesian Network

A NPBN was constructed that describes the NLFEA ultimate limit state response of reinforced concrete beams, to enable quick assessment of the resistance for conditional material and geometry parameters. (See Figure 8.1) The model can be extremely useful to assess the resistance and probability of failure of existing structures, or for quality control of new structures. The probability of failure can be assessed through Monte Carlo Simulation for a specific design load from EN 1991-1-1[17].

The dependence between variables was based on physical logic. The dependency between geometric variables is physically less substantiated, but clear correlation was present within the range of benchmarks. Some limitations arose during construction of the model due to the discrete geometry nodes. Multiple geometry nodes were perfectly correlated to the type of experiment, and therefore would not add information to the model. As a consequence, the model application is restricted to the typical configurations of the evaluated benchmarks.

9.2. Discussion on Results

The results have been presented and partially discussed in the previous chapters. The interpretation of these results is described and compared to findings of other research accordingly.

Model Uncertainty

The model uncertainty has been quantified in other research based on a semi-probabilistic approach, which cannot guarantee safety standards adequately. (Strauss et al.[11]) Moreover, the effect of different parameters on the model uncertainty can not be reviewed. In this research, a full probabilistic approach was applied that does consider material uncertainties explicitly besides the model uncertainty. A comparison of the model uncertainty with the semi-probabilistic approach was displayed in Table 6.4.

The mean model uncertainty can be directly compared, and was found similar in magnitude for the ductile failure mode. The model uncertainty of the brittle failure mode was found as 1.27, compared to 1.13 and 1.20 in Engen et al., de Putter[5,7]. These are explainable differences, as the selection of benchmarks varied along with noticeable differences in the used solution strategy.

Lower coefficients of variation were found for both failure modes, which can be explained by the lower standard deviation as more samples per benchmark were used. ($N = 20$) In general, the results agree that the brittle failure mode is more difficult to predict as a higher model uncertainty and coefficient of variation are observed.

Convergence & Discretization

In consideration of time efficiency, the analysis was performed with a relatively large mesh size ($h/10$), a low maximum number of iterations per load-step (40), and a varying load-step. For the brittle failure mode, which is more difficult to predict due to the complexity of stress redistribution for cracking concrete, this led in some cases to non-converged results. These results were still accepted as the accuracy for smaller mesh and more iterations per load-step did not vary significantly. To improve convergence and accuracy of the brittle failure mode, it may be more appropriate to use a mesh size $h/20$ and a maximum number of iterations >100 as suggested by de Putter[7]. This does however come at a cost of computational time, and in Engen et al.[5] the effect of mesh size on the model uncertainty was found insignificant.

One exception was observed for beam B-N4 from Ashour[29]. (red dots, $\chi < 0.3$ in Figure 5.4) An unusual low ductility index indicated a brittle failure mode whereas a ductile failure mode was expected.

This beam was assigned as over-reinforced with a very high concrete strength. The relatively large element size induced discretization problems near the loading plate, which resulted in an erroneous high plastic dissipated energy in the concrete, and thus a low ductility index. As the magnitude of the found resistance was not divergent, this data was included in the analysis.

Reliability Method

The analysis was performed on a wide variety of benchmarks to establish a reliability method applicable to different types of reinforced concrete beams. (Equation 6.8) Although a clear difference between the model uncertainty of beams with and without shear reinforcement was observed, the total data-set was used to define safety factors for the reliability method. The higher mean model uncertainty and coefficient of variation of the beams without shear reinforcement can affect the magnitude of the safety factor for the brittle failure mode. It may be more appropriate to exclude beams without shear reinforcement, and define the safety factor for beams with shear reinforcement only.

A modest positive relation for the model uncertainty with respect to the beam height was observed, due to which the derived models should be applied with caution to beams of larger size, deep beams in particular. Further research on an extended set of benchmarks is recommended .

In comparison to the available reliability methods from *fib* Model Code 2010 [2], an exact similar value for the ductile failure mode was found as for method GRF that is formulated for different types of structures. This seems on the low side, as a similar safety factor was found while a specific set of benchmarks was evaluated, and deviations in geometry and boundary conditions were not explicitly considered. The full comparison in Table 7.1 showed that improved accuracy and reduced coefficients of variation are feasible.

Non-Parametric Bayesian Network

The model was validated based on the calibration score d-Cal. The validation was improved significantly when beams without shear reinforcement were excluded from the data-set. This implies that a significant different mechanical response exists, and that the NPBN can best be formulated for a similar type of beam configuration.

In section 8.3 the model application was demonstrated. However, the conditional results were found unsubstantial as very large standard deviations were incurred. It was aforementioned that the model was limited due to the discrete geometry variables and as parameters for the configuration of shear reinforcement and the loading condition were not included. Moreover, the response was found to be affected by the typical configurations of the experimental tests performed per benchmark study. Certain ranges of material parameters and dimensions were inherently connected to a specific research. This implicates that the model application is limited to the specific configurations of the benchmarks. To improve the model usability, addition of continuous geometry parameters and a wider overlapping data-set is necessary.

9.3. Conclusions to Research Questions

Conclusions are presented by answering the research questions as formulated in section 1.2. First, the sub-questions are answered. Subsequently, the main research question is answered.

1. Can an efficient sampling strategy be applied to adequately describe the total space of design-related uncertainties?

An efficient sampling strategy for a full probabilistic approach was necessary due to the large computational times in NLFEA. The Latin hypercube sampling strategy has shown to provide representative samples of the material uncertainties that concur with the prior known marginal and joint distributions from Graubner and Brehm, Strauss et al.[10,11]. The iterative spatial optimization ensured that the samples covered the total space of uncertainties.

Moreover, the resulting empirical cumulative distribution functions of the individual benchmarks reasonably matched the fitted log-normal distributions of the ductile and brittle failure modes for a sample size $N = 20$, as shown in Figure 6.7. This indicates that an efficient data-set can be generated by an optimized Latin hypercube sampling strategy, to perform a full probabilistic analysis with benchmarking by NLFEA.

2. Can the benchmarks be modelled efficiently in NLFEA according to a single solution strategy?

The benchmarks were modelled in a 2D plane with symmetry conditions in software program Diana based on a total strain crack model and Von Mises plasticity. Guidelines from Hendriks et al.[3] were followed for the constitutive, kinematic and equilibrium relations. The used solution strategy (Table 5.1) was found applicable to beams with shear reinforcement, but less accurate for beams without shear reinforcement. The beams without shear reinforcement exhibited a relatively large model uncertainty and coefficient of variation, which implies that the used solution strategy is not suitable to beams without shear reinforcement.

The solution strategy was kept constant as much as possible to avoid biased results due to modelling choices. Most of the constitutive, kinematic and equilibrium conditions could be well applied to the beams with shear reinforcement. The mesh size, load-step and maximum number of iterations however, were found to be very beam specific. The chosen element size of $h/10$ caused discretization problems or non-converged results in a few cases. Similarly, the load-step for the displacement controlled analysis was reduced as non-convergence could occur for beams failing in a brittle manner. The maximum number of iterations was set equal to 40, but could be chosen higher to improve convergence and accuracy of the brittle failure mode especially.

The aforementioned actions come at the cost of increased computational time, which was undesirable for the large amount of analysis to be performed. It can be concluded that it remains complicated to select one solution strategy on forehand that is both time efficient and accurate for different types of reinforced concrete structures.

3. What is the relation between the ductility index and the model uncertainty?

The ductility index was found applicable for an objective distinction between failure modes based on the proposed boundary of $\chi = 0.6$ by Engen et al.[5]. However, analysis with a ductility index near this boundary require additional attention. By visual inspection, the numerical failure mode corresponded better to a value of $\chi = 0.65$. In contrary, the experimental failure mode was correctly predicted for a ductility index towards $\chi = 0.55$, which can be explained by the systematic underestimation of the shear capacity in NLFEA. After consideration, the original boundary of $\chi = 0.6$ was accepted for further analysis.

A statistical significant difference of the mean model uncertainty and coefficients of variation was observed between the ductile and brittle failure modes. (Figure 6.2) The brittle failure mode showed a high model uncertainty with a large variance. The ductile failure mode exhibited a lower model uncertainty and variance, but also overestimated the resistance more often. For the ductile failure mode, a mean model uncertainty of $\theta_d = 1.03$ with a coefficient of variation of 9% was found. Whereas for the brittle failure mode, a mean model uncertainty of $\theta_b = 1.27$ with a coefficient of variation of 13% was found. In comparison to the entire data-set, a mean model uncertainty of $\theta = 1.16$ with a coefficient of variation of 15% was found. Thereby, quantification of the model uncertainty and design resistance with respect to the failure mode was considered appropriate and beneficial.

4. Does distinction of the failure mode based on the ductility index enable a more accurate and robust reliability method?

A reliability method was formulated in Equation 6.8, which relies on a global approach and failure mode distinction. The design resistance is formulated as the numerical resistance for mean input parameters, divided by an associated safety factor for a ductile or brittle failure mode. Safety factors were defined for a 50 year design lifetime with a sensitivity factor $\alpha = 0.8$ and reliability index $\beta = 3.8$. (EN 1990)[15] This resulted in safety factors $\gamma_d = 1.27$ and $\gamma_b = 1.17$ for the ductile and brittle failure mode respectively. More favourable safety factors may be derived by a more accurate description of the marginal distributions for specific types of concrete and reinforcement.

A comparison between the proposed method and existing reliability methods was made by assessment of the unity check. (Table 7.1) The proposed reliability method showed lower coefficients of variation and on average a higher unity check. From the existing reliability models, the global analysis method GRF was found most robust and efficient, followed up by method ECOV and then PRF. Method PRF showed the least encouraging results in terms of efficiency, while method ECOV only resulted in accurate estimates for ductile failure modes and less for brittle failure modes.

Overall, the proposed reliability method showed promising signs for an increased efficiency along with reduced variance. The full probabilistic approach with benchmarking has shown to result in a more efficient reliability method that respects safety standards. Especially if reinforced concrete beams are designed to fail in a ductile manner, a considerable efficient design by NLFEA can be achieved with a mean unity check of 77%. For a brittle failure mode, a mean unity check of 66% was attained.

5. Can the NLFEA response of concrete beams be captured by a standalone model to be used for extensive analysis possibilities?

It has been demonstrated how a NPBN for the NLFEA response of reinforced concrete beams can be designed and used. The model was validated based on the calibration score d-Cal. Comparison of the empirical and empirical normal rank correlation matrices indicated that the data could be well represented by the Gaussian copula, enabling the response to be described by a NPBN. Evaluation of the empirical normal and Bayesian network rank correlation matrices was also validated, but suggested that the NPBN could be improved to describe the dependencies more adequately. The model validation was improved significantly after exclusion of the data related to beams without shear reinforcement, indicating that the NPBN is best designed for a typical type of beam configuration.

However, limitations of the model presented itself by display of the model application in section 8.3. The conditional results were classified as unsubstantial due to large standard deviations. The limitations arose due to the discrete geometry parameters and the composition of the data-set. The dimensions and material parameters were inherently connected to specific types of research, which affected the response of the NPBN. The foundation of a NPBN for the NLFEA resistance of reinforced concrete beams has been demonstrated, but further research is needed to improve usability.

Can the quantification of uncertainties related to NLFEA be improved to enhance safe and efficient application for the design of reinforced concrete beam elements?

The research focused on two main parts. First, it has been demonstrated how a full probabilistic approach can be applied to define a reliability method for reinforced concrete beams. A reliability method as a function of the failure mode was statistically appropriate and resulted in improved efficiency. For a 50 year design lifetime, a mean unity check of 77% was found for the ductile failure mode and a mean unity check of 66% for the brittle failure mode. For specific types of concrete and reinforcement, reduced coefficients of variation for the material parameters could lead to even higher efficiency.

Secondly, a standalone multivariate NPBN was developed. Although the model itself was limited to the specific configuration of benchmarks, it has been demonstrated how such a model can be established and used to assess reliability of reinforced concrete beams. On this part, further research is necessary to extend the model usability.

The findings of this study suggest that design of reinforced concrete beams by NLFEA can be applied for efficient design, while respecting safety standards. The full probabilistic approach enabled a proper quantification of the design resistance combined with a distinction between failure modes. Thereby, this research contributes to the implementation of NLFEA for the design of reinforced concrete structures.

9.4. Recommendations

Following from the discussion, several recommendations are made for further research related to application of NLFEA for reinforced concrete beams.

- For extensive use of the proposed reliability method, it is recommended to expand the analysis to benchmarks of larger size (deep beams and longer span), prestressed beams and continuous beams. The proposed model might be applicable, but this should be confirmed by further research. Prestressing could induce additional uncertainty parameters by prestressing losses, beams of larger size are susceptible to a size affect potentially accompanied with a higher model uncertainty, and continuous beams can suffer different failure mechanisms. Further improvements could be made by addition of coefficients of variation within the reliability method for specific types of concrete and reinforcement.

- A better quantification of the ductility index boundary is necessary to improve robustness of the proposed reliability method. This might be achieved by separation of the ductility index for longitudinal and shear reinforcement, or by reviewing the relative change of the ductility index as a function of the load-step as described in section C.2.

- Considerably more work needs to be done to improve the usability of the NPBN. A larger sample size and a wider selection of benchmarks could improve the NPBN significantly. A more extensive model could be made by including shear reinforcement parameters and to include uncertainties of geometry parameters as continuous instead of discrete nodes. Preferably, the model is defined for a specific type of beam configuration, for example for beams with shear reinforcement within a certain range of shear span over depth ratio. The NPBN could also be coupled to a limit state function to assess the probability of failure directly for certain design loads.

Bibliography

[1] EN 1992-1-1. Eurocode 2: Design of concrete structures—part 1-1: General rules and rules for buildings. *European Committee: Brussels, Belgium*, 2005.

[2] *fib* Model Code 2010. *Volume 2*. International Federation for Structural Concrete (fib), Walraven, J.C. and Bigaj-van Vliet, A., 2012. ISBN 978-2-88394-106-9.

[3] M.A.N. Hendriks, A. de Boer, and B. Belletti. Guidelines for nonlinear finite element analysis of concrete structures. *Rijkswaterstaat Technisch Document (RTD), Rijkswaterstaat Centre for Infrastructure, RTD*, 1016:2012, 2012.

[4] B. Belletti, C. Damoni, and M.A.N. Hendriks. Development of guidelines for nonlinear finite element analyses of existing reinforced and prestressed beams. *European Journal of Environmental and Civil Engineering*, 15:1361–1384, 11 2011. doi: 10.1080/19648189.2011.9714859.

[5] M. Engen, M.A.N. Hendriks, J.A. Øverli, and E. Åldstedt. Non-linear finite element analyses applicable for the design of large reinforced concrete structures. *European Journal of Environmental and Civil Engineering*, 23(11):1381–1403, 2019.

[6] C. Pacoste, M. Plos, and M. Johansson. Recommendations for finite element analysis for the design of reinforced concrete slabs. Technical report, Kungl. tekniska högskolan, 2012.

[7] A. de Putter. Towards a uniform and optimal approach for safe nlfea of reinforced concrete beams: Quantification of the accuracy of multiple solution strategies using a large number of samples. *TU Delft repository*, 2020.

[8] P. Castaldo, D. Gino, and G. Mancini. Safety formats for non-linear finite element analysis of reinforced concrete structures: Discussion, comparison and proposals. *Engineering Structures*, 193:136–153, 2019.

[9] IEA UN. Global status report for buildings and construction (2019). *Avail-able at https://www. gbpn. org/china/newsroom/2019-global-status-report-buildings-and-constr uction. Access date*, 15, 2020.

[10] C.A. Graubner and E. Brehm. Jcss probabilistic model code part 3: Resistance models 3.2 masonry properties. Technical report, Technical report, JCSS, 2011.

[11] A. Strauss, D. Zimmermann, T.and Lehkỳ, D. Novák, and Z. Keršner. Stochastic fracture-mechanical parameters for the performance-based design of concrete structures. *Structural Concrete*, 15(3):380–394, 2014.

[12] Y. Xiao, Z. Chen, J. Zhou, Y. Leng, and R. Xia. Concrete plastic-damage factor for finite element analysis: Concept, simulation, and experiment. *Advances in Mechanical Engineering*, 9(9): 1687814017719642, 2017.

[13] J.C. Walraven and C.R. Braam. *Prestressed Concrete CIE3150/4160*. Faculty of Civil Engineering and Geosciences, TU Delft, 2015. ISBN 06917300086.

[14] Committee 445 ASCE-ACI. Recent approaches to shear design of structural concrete. *Journal of structural engineering*, 124(12):1375–1417, 1998.

[15] EN 1990. Eurocode 0: Basis of structural design. *European Committee: Brussels, Belgium*, 2005.

[16] NEN-EN 13670. Dutch standard: Execution of concrete structures. *European Committee: Brussels, Belgium*, 2005.

[17] EN 1991-1-1. Eurocode 1: Actions on structures. *European Committee: Brussels, Belgium*, 2005.

[18] F. Hartmann and C. Katz. *Structural analysis with finite elements*. Springer Science & Business Media, 2013.

[19] T. Rabczuk, J. Akkermann, and J. Eibl. A numerical model for reinforced concrete structures. *International Journal of Solids and Structures*, 42(5-6):1327–1354, 2005.

[20] A. Petrík and R. Ároch. Usage of true stress-strain curve for fe simulation and the influencing parameters. In *IOP Conference Series: Materials Science and Engineering*, volume 566-1, page 012025. IOP Publishing, 2019.

[21] V. Cervenka. Global safety format for nonlinear calculation of reinforced concrete. *Beton-und Stahlbetonbau*, 103(S1):37–42, 2008.

[22] M. Engen, M.A.N. Hendriks, J. Köhler, J.A. Øverli, and E. Åldstedt. A quantification of the modelling uncertainty of non-linear finite element analyses of large concrete structures. *Structural Safety*, 64:1–8, 2017.

[23] N.L. Tran, C.A. Graubner, and G.A. Rombach. An efficient latin hypercube sampling for probabilistic nonlinear finite element analysis of reinforced concrete structures. In *7th International Conference on Structural Engineering, Mechanics and Computation*, 2019.

[24] S.N. Jonkman, R.D.J.M. Steenbergen, O. Morales-Nápoles, A.C.W.M. Vrouwenvelder, and J.J.C.C. Vrijling. Probabilistic design: Risk and reliability analysis in civil engineering. *Lecture Notes CIE4130. Delft University of Technology*, 2015.

[25] C. Genest and A. Favre. Everything you always wanted to know about copula modeling but were afraid to ask. *Journal of hydrologic engineering*, 12(4):347–368, 2007.

[26] K. Ickstadt, M. Bornkamp, B.and Grzegorczyk, J. Wieczorek, M.R. Sheriff, H.E. Grecco, and E. Zamir. Nonparametric bayesian networks. *Bayesian Stat*, 9:283, 2011.

[27] B.G. Marcot and T.D. Penman. Advances in bayesian network modelling: Integration of modelling technologies. *Environmental modelling & software*, 111:386–393, 2019.

[28] A. Hanea, O. Morales-Nápoles, and D. Ababei. Non-parametric bayesian networks: Improving theory and reviewing applications. *Reliability Engineering & System Safety*, 144:265–284, 2015.

[29] S.A. Ashour. Effect of compressive strength and tensile reinforcement ratio on flexural behavior of high-strength concrete beams. *Engineering structures*, 22(5):413–423, 2000.

[30] Z. Bazant and J. Planas. *Fracture and size effect in concrete and other quasi-brittle materials*, volume 16. CRC press, 1997.

[31] D. Paprotny, O. Morales-Nápoles, D.T.H. Worm, and E. Ragno. Banshee–a matlab toolbox for non-parametric bayesian networks. *SoftwareX*, 12:100588, 2020.

[32] M.A. Mendoza-Lugo, D.J. Delgado-Hernández, and O. Morales-Nápoles. Reliability analysis of reinforced concrete vehicle bridges columns using non-parametric bayesian networks. *Engineering Structures*, 188:178–187, 2019.

[33] M.A. Rashid and M.A. Mansur. Reinforced high-strength concrete beams in flexure. *ACI Structural Journal*, 102(3):462, 2005.

[34] B. Bresler and A.C. Scordelis. Shear strength of reinforced concrete beams. In *Journal Proceedings*, volume 60-1, pages 51–74, 1963.

[35] F.J. Vecchio and W. Shim. Experimental and analytical reexamination of classic concrete beam tests. *Journal of Structural Engineering*, 130(3):460–469, 2004.

A | Data Description

The data for experimental results on the ultimate load on reinforced concrete beams was obtained from four different research. An overview of the configuration of the main geometry and material parameters is shown in Figure A.1. The sequentially displayed parameters are: concrete mean compressive strength, concrete mean tensile strength, reinforcement yield strength, beam span length, beam height and longitudinal reinforcement ratio. The benchmarks govern a variety in experimental failure mechanisms as described in Table A.1. The test arrangements and important differences per research are highlighted accordingly.

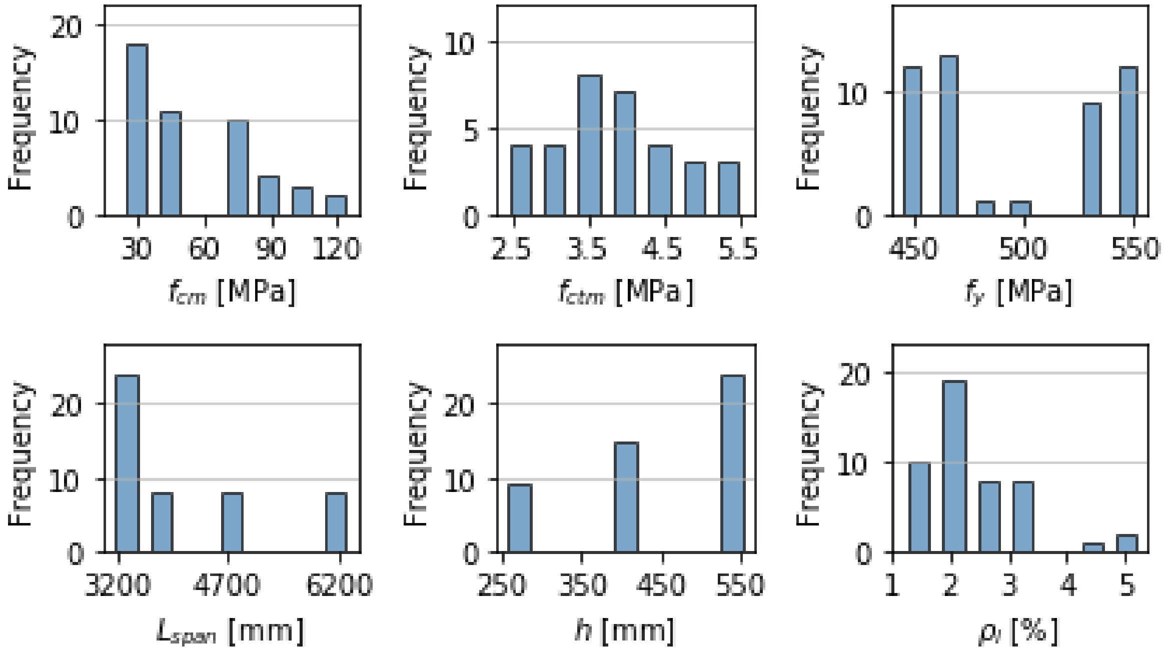

Figure A.1: Overview of the variety of geometry and material parameters from the benchmark experiments.

Ashour (1998)

"Effect of compressive strength and tensile reinforcement ratio on flexural behavior of high-strength concrete beam" (Ashour)[29]

In total nine beams with high-strength concrete were loaded by a four-point bending test after 28 days of hardening. All beams failed in a flexural manner. Mean concrete compressive strengths of 48, 78 and 102 MPa were used in combination with varying longitudinal tensile reinforcement ratio's of 1.18, 1.77 and 2.37%. The layout of the beams, including stirrups and the cross section, is shown in Figure A.2. Shear reinforcement and top reinforcement was applied over the shear span and the longitudinal reinforcement was anchored within the concrete. The used reinforcement consisted of locally available deformed steel bars. Ordinary Portland cement (Type-I) was used, for which the mean compressive strength was derived from cylinders tested under compression. A constant distance of 500 mm between the loading points was used, while a force controlled hydraulic testing machine implemented 25 to 35 increments until failure occurred.

The ultimate strength of the reinforcing bars was unspecified in the research and was therefore assumed as $1.08 * f_y$. Loading and support plate dimensions were assumed equal to the width of beam and 150 millimeter. The mean Young's modulus for steel was taken as 210 GPa.

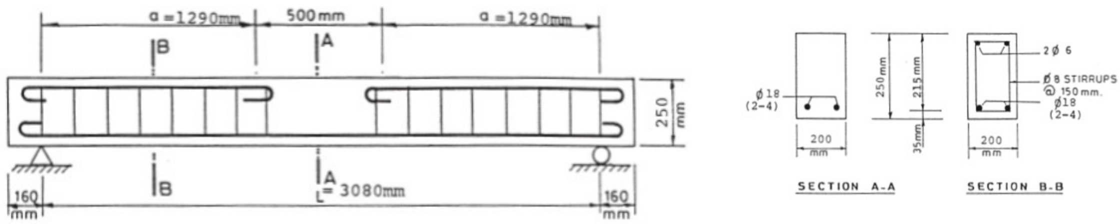

Figure A.2: Experimental layout from Ashour[29].

Bresler-Scordelis (1963)

"Experimental and Analytical Reexamination of Classic Concrete Beam Tests" (Bresler and Scordelis)[34]

Twelve benchmarks were included from the Bresler-Scordelis tests. Nine of the twelve beams failed due to shear. The beams were designed with high reinforcement ratio's to make the beams shear-critical. The beams were designed with different longitudinal reinforcement ratio, shear reinforcement configuration, span length, cross section dimensions, and concrete strength. The test arrangement used a monotonic force controlled centre-point loading. The force increments were reduced in magnitude if cracks started to develop. All beams were tested at an age of thirteen days, which is early compared to the standard 28 days.

To prevent bond failure, the longitudinal reinforcement was anchored to the outside of the beams with anchor plates and nuts. The test set-up is displayed in Figure A.3.

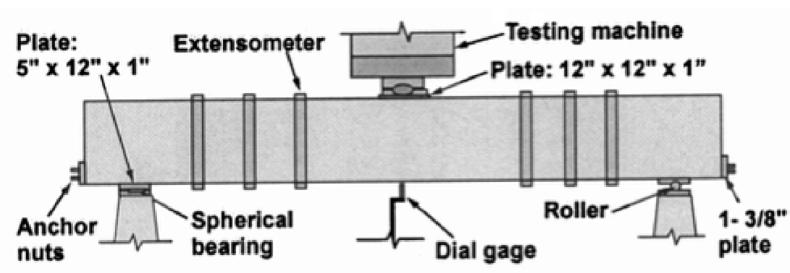

Figure A.3: Experimental layout from Bresler and Scordelis[34].

Vecchio & Shim (2004)

"Experimental and Analytical Reexamination of Classic Concrete Beam Tests" (Vecchio and Shim)[35]

Twelve experimental test results were obtained. The configuration of the beams was nominally identical to the Bresler-Scordelis beams in terms of cross section dimensions, reinforcement configuration and concrete strength. Details related to the longitudinal reinforcement anchor plates, the loading plates, and the support plates were also preserved. Similar failure mechanisms were observed for both research. However, some differences between both experimental tests were present. A displacement-controlled loading system was used to measure the post-peak response. The age at testing differed from 38 to 127 days, which is significantly older than for the Bresler-Scordelis tests. Furthermore, some deviations in concrete and reinforcement strength occurred due to heterogeneity and the use of available reinforcing bars.

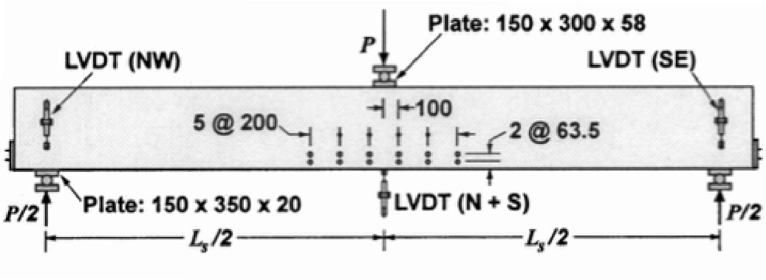

Figure A.4: Experimental layout from Vecchio and Shim [35].

Rashid & Mansur (2015)

"Reinforced High-Strength Concrete Beams in Flexure" (Rashid and Mansur)[33]

In total sixteen beams were tested with varying concrete strength, reinforcement ratio's and shear reinforcement spacing. The shear reinforcement was placed along the entire length of the beam and the longitudinal reinforcement was anchored externally at shown in Figure A.5. The beams were tested under four-point loading by a deflection-controlled hydraulic actuator.

The beams were designed to fail in a ductile manner. All sixteen beams were classified to fail in flexural-tension. The mean concrete compressive and tensile strength were derived from several tests on cylinders and prisms. The beams were cured for fourteen days in a moist environment and air-dried before testing. The load was applied by displacement-controlled hydraulic actuator and a constant gauge length of 450 millimeter was used.

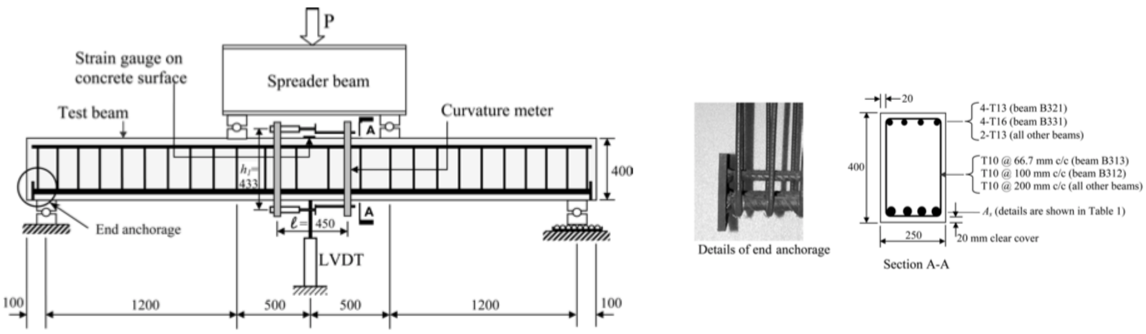

Figure A.5: Experimental layout from Rashid and Mansur [33].

Table A.1: Overview of dimensions and experimental results of selected benchmarks. (Ashour, Rashid and Mansur, Bresler and Scordelis, Vecchio and Shim)[29,33–35]

No.	Code	Ref.	f_{cm} [MPa]	ρ [%]	a [mm]	d [mm]	h [mm]	FM	P_u [kN]	b_w [mm]	s [mm]	f_y [MPa]
0	B-H2	[29]	102,4	1,18	1290	198	250	FT	88,06	200	150	530
1	B-H3	[29]	102,4	1,77	1290	198	250	FT	128,31	200	150	530
2	B-H4	[29]	102,4	2,37	1290	198	250	FT	167,60	200	150	530
3	B-M2	[29]	78,5	1,18	1290	198	250	FT	89,84	200	150	530
4	B-M3	[29]	78,5	1,77	1290	198	250	FT	123,89	200	150	530
5	B-M4	[29]	78,5	2,37	1290	198	250	FT	160,88	200	150	530
6	B-N2	[29]	48,6	1,18	1290	198	250	FT	90,19	200	150	530
7	B-N3	[29]	48,6	1,77	1290	198	250	FT	124,96	200	150	530
8	B-N4	[29]	48,6	2,37	1290	198	250	FT	154,34	200	150	530
9	BS-A1	[34]	24,1	1,50	1830	466	561	VC	468	307	210	555
10	BS-A2	[34]	24,3	1,89	2285	464	559	VC	490	305	210	555
11	BS-A3	[34]	35,1	2,25	3200	466	561	FC	468	307	210	555
12	BS-B1	[34]	24,8	2,01	1830	461	556	VC	446	231	190	555
13	BS-B2	[34]	23,2	2,01	2285	466	561	VC	400	229	190	555
14	BS-B3	[34]	38,8	2,53	3200	461	556	FC	356	229	190	555
15	BS-C1	[34]	29,6	1,49	1830	464	559	VC	312	155	210	555
16	BS-C2	[34]	23,8	3,04	2285	464	559	VC	324	152	210	555
17	BS-C3	[34]	35,1	3,00	3200	459	554	FC	270	155	210	555
18	BS-OA1	[34]	22,6	1,50	1830	461	556	DT	334	310	-	555
19	BS-OA2	[34]	23,7	1,88	2285	466	561	DT	356	305	-	555
20	BS-OA3	[34]	37,6	2,27	3200	462	556	DT	378	307	-	555
21	VS-A1	[35]	22,6	1,43	1830	457	552	VC	459	305	210	441
22	VS-A2	[35]	25,9	1,84	2285	457	552	VC	439	305	210	441
23	VS-A3	[35]	43,5	2,26	3200	457	552	FC	420	305	168	441
24	VS-B1	[35]	22,6	1,90	1830	457	552	VC	434	229	190	441
25	VS-B2	[35]	25,9	1,90	2285	457	552	VC	365	229	190	441
26	VS-B3	[35]	43,5	2,45	3200	457	552	FC	342	229	152	441
27	VS-C1	[35]	22,6	1,67	1830	457	552	VC	282	152	210	441
28	VS-C2	[35]	25,9	2,86	2285	457	552	VC	290	152	210	441
29	VS-C3	[35]	43,5	2,86	3200	457	552	FC	265	152	168	441
30	VS-OA1	[35]	22,6	1,43	1830	457	552	DT	331	305	-	441
31	VS-OA2	[35]	25,9	1,84	2285	457	552	DT	320	305	-	441
32	VS-OA3	[35]	43,5	2,26	3200	457	552	DT	385	305	-	441
33	A111	[33]	42,8	1,25	1200	357,5	400	FT	342,84	250	200	503,2
34	A211	[33]	42,8	2,20	1200	357,5	400	FT	461,3	250	200	460
35	B211a	[33]	73,6	2,20	1200	357,5	400	FT	500,9	250	200	460
36	B311	[33]	72,8	3,46	1200	340,8	400	FT	751,96	250	200	460
37	B312	[33]	72,8	3,46	1200	340,8	400	FT	730,22	250	100	460
38	B313	[33]	72,8	3,46	1200	340,5	400	FT	742,94	250	66,7	460
39	B321	[33]	77	3,46	1200	340,8	400	FT	765,06	250	200	460
40	B331	[33]	72,8	3,46	1200	340,8	400	FT	772,8	250	200	460
41	B411	[33]	77	4,73	1200	332,5	400	FT	950,4	250	200	460
42	C211	[33]	85,6	2,71	1200	350,8	400	FT	650,42	250	200	473
43	C311	[33]	88,1	3,22	1200	346,7	400	FT	730,12	250	200	482,4
44	C411	[33]	85,6	4,26	1200	335	400	FT	901,4	250	200	473,5
45	C511	[33]	88,1	5,31	1200	322	400	FT	880,6	250	200	467,2
46	D211	[33]	114,5	2,20	1200	357,5	400	FT	605	250	200	460
47	E211	[33]	126,2	2,20	1200	357,5	400	FT	595,2	250	200	460

Diagonal-Tension (DT), Shear-Compression (VC), Flexure–Compression (FC), Flexure-Tension (FT).

B | Python Scripts

B.1. Optimized Latin Hypercube Sampling

```python
 __all__ = ['lhs']

def lhs(n, samples=None, criterion=None, iterations=None):
    if criterion.lower() in ('centermaximin', 'cm'):
            H = _lhsmaximin(n, samples, iterations, 'centermaximin')
    return H


def _lhscentered(n, samples):
    # Generate the intervals
    cut = np.linspace(0, 1, samples + 1)

    # Fill points uniformly in each interval
    u = np.random.rand(samples, n)
    a = cut[:samples]
    b = cut[1:samples + 1]
    _center = (a + b)/2

    # Make the random pairings
    H = np.zeros_like(u)
    for j in range(n):
        H[:, j] = np.random.permutation(_center)
    return H


def _lhsmaximin(n, samples, iterations, lhstype):
    maxdist = 0

    # Maximize the minimum distance between points
    for i in range(iterations):
        Hcandidate = _lhscentered(n, samples)
        d = _pdist(Hcandidate)
        if maxdist<np.min(d):
            maxdist = np.min(d)
            H = Hcandidate.copy()
    return H


def _pdist(x):
    x = np.atleast_2d(x)
    assert len(x.shape)==2, 'Input array must be 2d-dimensional'

    m, n = x.shape
    if m<2:
        return []

    d = []
    for i in range(m - 1):
        for j in range(i + 1, m):
            d.append((sum((x[j, :] - x[i, :])**2))**0.5)
```

```
    return np.array(d)


"""LHS for concrete parameters"""
def LHSconcrete(N,iters):
    f_cm= 40 #MPa
    f_ck= f_cm-8

    if f_ck<= 30:
        f_ctm=0.30*f_ck**(2/3)
    else:
        f_ctm=2.12*np.log(1+f_cm/10)

    E_c = 21.5*(f_cm/10)**(1/3) #GPa
    eps_uc = 3.5  #Promile

    design = lhs(4, samples=N,criterion= 'centermaximin', iterations=iters)
    means = np.array([f_cm, f_ctm, E_c, eps_uc])
    CoV = np.array([0.06,0.30,0.15,0.15])
    stdevs = means*CoV

    mu_n = np.zeros(len(means))
    sig_n=np.zeros(len(means))

    for i in range(len(means)):
        mu_n[i]= np.log(means[i]**2/(np.sqrt(stdevs[i]**2+means[i]**2))) #convert LN_mu to N_mu
        sig_n[i]= np.sqrt(np.log(1+(stdevs[i]**2/means[i]**2))) #convert LN_sigma to N_sigma
        design[:,i]= norm(loc=mu_n[i],scale=sig_n[i]).ppf(design[:,i])

    design=np.exp(design)

    x= np.linspace(0,1,N+1)
    x_t = np.exp(norm(loc=mu_n[0], scale=sig_n[0]).ppf(x))
    y_t = np.exp(norm(loc=mu_n[1], scale=sig_n[1]).ppf(x))

    df_concrete = pd.DataFrame((design),columns=['fc','fctm','Ec','eps_u'])

    return df_concrete
LHSconcrete(N=20,iters=10000)


"""LHS for steel parameters incl correlation"""
def LHSreinfo(N,iters):
    f_y= 435 #MPa
    f_u= 500
    E_s= 210 #GPa
    nu_s= 0.30
    eps_us=25 #promile

    CoV = np.array([0.07,0.04,0.03,0.03,0.06])
    means = np.array([f_y, f_u, E_s, nu_s,eps_us])
    stdevs = means*CoV

    design = lhs(5, samples=N,criterion= 'centermaximin', iterations=iters)

    mu_n = np.zeros(len(means))
    sig_n=np.zeros(len(means))
    for i in range(len(means)):
        mu_n[i]= np.log(means[i]**2/(np.sqrt(stdevs[i]**2+means[i]**2))) #convert LN_mu to N_mu
```

```
        sig_n[i]= np.sqrt(np.log(1+(stdevs[i]**2/means[i]**2))) #convert LN_sigma to N_sigma
        design[:,i]= norm(loc=0,scale=1).ppf(design[:,i]) #Uniform to N(0,1) sample

    corr= np.array([
        [  1, 0.75, 0, 0, -0.45],
        [ 0.75, 1, 0, 0,  -0.65],
        [ 0, 0, 1, 0, 0  ],
        [0, 0, 0, 1, 0],
        [-0.45, -0.65, 0, 0, 1 ]])

    df_std= np.ones(5)
    df_std = np.diag([df_std[0],df_std[1],df_std[2],df_std[3],df_std[4]])
    df_cov  = np.dot(np.dot(df_std,corr),df_std) #covariance matrix

    c = cholesky(df_cov, lower=False)
    y = np.dot(design,c) # Convert the data to correlated normal variables.
    for i in range(5):
        design[:,i]= sig_n[i]*y[:,i]+mu_n[i]  #convert to N with LN parameters

    design=np.exp(design) #convert the normal sample to LN
    df_reinfo = pd.DataFrame((design),columns=['fy','fu','Es','nu_s','eps_us'])

    x= np.linspace(0,1,N+1)
    x_t = np.exp(norm(loc=mu_n[0], scale=sig_n[0]).ppf(x))
    y_t = np.exp(norm(loc=mu_n[1], scale=sig_n[1]).ppf(x))
    return df_reinfo

LHSreinfo(N=20,iters=10000)
```

B.2. Diana Model

```
### INPUT
[f_c,f_ctm,rho,a,d,ad,h,P_u,b_w] = [42.8, 3.20, 1.25, 1200, 357.5, 1.32, 400, 342.84, 250]
[s_d, s, s_fy, s_fu, s_E, l_load, w_load] = [10, 200, 541, 585.3, 210000, 250, 150]
[l_supp, w_supp, f_y, f_u, E_s, A_long] = [250, 150, 503.2, 543.5, 210000, 1119.2]
[L_beam, L_span, A_top, fy_top, fu_top] = [3600, 3400, 265.5, 472, 510]
[Es_top, c_top, typ, mid_span] = [210000, 20, 2, 1000]

########################################################################
Load_step = "0.15(80)"   #XX(YY) -> XX displacement step, YY=number of steps
iters= 40

Mesh_size = h/10
hp = 50  # height plates in mm
F = -P_u*1000/2 #N
index_num = 33 #Beam index number of excel file
N=20  #sample size

########################################################################
### fc, fctm, Ec,G_f
concr=([[ 44.2818429 ,   6.00669656,  33.56112902, 176.76897704],
       [ 40.39541737,   1.90054255,  40.9836041 , 169.37480879],
       [ 43.21027213,   3.86017983,  30.84257711, 163.47008334],
       [ 42.88406715,   4.21760356,  37.74089853, 125.04131621],
       [ 46.57368302,   4.73605339,  35.50909088, 132.14792013],
       [ 41.21935566,   5.15566739,  34.19997424, 146.12747721],
       [ 37.98719495,   3.71005634,  36.20180264, 139.01854684],
       [ 40.83163491,   3.07703748,  31.576492  , 207.51041337],
       [ 45.77327015,   2.2142589 ,  32.91894584, 112.07947529],
       [ 39.19099614,   2.41044209,  32.26208077, 149.92422261],
       [ 42.24155372,   3.44152744,  46.24435333, 116.97237822],
       [ 42.56287131,   2.56805495,  29.07809615, 105.84099947],
       [ 41.57670602,   3.31712666,  34.84579176, 158.44502278],
       [ 44.70232543,   2.95737062,  27.85044474, 135.58144282],
       [ 45.18505193,   4.4453809 ,  25.77017721,  95.47556614],
       [ 41.9148486 ,   3.19628594,  39.6855815 , 142.5146115 ],
       [ 43.90124198,   2.83496185,  36.93888156, 153.9903604 ],
       [ 43.54707442,   3.5716399 ,  42.79016696, 187.1880868 ],
       [ 39.87630828,   4.02685574,  30.0291727 , 121.19755364],
       [ 48.04958708,   2.7067462 ,  38.63896251, 128.65853514]])

### fy, fu, Es, nu,epsilon_su
reinfo=([[4.86296802e+02, 5.27280695e+02, 2.08718292e+02, 2.94536786e-01,
        2.74301989e+01],
       [5.75692431e+02, 5.74940412e+02, 2.02786766e+02, 2.91576178e-01,
        2.37796980e+01],
       [4.37691284e+02, 5.39266031e+02, 2.13702851e+02, 2.95811632e-01,
        2.52522660e+01],
       [5.08652872e+02, 5.39595643e+02, 2.12781866e+02, 2.99301641e-01,
        2.30068344e+01],
       [4.99775789e+02, 5.48545130e+02, 1.97921807e+02, 2.82745438e-01,
        2.55397567e+01],
       [5.29195609e+02, 5.38818920e+02, 2.09511149e+02, 3.10391808e-01,
        2.54794570e+01],
       [4.63180864e+02, 5.40814273e+02, 2.11099589e+02, 3.06736794e-01,
        2.33392222e+01],
       [5.18151792e+02, 5.55119745e+02, 2.11921254e+02, 3.05289787e-01,
        2.54896038e+01],
```

```
        [5.44011161e+02, 5.41084183e+02, 2.14715756e+02, 3.03974094e-01,
         2.65512276e+01],
        [4.76148244e+02, 5.33520553e+02, 2.07068142e+02, 3.00429602e-01,
         2.42797847e+01],
        [5.04177203e+02, 5.16561726e+02, 2.19166993e+02, 2.97012922e-01,
         2.70598878e+01],
        [4.90912637e+02, 5.46428218e+02, 2.22614913e+02, 3.13095705e-01,
         2.46776075e+01],
        [5.35866472e+02, 5.55669813e+02, 2.15872748e+02, 3.18021304e-01,
         2.38091240e+01],
        [4.53910299e+02, 5.15714679e+02, 2.17274266e+02, 3.02744649e-01,
         2.58022259e+01],
        [4.70220798e+02, 5.41227625e+02, 2.05203133e+02, 3.01570842e-01,
         2.54428448e+01],
        [4.81425552e+02, 5.22824233e+02, 2.04103325e+02, 3.08389641e-01,
         2.50351728e+01],
        [5.13279840e+02, 5.34850742e+02, 2.01035498e+02, 2.98168988e-01,
         2.41116374e+01],
        [5.23394653e+02, 5.53761133e+02, 2.10300721e+02, 2.93147332e-01,
         2.67950074e+01],
        [5.55121927e+02, 5.88978259e+02, 2.07909045e+02, 2.89695380e-01,
         2.28484914e+01],
        [4.95378230e+02, 5.50846682e+02, 2.06175750e+02, 2.87193569e-01,
         2.40508978e+01]])

#################################################################################
newProject( "./Base_model/Base_model", 100 )
setModelAnalysisAspects( [ "STRUCT" ] )
setModelDimension( "2D" )
setDefaultMeshOrder( "QUADRATIC" )
setDefaultMesherType( "HEXQUAD" )
setDefaultMidSideNodeLocation( "LINEAR" )
setUnit( "LENGTH", "MM" )
setUnit( "FORCE", "N" )

### GEOMETRY
createSheet( "Concrete", [[ 0, 0, 0 ],[ L_beam/2, 0, 0 ],[ L_beam/2, h, 0 ],[ 0, h, 0 ]] )
createSheet( "Supp_plate", [[ 0.5*(L_beam-L_span-w_supp), 0, 0 ],
[ 0.5*(L_beam-L_span-w_supp), -hp, 0 ], [ 0.5*(L_beam-L_span), -hp, 0 ],
[ 0.5*(L_beam-L_span+w_supp), -hp, 0 ],[ 0.5*(L_beam-L_span+w_supp), 0, 0 ]] )
if typ==1.0:
    createSheet("Load_plate",[[0.5*(L_beam-w_load),h,0],[L_beam/2,h,0],[L_beam/2,h+hp,0],
    [ 0.5*(L_beam-0.5*w_load), h+hp, 0 ],[ 0.5*(L_beam-w_load), h+hp, 0 ]] )
    createPointNodeGroupItem( "Node_load", "Geom node group 1" )
    attach( GEOMETRYNODEGROUPITEM, "Node_load", "Load_plate", [[ 0.5*(L_beam), h+hp, 0 ]] )
if typ==2.0:
    createSheet("Load_plate",[[0.5*(L_beam-w_load-mid_span),h,0],[0.5*(L_beam-mid_span+w_load),
    h, 0], [ 0.5*(L_beam-mid_span+w_load), h+hp, 0 ],[ 0.5*(L_beam-mid_span), h+hp, 0 ],
    [ 0.5*(L_beam-w_load-mid_span), h+hp, 0 ]] )
    createPointNodeGroupItem( "Node_load", "Geom node group 1" )
    attach(GEOMETRYNODEGROUPITEM,"Node_load","Load_plate",[[ 0.5*(L_beam-mid_span), h+hp, 0 ]])

createLine( "Reinfo_low", [ 0, h-d, 0 ], [ L_beam/2, h-d, 0 ] )
addGeometry( "Element geometry 1", "SHEET", "MEMBRA", [] )
setParameter( "GEOMET", "Element geometry 1", "THICK", b_w )
rename( "GEOMET", "Element geometry 1", "Thickness" )

### ASSIGN TOP REINFO
if A_top >= 0.5:
```

```
    createLine( "Reinfo_top", [ 0, h-c_top, 0 ], [ L_beam/2, h-c_top, 0 ] )
    addMaterial( "Reinfo_top", "REINFO", "VMISES", [] )
    setParameter( "MATERIAL", "Reinfo_top", "LINEAR/ELASTI/YOUNG", Es_top )  #Es
    setParameter( "MATERIAL", "Reinfo_top", "PLASTI/YLDTYP", "JSCE12" )
    setParameter("MATERIAL","Reinfo_top","PLASTI/HARDI5/REJSCE",[ fy_top, fu_top,25/1000 ])
    addGeometry( "Bar_Area_top", "RELINE", "REBAR", [] )
    setParameter( "GEOMET", "Bar_Area_top", "REIEMB/CROSSE", A_top )
    setShapeType( REINFORCEMENTSHAPE, [ "Reinfo_top" ] )
    assignMaterial( "Reinfo_top", "SHAPE", [ "Reinfo_top" ] )
    assignGeometry( "Bar_Area_top", "SHAPE", [ "Reinfo_top" ] )
    resetElementData( "SHAPE", [ "Reinfo_top" ] )
    setReinforcementDiscretization( [ "Reinfo_top" ], "ELEMENT" )

### SUPPORT CONDITIONS
addSet( "GEOMETRYSUPPORTSET", "Supports" )
createPointSupport( "Support_left", "Supports" )
setParameter( GEOMETRYSUPPORT, "Support_left", "AXES", [ 1, 2 ] )
setParameter( GEOMETRYSUPPORT, "Support_left", "TRANSL", [ 0, 1, 0 ] )
setParameter( GEOMETRYSUPPORT, "Support_left", "ROTATI", [ 0, 0, 0 ] )
attach( GEOMETRYSUPPORT, "Support_left", "Supp_plate", [[ 0.5*(L_beam-L_span), -hp, 0 ]] )

createLineSupport( "Support_right", "Supports" )
setParameter( "GEOMETRYSUPPORT", "Support_right", "AXES", [ 1, 2 ] )
setParameter( "GEOMETRYSUPPORT", "Support_right", "TRANSL", [ 1, 0, 0 ] )
setParameter( "GEOMETRYSUPPORT", "Support_right", "ROTATI", [ 0, 0, 0 ] )
attach( "GEOMETRYSUPPORT", "Support_right", "Concrete", [[ L_beam/2, h/2, 0 ]] )
if typ==1.0:
    attach( "GEOMETRYSUPPORT", "Support_right", "Load_plate", [[ L_beam/2, h+hp/2, 0 ]] )

### LOADS
addSet( "GEOMETRYLOADSET", "Loads" )
createPointLoad( "Point_load", "Loads" )
setParameter( "GEOMETRYLOAD", "Point_load", "FORCE/VALUE", F )  #Newton
setParameter( "GEOMETRYLOAD", "Point_load", "FORCE/DIRECT", 2 )
if typ==1.0:
    attach( "GEOMETRYLOAD", "Point_load", "Load_plate", [[ 0.5*L_beam, h+hp, 0 ]] )
if typ==2.0:
    attach("GEOMETRYLOAD","Point_load","Load_plate",[[0.5*(L_beam-mid_span),h+hp,0]])

### ASSIGN PLATES
addMaterial( "Plates_material", "MCSTEL", "ISOTRO", [] )
setParameter( "MATERIAL", "Plates_material", "LINEAR/ELASTI/YOUNG", 210000 )
setParameter( "MATERIAL", "Plates_material", "LINEAR/ELASTI/POISON", 0.3 )
setParameter( "MATERIAL", "Plates_material", "LINEAR/MASS/DENSIT", 0 )
setElementClassType( "SHAPE", [ "Supp_plate", "Load_plate" ], "MEMBRA" )
assignMaterial( "Plates_material", "SHAPE", [ "Supp_plate", "Load_plate" ] )
assignGeometry( "Thickness", "SHAPE", [ "Supp_plate", "Load_plate" ] )

### INTERFACES
addMaterial( "Interface_material", "INTERF", "ELASTI", [] )
setParameter( "MATERIAL", "Interface_material", "LINEAR/IFTYP", "LIN2D" )
setParameter( "MATERIAL", "Interface_material", "LINEAR/ELAS2/DSNY", 30000 )
setParameter( "MATERIAL", "Interface_material", "LINEAR/ELAS2/DSSX", 30 )
addGeometry( "Interface_thickness", "LINE", "STLIIF", [] )
setParameter( "GEOMET", "Interface_thickness", "LIFMEM/THICK", 10 )
setParameter( GEOMET, "Interface_thickness", "LOCAXS", False )
createConnection( "Interface_plates", "INTER", "SHAPEEDGE" )
setParameter( "GEOMETRYCONNECTION", "Interface_plates", "MODE", "AUTO" )
attachTo( "GEOMETRYCONNECTION", "Interface_plates", "SOURCE", "Supp_plate",
```

```
[[ (L_beam-L_span)/2, 0, 0 ]] )

if typ==1.0:
    attachTo( ”GEOMETRYCONNECTION”, ”Interface_plates”, ”SOURCE”, ”Load_plate”,
    [[ 0.5*(L_beam-0.5*l_load), h, 0 ]] )
if typ==2.0:
    attachTo( ”GEOMETRYCONNECTION”, ”Interface_plates”, ”SOURCE”, ”Load_plate”,
    [[ 0.5*(L_beam-mid_span), h, 0 ]] )
setElementClassType( ”GEOMETRYCONNECTION”, ”Interface_plates”, ”STLIIF” )
assignMaterial( ”Interface_material”, ”GEOMETRYCONNECTION”, ”Interface_plates” )
assignGeometry( ”Interface_thickness”, ”GEOMETRYCONNECTION”, ”Interface_plates” )
setParameter( ”GEOMETRYCONNECTION”, ”Interface_plates”, ”FLIP”, False )
resetElementData( ”GEOMETRYCONNECTION”, ”Interface_plates” )

#### STIRRUPS
if s >=0.5:
    createLine(”stirrups”,[0.5*(L_beam-L_span)+45,h-d,0],[0.5*(L_beam-L_span)+45,h-c_top,0])
    duplicateShape( ”stirrups”, ”stirrups 1” )
    translate( [ ”stirrups 1” ], [ s, 0, 0 ] )
    duplicateShape( ”stirrups 1”, ”stirrups 2” )
    translate( [ ”stirrups 2” ], [ s, 0, 0 ] )
    duplicateShape( ”stirrups 2”, ”stirrups 3” )
    translate( [ ”stirrups 3” ], [ s, 0, 0 ] )
    duplicateShape( ”stirrups 3”, ”stirrups 4” )
    translate( [ ”stirrups 4” ], [ s, 0, 0 ] )
    duplicateShape( ”stirrups 4”, ”stirrups 5” )
    translate( [ ”stirrups 5” ], [ s, 0, 0 ] )
    duplicateShape( ”stirrups 5”, ”stirrups 6” )
    translate( [ ”stirrups 6” ], [ s, 0, 0 ] )
    duplicateShape( ”stirrups 6”, ”stirrups 7” )
    translate( [ ”stirrups 7” ], [ s, 0, 0 ] )
    duplicateShape( ”stirrups 7”, ”stirrups 8” )
    translate( [ ”stirrups 8” ], [ s, 0, 0 ] )

    addMaterial( ”Stir_mat”, ”REINFO”, ”VMISES”, [] )
    setParameter( ”MATERIAL”, ”Stir_mat”, ”LINEAR/ELASTI/YOUNG”, s_E )
    setParameter( ”MATERIAL”, ”Stir_mat”, ”PLASTI/YLDTYP”, ”JSCE12” )
    setParameter( ”MATERIAL”, ”Stir_mat”, ”PLASTI/HARDI5/REJSCE”, [ s_fy, s_fu,25/1000 ] )
    addGeometry( ”stirrup_area”, ”RELINE”, ”REBAR”, [] )
    setParameter( ”GEOMET”, ”stirrup_area”, ”REIEMB/CROSSE”, 0.25*3.14*s_d**2 )
    setShapeType( REINFORCEMENTSHAPE, [ ”stirrups”, ”stirrups 1”, ”stirrups 2”,”stirrups 3”,
    ”stirrups 4”, ”stirrups 5”,”stirrups 6”, ”stirrups 7”, ”stirrups 8” ] )
    assignMaterial(”Stir_mat”,”SHAPE”,[”stirrups”,”stirrups 1”,”stirrups 2”,”stirrups 3”,
    ”stirrups 4”, ”stirrups 5”,”stirrups 6”, ”stirrups 7”, ”stirrups 8”  ] )
    assignGeometry(”stirrup_area”,”SHAPE”,[”stirrups”,”stirrups 1”,”stirrups 2”,”stirrups 3”,
    ”stirrups 4”, ”stirrups 5”,”stirrups 6”, ”stirrups 7”, ”stirrups 8”  ] )
    resetElementData(”SHAPE”,[”stirrups”,”stirrups 1”,”stirrups 2”,”stirrups 3”,”stirrups 4”,
    ”stirrups 5”,”stirrups 6”, ”stirrups 7”, ”stirrups 8”  ] )
    setReinforcementDiscretization( [ ”stirrups”, ”stirrups 1”, ”stirrups 2”,”stirrups 3”,
    ”stirrups 4”, ”stirrups 5”,”stirrups 6”, ”stirrups 7”, ”stirrups 8”  ], ”ELEMENT” )


for i in range(N):
    ### ASSIGN CONCRETE MATERIAL
    concrete= concr[i]
    reinforcement= reinfo[i]
    f_cd,f_ctm,E_c,G_f = [concrete[0],concrete[1],concrete[2],concrete[3]]
    f_y,f_u,E_s,nu_s,eps_s = [reinforcement[0],reinforcement[1],reinforcement[2],
    reinforcement[3],reinforcement[4]]
```

```
    G_c = 250*G_f

    addMaterial( "Concrete_material", "CONCR", "TSCR", [] )
    setParameter( "MATERIAL", "Concrete_material", "LINEAR/ELASTI/YOUNG", 1000*E_c )
    setParameter( "MATERIAL", "Concrete_material", "LINEAR/ELASTI/POISON", 0.2 )
    setParameter( "MATERIAL", "Concrete_material", "LINEAR/MASS/DENSIT", 2.756*10**9 )
    setParameter( "MATERIAL", "Concrete_material", "MODTYP/TOTCRK", "ROTATE" )
    setParameter( "MATERIAL", "Concrete_material", "TENSIL/TENCRV", "HORDYK" )
    setParameter( "MATERIAL", "Concrete_material", "TENSIL/TENSTR", f_ctm )
    setParameter( "MATERIAL", "Concrete_material", "TENSIL/CBSPEC", "GOVIND" )
    setParameter( "MATERIAL", "Concrete_material", "TENSIL/RESTST", 0 )
    setParameter( "MATERIAL", "Concrete_material", "TENSIL/POISRE/POIRED", "DAMAGE" )
    setParameter( "MATERIAL", "Concrete_material", "TENSIL/GF1", G_f/1000 )
    setParameter( "MATERIAL", "Concrete_material", "TENSIL/RESTST", 0 )
    setParameter( "MATERIAL", "Concrete_material", "COMPRS/COMCRV", "PARABO" )
    setParameter( "MATERIAL", "Concrete_material", "COMPRS/COMSTR", f_cd )
    setParameter( "MATERIAL", "Concrete_material", "COMPRS/GC", G_c/1000 )
    setParameter( "MATERIAL", "Concrete_material", "COMPRS/RESCST", 0 )
    setParameter( "MATERIAL", "Concrete_material", "COMPRS/REDUCT/REDCRV", "VC1993" )
    setParameter( "MATERIAL", "Concrete_material", "COMPRS/REDUCT/REDMIN", 0.4 )
    setParameter( "MATERIAL", "Concrete_material", "COMPRS/CONFIN/CNFCRV", "VECCHI" )
    setElementClassType( "SHAPE", [ "Concrete" ], "MEMBRA" )
    assignMaterial( "Concrete_material", "SHAPE", [ "Concrete" ] )
    assignGeometry( "Thickness", "SHAPE", [ "Concrete" ] )

    ### ASSIGN REINFO
    addMaterial( "Reinfo", "REINFO", "VMISES", [] )
    setParameter( "MATERIAL", "Reinfo", "LINEAR/ELASTI/YOUNG", 1000*E_s )
    setParameter( "MATERIAL", "Reinfo", "PLASTI/YLDTYP", "JSCE12" )
    setParameter( "MATERIAL", "Reinfo", "PLASTI/HARDI5/REJSCE", [ f_y, f_u,eps_s/1000 ] )
    addGeometry( "Element geometry 3", "RELINE", "REBAR", [] )
    rename( "GEOMET", "Element geometry 3", "Bar_Area" )
    setParameter( "GEOMET", "Bar_Area", "REIEMB/CROSSE", A_long )
    setShapeType( REINFORCEMENTSHAPE, [ "Reinfo_low" ] )
    assignMaterial( "Reinfo", "SHAPE", [ "Reinfo_low" ] )
    assignGeometry( "Bar_Area", "SHAPE", [ "Reinfo_low" ] )
    resetElementData( "SHAPE", [ "Reinfo_low" ] )
    setReinforcementDiscretization( [ "Reinfo_low" ], "ELEMENT" )

    ### MESH
    setElementSize( [ "Concrete", "Supp_plate", "Load_plate" ], Mesh_size, -1, True )
    setMesherType( [ "Concrete", "Supp_plate", "Load_plate" ], "HEXQUAD" )
    setMidSideNodeLocation( [ "Concrete", "Supp_plate", "Load_plate" ], "LINEAR" )
    generateMesh( [] )
    if typ==1.0:
        p1 = findNodesInBox( 0.5*(L_beam)-1, 0.5*(L_beam)+1, h+hp-1, h+hp+1, 0, 0 )
    if typ==2.0:
        p1 =findNodesInBox(0.5*(L_beam-mid_span)-1,0.5*(L_beam-mid_span)+1,h+hp-1,h+hp+1,0,0)

    ### ADD ANALYSIS
    Analysis_name= "Analysis%s_%s" %(index_num,i)
    addAnalysis( Analysis_name )
    addAnalysisCommand( Analysis_name, "NONLIN", "Structural nonlinear" )
    setAnalysisCommandDetail(Analysis_name,"Structural nonlinear","EXECUT(1)/ITERAT/MAXITE",iters)
    setAnalysisCommandDetail(Analysis_name, "Structural nonlinear",
    "EXECUT(1)/ITERAT/CONVER/DISPLA", False )
    addAnalysisCommandDetail(Analysis_name,"Structural nonlinear","EXECUT(1)/ITERAT/CONVER/ENERGY")
    setAnalysisCommandDetail( Analysis_name, "Structural nonlinear",
    "EXECUT(1)/ITERAT/CONVER/ENERGY", True )
```

```
    setAnalysisCommandDetail( Analysis_name, "Structural nonlinear",
    "EXECUT(1)/ITERAT/CONVER/ENERGY/NOCONV", "CONTIN" )
    setAnalysisCommandDetail( Analysis_name, "Structural nonlinear",
    "EXECUT(1)/ITERAT/CONVER/FORCE/NOCONV", "CONTIN" )
    setAnalysisCommandDetail( Analysis_name, "Structural nonlinear",
    "EXECUT(1)/LOAD/STEPS/EXPLIC/SIZES", Load_step )
    addAnalysisCommandDetail(Analysis_name,"Structural nonlinear","EXECUT(1)/LOAD/LOADNR")
    setAnalysisCommandDetail(Analysis_name,"Structural nonlinear","EXECUT(1)/LOAD/LOADNR",1)
    addAnalysisCommandDetail( Analysis_name, "Structural nonlinear",
    "EXECUT(1)/LOAD/STEPS/EXPLIC/ARCLEN" )
    setAnalysisCommandDetail( Analysis_name, "Structural nonlinear",
    "EXECUT(1)/LOAD/STEPS/EXPLIC/ARCLEN", True )
    addAnalysisCommandDetail( Analysis_name, "Structural nonlinear",
    "EXECUT(1)/LOAD/STEPS/EXPLIC/ARCLEN/REGULA/SET" )
    setAnalysisCommandDetail( Analysis_name, "Structural nonlinear",
    "EXECUT(1)/LOAD/STEPS/EXPLIC/ARCLEN/REGULA/SET(1)/NODES(1)/RNGNRS","\"Geom node group 1\"")
    setAnalysisCommandDetail( Analysis_name, "Structural nonlinear",
    "EXECUT(1)/LOAD/STEPS/EXPLIC/ARCLEN/REGULA/SET(1)/DIRECT", 2 )
    setAnalysisCommandDetail(Analysis_name,"Structural nonlinear","EXECUT(1)/ITERAT/LINESE",True)
    addAnalysisCommandDetail(Analysis_name,"Structural nonlinear","EXECUT(1)/LOGGIN/ENERGY")
    setAnalysisCommandDetail(Analysis_name,"Structural nonlinear","OUTPUT(1)/SELTYP", "USER")
    addAnalysisCommandDetail( Analysis_name, "Structural nonlinear", "OUTPUT(1)/USER" )
    addAnalysisCommandDetail( Analysis_name, "Structural nonlinear",
    "OUTPUT(1)/USER/DISPLA(1)/TOTAL/TRANSL/GLOBAL" )
    addAnalysisCommandDetail( Analysis_name, "Structural nonlinear",
    "OUTPUT(1)/USER/DISPLA(2)/TOTAL/TRANSL/LOCAL" )
    addAnalysisCommandDetail(Analysis_name,"Structural nonlinear","OUTPUT(1)/USER/STRAIN(1)/CRACK")
    addAnalysisCommandDetail(Analysis_name,"Structural nonlinear","OUTPUT(1)/USER/STRAIN(2)/CRKWDT")
    addAnalysisCommandDetail(Analysis_name,"Structural nonlinear","OUTPUT(1)/USER/STRAIN(3)/TOTAL")
    addAnalysisCommandDetail( Analysis_name, "Structural nonlinear", "OUTPUT(1)/USER/STRESS" )
    addAnalysisCommandDetail(Analysis_name,"Structural nonlinear","OUTPUT(1)/USER/FORCE(1)/EXTERN")

    runSolver( Analysis_name )
    showView( "RESULT" )
    selectResult( {"component": "TDtY", "result": "Displacements", "type": "Node"} )

    output1 = outputBlocks( Analysis_name )[0]
    p1 = p1[0]
    Result_name= "load_facs%s_%s.csv" %(index_num,i)
    resCases = resultCases(Analysis_name, output1)
    exportResults( Result_name,
                { "analysis"   : Analysis_name,
                  "block"      : output1,
                  "result"     : 'External Forces',
                  "components" : [ 'FEY' ],
                  "cases"      : resCases,
                  "nodes"      : [p1] } )
```

C NLFEA

C.1. Load-Steps

Table C.1: Overview of the used load-steps per benchmark.

Beam index	Load-step	Beam index	Load-step	Beam index	Load-step
B-H2	0.30(70)	BS-C2	0.03(100)	VS-OA3	0.04(80)
B-H3	0.30(70)	BS-C3	0.03(100)	A111	0.20(100)
B-H4	0.30(70)	BS-OA1	0.05(125)	A211	0.15(80)
B-M2	0.30(60)	BS-OA2	0.05(90)	B211a	0.20(100)
B-M3	0.30(40)	BS-OA3	0.03(110)	B311	0.05(80)
B-M4	0.15(60)	VS-A1	0.05(110)	B312	0.15(80)
B-N2	0.30(60)	VS-A2	0.05(90)	B313	0.15(80)
B-N3	0.15(35)	VS-A3	0.04(95)	B321	0.05(80)
B-N4	0.075(60)	VS-B1	0.05(90)	B331	0.05(80)
BS-A1	0.03(160)	VS-B2	0.05(105)	B411	0.05(80)
BS-A2	0.03(120)	VS-B3	0.03(100)	C211	0.20(100)
BS-A3	0.03(100)	VS-C1	0.05(90)	C311	0.20(100)
BS-B1	0.05(90)	VS-C2	0.05(75)	C411	0.15(80)
BS-B2	0.04(95)	VS-C3	0.04(95)	C511	0.075(80)
BS-B3	0.04(95)	VS-OA1	0.10(80)	D211	0.20(100)
BS-C1	0.05(100)	VS-OA2	0.06(100)	E211	0.13(150)

C.2. Ductility Index per Load-step

It can be argued whether the ductility index should be defined at a point where the beam has truly failed, or at its maximum capacity. For this case, the effect of defining the ductility index at the maximum load and one load-step afterwards was investigated. The effect was investigated by a visual inspection of the deformed finite element models and the magnitude of the ductility index.

In Figure C.1, the logged ductility index is showed as function of the load-step for the 48 benchmarks based on mean input parameters. From visual inspection it was observed that defining the ductility index at one load-step after the maximum load resulted in a wrong prediction of the failure mode. This can be explained due to the relative change of the ductility index. If a brittle failure mode occurred, the concrete would fail and in the next load-step a significant part of the load would be absorbed by the reinforcement, resulting in an increased ductility index. In the upper graph, it can be seen that many of the brittle failure mechanisms (red) could result in a ductile failure mechanism if the ductility index were to be affirmed one load-step behind the maximum load. For the ductile failure mechanism (blue), the opposite would occur although for this data-set most would not drop below the boundary of $\chi = 0.6$.

In the lower graph, the derivative of the ductility index is displayed to indicate the relative change. After failure, the brittle failure mode exhibits a positive change while the ductile failure mode would exhibit a negative change. Both affect the magnitude of the ductility index significantly, and resulted in wrong predictions of the failure mode. Therefore, the ductility index was found to be best defined at the load-step belonging to the maximum resistance. However, the relative change of the ductility index could be used as indicator of the numerical failure mode as a function of the load-step.

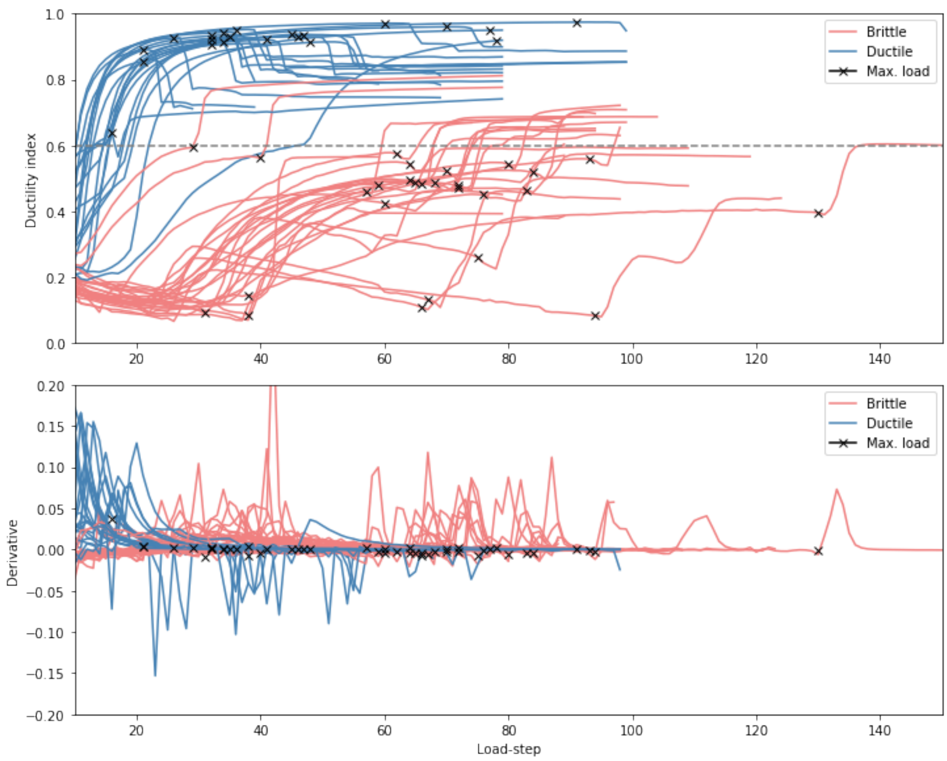

Figure C.1: Ductility index (top) and derivative of the ductility index (bottom) as function of the load-step for mean input variables of 48 benchmarks.

C.3. Load-Displacement Curves

In Figure C.2, the numerical load-displacement curve (left) is compared to the experimental load-displacement curve (right) from Ashour [29]. All beams are expected to fail in a ductile manner and both graphs show clear agreement. Only one exception can be observed for beam index 8 (BN4), which was earlier discussed to fail prematurely due to a failure of shear reinforcement.

In figure Figure C.3, the numerical load-displacement curves are compared to the experimental load-displacement curve from Vecchio and Shim [35]. These beams are expected to experience a brittle failure mode, and therefore are more difficult to predict. The top three graphs are beams without shear reinforcement and these show the least consistency. This again indicates that a different crack model (fixed instead of rotating) may be better suited to these benchmarks. The other numerical output shows better agreement to the experimental observed load-displacement curves. Contrary to the ductile failure mode, a systematic underestimation of the maximum load is observed.

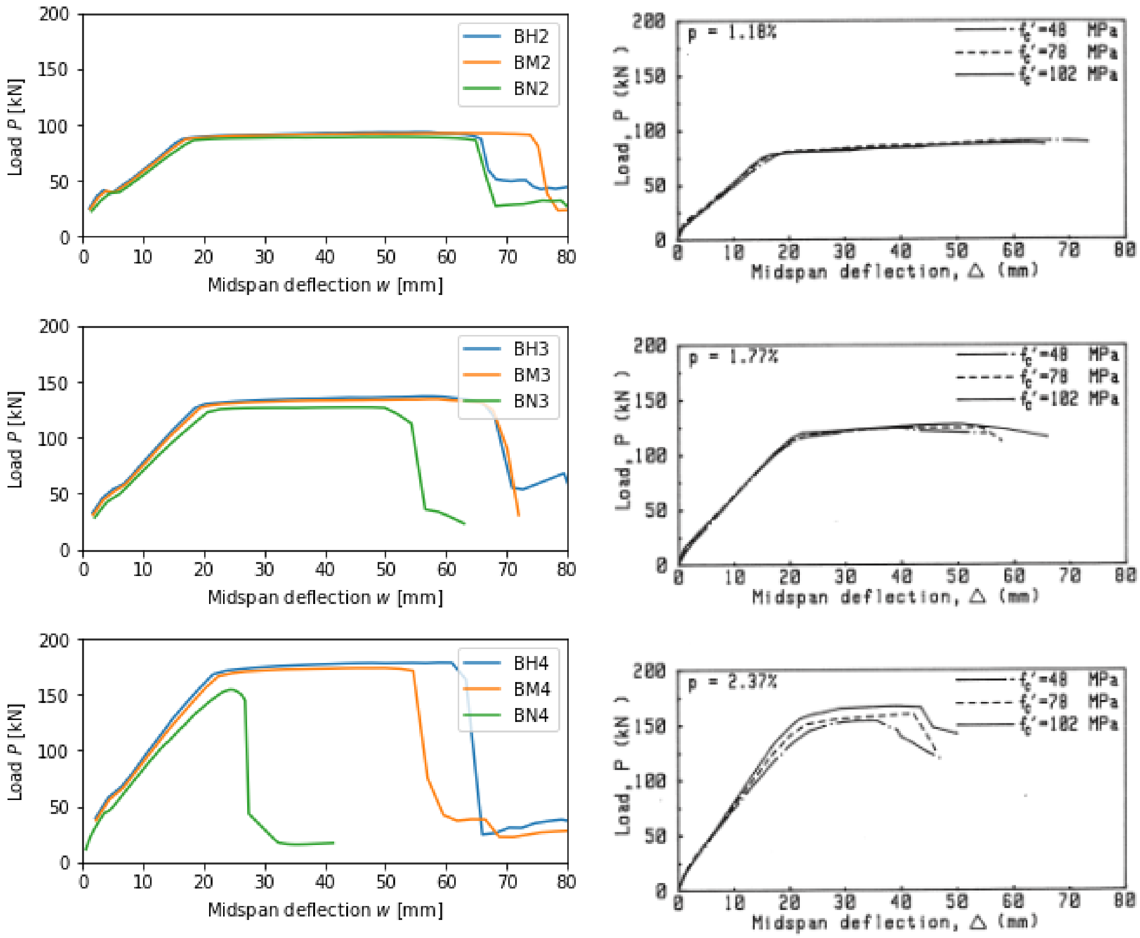

Figure C.2: Comparison of the numerical (left) and experimental (right) load-displacement curves from Ashour [29].

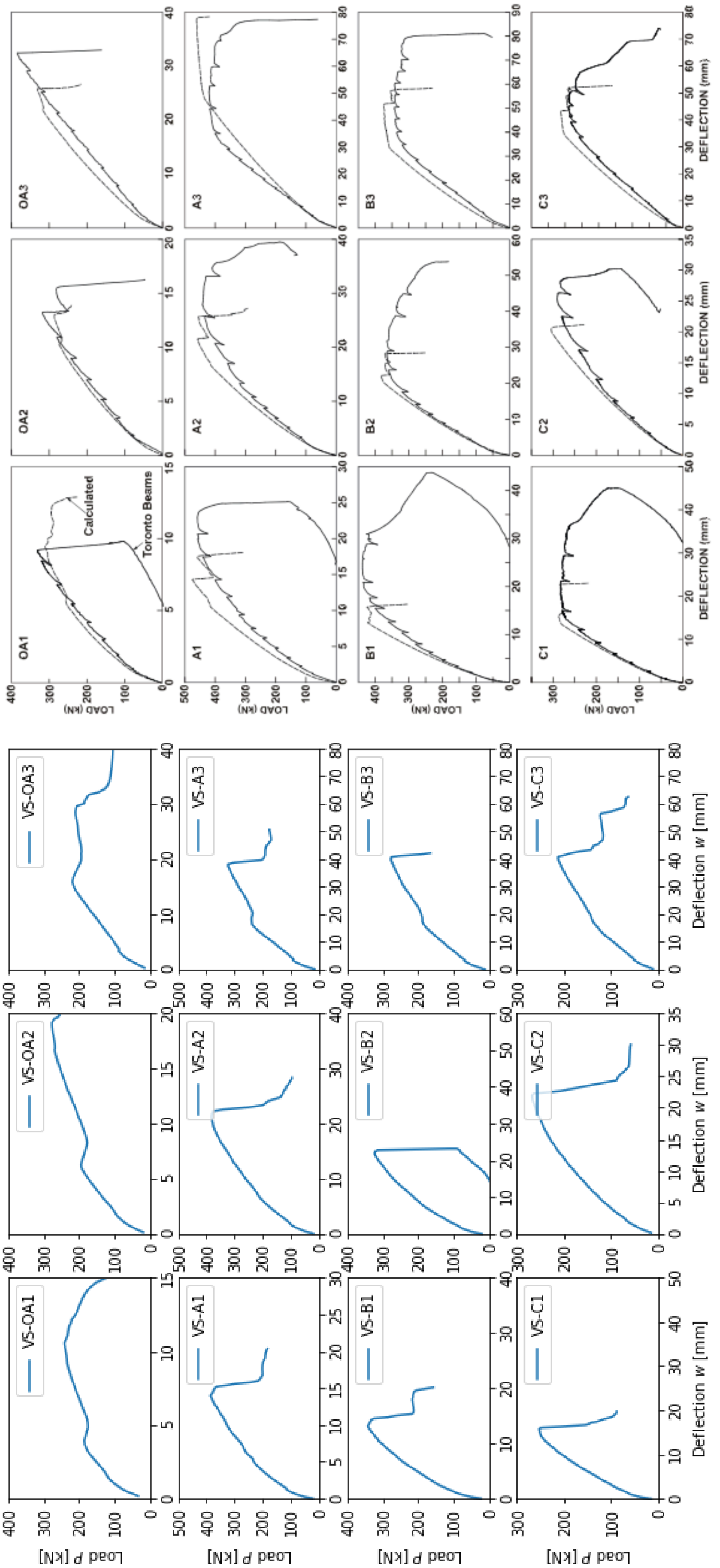

Figure C.3: Comparison of the numerical (left) and experimental (right) load-displacement curves from Vecchio and Shim[35].

D | Model Application

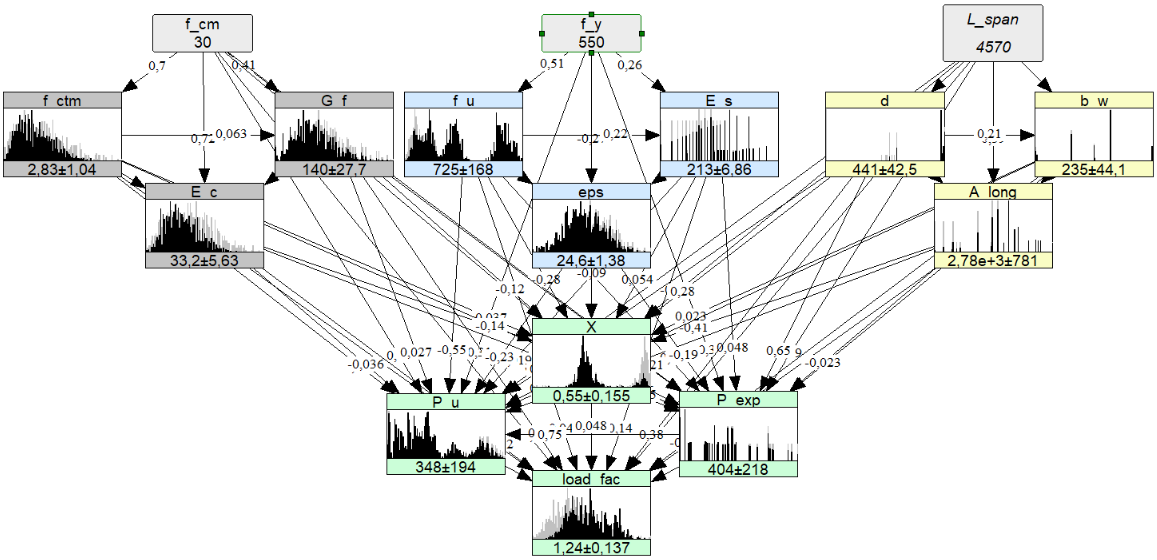

Figure D.1: Example of the change in distributions for conditional strength and geometry parameters, visible by shaded histograms.